# Subseasonal Forecasting of Fire Weather Using Recurrent Neural Networks

by

Jessica Zerb

A thesis submitted in partial fulfillment of the requirements for the degree of

Master of Science
in
Forest Biology and Management

Department of Renewable Resources
University of Alberta

## Abstract

Fire weather indices are used by fire management agencies around the world to estimate potential wildfire danger. This allows for resources to be allocated effectively and to warn communities of potential wildfire hazards. Currently, monitoring and short-term forecasting of fire weather depends on the use of observed surface and upper air weather and numerical weather prediction systems. Fire weather forecasting at the subseasonal and seasonal time scale has been largely reliant on continued improvements to global circulation models. However, such models may lead to large uncertainties in the prediction of surface meteorology at timescales greater than five to seven days, which may result in low predictive skill for fire weather indices. To resolve this, large scale atmospheric patterns (teleconnections) are frequently used to predict seasonal variations in weather. Here we consider a deep learning data-centric approach to predict fire weather indices on a sub-seasonal time scale (1-5 weeks). This approach uses teleconnections such as the El Niño-Southern Oscillation (ENSO) and the Atlantic Multidecadal (AMO) as covariates. We apply a long short term memory (LSTM) recurrent neural network for time series forecasting of the Build-Up Index (BUI), an output of the Canadian Fire Weather Index System. Weekly averages of BUI are calculated using the fifth version of the European Centre for Medium-Range Weather Forecasts Reanalysis (ERA5) data. The ERA5 data is aggregated onto 4.87 x $10^5$ $m^2$ hexels across Canada. Active fire season data from April to October is split into training and testing datasets which span 80% (1981 - 2012) and 20% (2013 - 2020) of the total time period respectively. After, hyperparameter tuning the LSTM model showed improved results in 1-3 week forecasts in the western half of Canada when compared to

baseline forecasts of climatology and persistence. These model results may assist provincial fire management agencies in long range planning.

## Preface

This thesis is an original work by Jessica Zerb. No part of this thesis has been previously published.

**Acknowledgements**

This thesis was only possible with the help of an incredible wildfire science community and group of expert researchers. I am extremely grateful for all of the people that have generously provided me with their time and support on my journey as a master's student. Thank you to everyone who has helped me along the way!

I wish to express my sincere appreciation to my supervisors, Dr. Michael Flannigan and Dr. Piyush Jain, for their incredible patience, understanding, and commitment towards this project. Both supervisors have helped in every single step of the way, and I could not be more grateful for their expert advice and guidance. This thesis has proven to be one of the most challenging projects I have ever worked on, and I would not have completed it if it were not for Mike and Piyush.

Mike, I would like to thank you for believing in me and my potential for research. You have been an incredible role model and guiding force as your passion and commitment to your students shines bright. Your wealth of knowledge and ability to communicate information with students is unparalleled and I hope to learn from you again soon! Thank you for inspiring me to continue learning no matter what stage of life I am in and that we should all strive to be life-long-learners.

Piyush, I would like to thank you for encouraging me to pursue a project that has allowed me to grow as a person, student, and professional. This project has challenged me in ways that I never

expected it would. Thank you for taking me under your wing and teaching me how to be a researcher! Your curiosity, patience, and drive for perfection has left me in awe every time we meet. Now I think “what would Piyush do” before coding a new line, debugging old code, or starting a new sentence. Truly, this thesis would not be where it is today without your expert knowledge and advice. It has been an incredible experience having you as a supervisor and I will be forever grateful.

This project was completed in the height of the COVID-19 pandemic, leaving many students (including myself) isolated and working from home. Thankfully, the students of the fire lab provided much needed virtual mental-health support via Zoom meetings and socially distanced gatherings. Thank you to Olivia Aftergood, Andrew Stack, Hilary Cameron, and Kate Bezooyen for supporting me at the early stages of my project. A special thank you to Kyle Elliot for keeping me accountable, studying over large cups of coffee, sending me hilarious memes, and dreaming of our future defense dates. You have helped me to stay sane throughout these strange times, and I could not be more thankful.

Thank you to the University of Alberta and staff in the Department of Renewable Resources for keeping track of the students and providing us with everything we needed during the transition to a work-from-home environment. Finally, thank you to The Canadian Partnership for Wildland Fire Science for providing the funding for this research.

## Table of Contents

## List of Tables

## List of Figures

model forecast is improved. Red indicates a positive MAE difference, where the climatology or persistence forecast is improved. Tones of green represent F1-scores, with darker shades showing higher accuracies.

Figure 3.12 Model 2 MAE comparisons of testing data (2013-2020) for LSTM model, climatology, and persistence forecasts for each hexel: (a) the difference between model MAE and climatology MAE, (b) the difference between model MAE and persistence MAE, and (c) the accuracy of model predictions. Blue indicates a negative MAE difference, where the LSTM model forecast is improved. Red indicates a positive MAE difference, where the climatology or persistence forecast is improved. Tones of green represent F1-scores, with darker shades showing higher accuracies.

Figure 3.13 Model 3 MAE comparisons of testing data (2013-2020) for LSTM model, climatology, and persistence forecasts for each hexel: (a) the difference between model MAE and climatology MAE, (b) the difference between model MAE and persistence MAE, and (c) the accuracy of model predictions. Blue indicates a negative MAE difference, where the LSTM model forecast is improved. Red indicates a positive MAE difference, where the climatology or persistence forecast is improved. Tones of green represent F1-scores, with darker shades showing higher accuracies.

Figure 3.14 Model 4 MAE comparisons of testing data (2013-2020) for LSTM model, climatology, and persistence forecasts for each hexel: (a) the difference between model MAE and climatology MAE, (b) the difference between model MAE and persistence MAE, and (c) the accuracy of model predictions. Blue indicates a negative MAE difference, where the LSTM model forecast is improved. Red indicates a positive MAE difference, where the climatology or persistence forecast is improved. Tones of green represent F1-scores, with darker shades showing higher accuracies.

## List of Acronyms

| | |
|---|---|
| AI | Artificial Intelligence |
| AMO | Atlantic Multidecadal Oscillations |
| ANN | Artificial Neural Network |
| AO | Arctic Oscillation |
| API | Application Programming Interface |
| BUI | Build-Up Index |
| CanSIPS | Canadian Seasonal to Inter-annual Prediction System |
| CIFFC | Canadian Interagency Forest Fire Centre |
| CFFDRS | Canadian Forest Fire Danger Rating System |
| CFWIS | Canadian Forest Fire Weather Index System |
| CNN | Convolution Neural Network |
| CWFIS | Canadian Wildland Fire Information System |
| DC | Drought Code |
| DL | Deep Learning |
| DMC | Duff Moisture Code |
| DNN | Deep Neural Network |
| ECCC | Environment and Climate Change Canada |
| ECMWF | European Centre for Medium-Range Weather Forecasts |
| ENSO | El-Nino Southern Oscillation |
| ERA5 | European Centre for Medium-Range Weather Forecasts Reanalysis 5$^{th}$ Generation |

| | |
|---|---|
| FFT | Fast Fourier Transform |
| FWI | Fire Weather Index |
| FFMC | Fine Fuel Moisture Code |
| GEM | Global Environmental Multiscale Model |
| ISI | Initial Spread Index |
| LR | Learning Rate |
| LSTM | Long-Short Term Memory |
| MAE | Mean Absolute Error |
| ML | Machine Learning |
| MSE | Mean Standard Error |
| NAEFS | North American Ensemble Forecast System |
| NOAA | National Oceanic and Atmospheric Administration |
| NWP | Numerical Weather Prediction |
| PDO | Pacific Decadal Oscillation |
| ReLu | Rectified Linear Unit |
| RMSE | Root Mean Square Error |
| RNN | Recurrent Neural Network |
| SD | Standard Deviation |
| SST | Sea Surface Temperature |
| WMO | World Meteorological Organization |

# Chapter 1 Introduction

## 1.1 Research Context

Wildland fire can have adverse effects on communities and human assets, yet it is a critical process of the Earth's system (Bond and Keeley, 2005). Despite the necessity of wildland fire for global processes and healthy ecosystems, studies have shown that Canada has experienced frequent extreme fire weather (Wang et al., 2015) and severe fire seasons (Kirchmeier-Young et al., 2017) in recent years. The frequency of large wildfires has increased in Canada over the last few decades (Hanes et al., 2019) which may be attributed to increased fuel on the landscape (Wang et al., 2015), hotter and drier weather (Flannigan and Harrington, 1988; Van Wagner, 1977), and longer fire seasons (Albert-Green et al., 2013). As wildfires are projected to increase in Canada (Flannigan et al., 2005; Coogan et al., 2019), the negative impacts are shown through community devastation, loss of life, air quality, and number of evacuations. Hundreds of millions of dollars are spent on fire suppression, mitigation and prevention every season, therefore, understanding and better predicting wildfires is crucial for emergency responses (Stocks and Martell, 2016). In predicting wildfire activity, the weather plays an essential role as hot, dry, and windy weather increase fuel drying rates which drive fire ignition and growth. Surface weather variables are indispensable in predicting wildfire danger and fire season severity (Stocks et al. 1989) and are necessary inputs to the Canadian Forest Fire Weather Index System (CFWIS). The CFWIS is heavily relied upon by fire management agencies across Canada for estimating fuel moisture and potential fire behavior.

Currently, forecasting short-term fire weather depends on the use of observed surface and upper air weather to run numerical weather prediction systems. In Canada, short-range and medium-range weather prediction systems including the Global Environmental Multiscale Model (GEM) and the North American Ensemble Forecast System (NAEFS) are most often used for 1-14 day forecasts (Environment and Climate Change Canada, 2022). Fire weather forecasting at the sub-seasonal (i.e. two weeks to two months. Vitart and Robertson, 2018) and seasonal time scale (i.e. several months) have been largely reliant on continued improvements to global circulation models such as the Canadian Seasonal to Inter-annual Prediction System (CanSIPS). However, such forecasts may lead to large uncertainties in the prediction of small-scale surface meteorology as they resolve various global weather patterns and atmospheric conditions. The CFWIS uses consecutive daily observations of temperature, relative humidity, windspeed, and 24-hour precipitation to calculate six variables that provide numeric ratings of relative potential for fuel moisture and fire behavior. Therefore, the accuracy of numerical weather prediction systems can have a large impact on the CFWIS outputs. Moreover, CanSIPS does not include relative humidity as a forecast variable which may limit forecasting skill with respect to CFWIS.

While the complexities of surface meteorology can make forecasting fire weather challenging, Machine Learning (ML) may offer a solution. Significant advances in ML have allowed it to perform well in environmental science applications (Tahmasebi et al., 2020). ML techniques can 'detect patterns in data…and…use the uncovered patterns to predict future data' (Murphy, 2012). These advancements may be particularly advantageous when forecasting fire weather using Recurrent Neural Networks (RNN). More specifically, Long Short Term Memory (LSTM) networks are variants of RNNs that are known to reduce computation time and improve model

outputs (Hochreiter and Schmidhuber, 1997). In combination with readily available weather datasets, ML may help to improve the current FWI system forecasting approach. With improved methods for predicting spatial fire risk, fire management agencies can allocate resources more effectively. Fire fighters and government officials can be deployed in high fire danger zones to apply preventative fuel treatments or to give early warning to communities.

### 1.2 Canadian Fire Regime and Weather

Wildland fire is a dominant disturbance regime to Canadian forests, particularly in the boreal region which spans 75% of Canada's 362 million hectares of forest (Natural Resources Canada, 2022). It is a critical process necessary to propagate various tree species, encourage landscape diversity, and direct energy flows (Stocks et al., 2002). While fire is an essential process in boreal forests, four main factors have influence on its activity: weather, fuels, ignition agents, and people (Flannigan et al., 2005). Specifically, wildfire ignition and spread usually occurs under hot, dry and windy weather (Flannigan et al., 2009).

It has been suggested in various studies that increasing temperatures have had the largest effect on changing wildland fire regimes (Gillett et al., 2004). The positive correlation between wildland fire and temperature can be explained by increased evapotranspiration and lightning activity, and lengthening of fire seasons (Flannigan et al., 2009). First, as temperatures increase, the rate of evapotranspiration increases since there is a larger amount of energy available to convert liquid water to water vapor. In turn, the increase of water vapor pressure deficit will decrease fuel moisture, thereby creating an environment conducive to fire. Increases in

temperature lead to frequent thunderstorm events as a result of increased convective energy. As a result, lightning-ignited wildfires could potentially increase in a warming climate (Price and Rind, 1994; Romps et al., 2014; Hessilt et al., 2022). However, Cary et al. (2006) and Flannigan et al. (2016) found that increasing precipitation is not enough to compensate for the rise in temperature with respect to fuel moisture. Therefore, fire danger is anticipated to increase due to the effects of climate change. Finally, increases in fire season length and summer drought may result in heighted frequency of large wildfires (Westerling et al., 2006).

Surface meteorology is strongly tied to high level atmospheric conditions. Temperature, precipitation, wind, and atmospheric moisture depend on both the vertical and horizontal state of the atmosphere. Blocking ridges in the upper atmosphere have been linked to fire outbreaks (Flannigan and Harrington, 1988; Jain and Flannigan, 2021). Westerly upper flows (evident in the upper troposphere) prevail and divert precipitation to the north or south of the ridge. As these precipitation-bearing systems are blocked, warm and dry weather dominate at the surface level and can last a few days or longer. Various studies have suggested that dry spells induced by blocking ridges are strongly related to increased fire activity (Sharma et al., 2022). Johnson and Wowchuk (1993) studied this process in the southern Canadian Rocky Mountains and suggested that positive anomalies were linked with more active fire seasons. Flannigan and Harrington (1988) suggested that the 700-hPa geopotential height anomaly was the predictor most often selected to relate meteorological variables to monthly provincial area burned in Canada from 1953-1980. As well, Skinner et al. (1999) found that the 500-hPa geopotential height anomalies were linked to large burned area over Canada and Alaska.

On a larger scale, teleconnections are characterized by reoccurring patterns of varying pressure and circulation in the atmosphere and sea surface temperatures in oceans. These oscillations occur on multiannual to multidecadal timescales and cover large geographical areas which result in weather variations across the globe. Teleconnections are an important element of atmospheric circulation, as proven in various studies by Troup (1965), Zhang and Battisti (1997), and Diaz et al., (2001). Several sea surface temperature (SST) and atmospheric pressure patterns have been discovered around the world, including the El Niño Southern Oscillation (ENSO), Atlantic Multidecadal Oscillation (AMO), Pacific Decadal Oscillation (PDO), and Arctic Oscillation (AO). More specifically, teleconnections like ENSO are characterized by two phases of alternating warm and cold events of sea surface temperatures in regions of the Pacific Ocean, called El Niño and La Niña, respectively. Immediate and time-lagged atmospheric variations throughout the world can often be attributed to teleconnections, as they have influence on surface weather over long timescales (Domeisen et al., 2019; Diaz et al., 2001). Variables such as temperature, precipitation, air pressure, humidity, wind patterns, and dry lightning have been systematically linked to teleconnections (Girardin et al., 2006). Therefore, teleconnections can also have an effect on fire weather. Blocking ridges that result in high fire activity seasons are linked to upper-level troughs in eastern North America and the North Pacific Ocean. The upper-level troughs often occur during the positive phase of the Pacific North American (PNA) pattern (Johnson and Wowchuk, 1993). Schoennagle (2005) found that the interaction between phases of ENSO and PDO were statistically significant and associated with large-fire occurrences across the Rocky Mountains. Skinner et al. (2006) found that the warm phase of ENSO and the positive phase of PDO leads to dry conditions and higher fire severity in western, northwestern, and northeastern Canada. Moreover, various studies have discovered relationships between fire

frequency, extent, area burned and atmospheric teleconnections in North America (Simard et al. 1985; Chu et al. 2002; Westerling and Swetnam 2003; Kitzberger et al. 2007; Trouet et al. 2009) and other parts of the world (González and Veblen 2006; Verdon et al. 2004; Cardil et al. 2023).

Although wildfires are recognized as natural and critical events on the boreal landscape, most provinces in Canada aim to contain their spread as soon as possible, particularly when values are at risk. The risk of wildfire spread during episodes of fire conducive weather and while unsuppressed can be high, and there is potential for loss of life, community devastation, destruction of infrastructure, and huge economic loss (Martell, 2001; Moritz et al., 2014). Therefore, using weather to predict wildfire danger has become an integral part in fire prevention and mitigation in Canada (Flannigan and Harrington, 1988; Turner and Lawson, 1978; Stocks et al. 1989).

### 1.3 Weather Forecasts and the CFWIS

Surface meteorology is a key factor in estimating future fire risk and behavior. In Canada, the Canadian Forest Fire Danger Rating System (CFFDRS) and its subsystem, the Canadian Forest Fire Weather Index System (CFWIS shortened to FWI) are used to estimate fire weather variables from surface meteorology (Van Wagner 1987; Stocks et al., 1989). The CFFDRS and the CWFIS rely on surface meteorology variables from several short-term weather prediction systems including the Global Environmental Multiscale Model (GEM) and the North American Ensemble Forecast System (NAEFS). These models are most often used for 1-14 day forecasts of relative potential for fire. GEM was developed primarily for weather forecasting, but is used

to address climate issues and air quality issues in Canada using a variable-resolution strategy (Côté et al., 1998). NAEFS is a collaborative product between North American governments that combines ensemble forecasts into a seamless grand ensemble that provides operational forecast guidance (Toth et al., 2006).

The CFWIS utilizes four weather variables: noon local standard time 2m temperature, 24-hour precipitation, 2m relative humidity, and 10m wind speeds, daily forecasts of six standard numeric ratings of relative potential for wildland fire are produced. These indices provide information on fuel moisture and expected fire behavior if an ignition occurs. The first three indices calculated are fuel moisture codes, which estimate the moisture content of fuels located at top (0-1.2cm), middle (1.2-7cm), and lower (7-18cm) layers of the forest floor (Lawson and Armitage, 2008). The Fine Fuel Moisture Code (FFMC) is the numeric rating of moisture content of litter and provides a general indication to the relative ease of ignition or flammability of fine fuels. The Duff Moisture Code (DMC) is the numeric rating of the average moisture at moderate depth and provides a general indication of fuel consumption or mid-sized debris. In addition to this, Flannigan and Wotton (1991) found that DMC functions as the most important predictor variable for estimating lightning-ignited wildfires in Ontario. The Drought Code (DC) is the numeric rating of the average moisture of deep layers and provides a general indication of the effects of seasonal drought. Both DMC and DC show a clear seasonal pattern, with higher values during the fire season months of April to September (Amiro et al., 2004). The second tier of standard numeric ratings are called fire behavior indices, which are used to provide an estimate of potential fire behavior based on the calculated fuel moisture codes. The Initial Spread Index (ISI) is a numeric rating of the expected rate of fire spread. The Fire Weather Index (FWI)

is a numeric rating of fire intensity. Finally, the Buildup Index (BUI) is a numeric rating of the total amount of fuel available for combustion and is calculated using the DMC and the DC which have strong correlation on seasonal timescales (Van Wagner, 1987). As a result, BUI is a useful metric for long term planning and provides a relative rating on accumulated moderate to deep layer fuels that are available for combustion. By using BUI as the main predictor in this study, forecast results may capture the effects of both the DC and DMC.

Extended forecasts can also be used by fire management operations for calculating FWI System ratings. Reaching estimates beyond fourteen days can provide even earlier warning signs to relative potential for fire. Forecasting fire weather indices at the sub-seasonal and seasonal time scale have been largely reliant on continued improvements to global circulation models such as the Canadian Seasonal to Inter-annual Prediction System (CanSIPS). However, forecast accuracy diminishes as the lead time increases for both probabilistic and deterministic forecasts (McCollor and Roland, 2009; Anderson et al., 2007). Decreasing forecast accuracy also limits the accuracy of FWI system ratings, which have become deeply ingrained into fire management decision processes (Stocks et al., 1989). Machine Learning (ML) has the potential to improve weather predictions, as shown in several studied (Hochreiter and Schmidhuber, 1997; Bauer et al., 2015; McGovern et al., 2017; Sanabria et al., 2013). However, ML has thus far been underutilized in the forecasting of fire weather (Jain et al., 2020).

## 1.4 Introduction to Machine Learning

Artificial intelligence (AI) is a data-centric approach that employs computer science and large data sets for efficient problem solving. The field of AI is further divided into subcategories, one being Machine Learning (ML). Within Machine Learning, lives the category of Deep Learning (DL). These terms are used to describe the process of computer algorithms and their ability to make predictions, classifications, and improve automatically through experience (Mitchell, 1997; Poole and Mackworth, 2010). A well-performing ML model is dependent on accurate datasets that allow the algorithm to learn patterns and relationships; however, ML methods are capable of accounting for underlying uncertainty in the data. As ML is still an emerging technology, major advancements have been made in recent years. The applications of ML span various fields including medicine (Rajkomar, 2019), law (Surden, 2014), engineering (Reich and Barai, 1999), business (Bose, 2001), and physical and environmental sciences (Carleo et al., 2019; Schmoldt, 2001; Olden et al., 2008). More specifically, Schmoldt (2001) discusses the motivation for using AI for ecosystem disturbances research such as wildfire, disease, and insects. Furthermore, various studies review the use of ML in environmental sciences such as forest ecology (Crisci et al., 2012; Liu et al., 2018), weather prediction (Krasnopolsky and Fox-Rabinovitz, 2006; McGovern et al., 2019), flood forecasting (Mosavi et al., 2018), remote sensing (Maxwell et al., 2018), geology (Rodriguez-Galiano et al., 2015), and geophysics (Jia and Ma, 2017). Although ML has been used extensively in various environmental fields, including wildfire research and management, many gaps remain (Jain et al., 2020). This presents a new opportunity to extend the typical forecasting period of fire weather indices.

ML involves developing algorithms that learn automatically from data, which eliminates some of the need for expert rules and human supervision. This enables the model to perform on larger unstructured datasets as ML algorithms create their own set of rules for determining data distributions and patterns. ML involves three different types of learning: supervised learning, unsupervised learning, and agent based learning. Supervised ML uses labeled datasets to train algorithms to predict outcomes. ML algorithms cross-validate and adjust weights until the model has been optimized. Several popular regression methods including linear and logistic regression are supervised ML algorithms. Whereas, unsupervised ML exposes patterns and clusters in data. For example, clustering is a common unsupervised learning technique that locates the natural groupings in data based on similarities or dissimilarities of features. Lastly, Agent Based ML can learn by interacting with the environment to extract information from incomplete or unknown datasets. Currently in wildfire science, weather prediction systems may result in reduced accuracy as they require user defined inputs. Therefore, these models, may be biased towards areas of interest, and require complex data formats (Jain et al., 2020). Moreover, the use of ML and data-centric models may help to improve the precision of current fire weather prediction systems as they reduce steps with human intervention through self-learning.

As well, Jain et al. (2020) suggest that ML has been under-utilized in fire management with respect to predictive analytics. Few studies have employed ML in fire weather predictions for various regions globally (Van Wagner, 1987; San-Miguel-Ayanz et al., 2012; Sanabria et al., 2013), yet it has been largely unexplored as a tool in Canadian fire regimes. By addressing this research gap, fire weather lead times may potentially be extended beyond the 1-14 day forecast offered by traditional numerical weather prediction systems like GEM and NAEFS.

## 1.5 Research Objectives

This thesis explores the use of ML to forecast BUI at the sub-seasonal timescale in Canada. Several research questions are addressed, including: (1) Is ML a viable option for forecasting FWI system values, such as BUI? (2) What is the influence of teleconnections such as ENSO and AMO on ML model performance? (3) Does ML outperform climatology or persistence forecasts, and where and at what lead time does it perform better? In this thesis, Chapter Two will discuss the data sources and methods used. Chapter Three presents the results of the ML model. Chapter Four is a discussion of results, potential sources of error, and suggestions for future work. Chapter Five summarizes results and concludes this research.

# Chapter 2 Data and Methods

The purpose of this study was to use ML to extend the forecasting lead time of BUI and to assess the potential of large scale teleconnections as covariates in model training. This chapter introduces the data and methods used in this thesis in the order of: study area, data and model covariates, Long Short-Term Memory (LSTM) networks, model development and training, and model performance and evaluation.

## 2.1 Study Area

This study was focused on forecasting fire weather indices for areas of Canada impacted by wildland fires. Wildland fire is prevalent in three of Canada's major biomes: the boreal forests, the temperate coniferous forests (west coast), and the temperate broadleaf and mixed forests (around the Great Lakes and east coast; Stocks et al., 2002 Hanes et al., 2019). These biomes are further divided into the ecozones as shown in Figure 2.1. Ecozones are large ecological units representing areas of similar climate, topography, and vegetation (Ecological Stratification Working Group, 1995). However, some areas of historically low fire activity and areas lacking robust data were excluded. The areas that were excluded from this study include portions of the ecozones: Arctic Cordillera, High Arctic, Low Arctic, Mixedwood Plains, Prairies, and the northern extents of the Hudson Plains, Taiga Cordillera, and Taiga Plains.

Although ecozones are typically representative of various forested regions in Canada, the study area was further aggregated into smaller regions consisting of tiling 17 hexagons, with each hexel

spanning an area of $4.87 \times 10^{11}\ m^2$ or $4.87 \times 10^{5}\ km^2$ (Figure 2.2). A hexagonal grid captures finer variability in fire weather data as opposed to the larger ecozone units. In addition to this, Birch et al. (2007) notes many reasons for choosing hexagonal grids over square grids in ecological studies. Of the various shapes that can be tiled together across the landscape, hexagons are ideal because they have a lower perimeter-to-area ratio, which lessens the sampling bias from edge effects. As well, points near the borders of hexagons are closer to the centroid than grids. The size of the hexels was chosen as a compromise between two important considerations: the scale of fire weather and number of individual models required. This means that the hexel size must capture the variations of fire weather at a scale that is most useful for fire management while keeping the number of models and model runs low to limit computation time. Finally, hexels one and fifteen were removed from the study due to the lack of fire activity within these regions, leaving a total of 15 hexels which were modeled individually.


Figure 2.1 Modified Ecozones of Canada as outlined by Ecological Stratification Working Group (1995). The Boreal Shield and Taiga Shield are split into East and West.

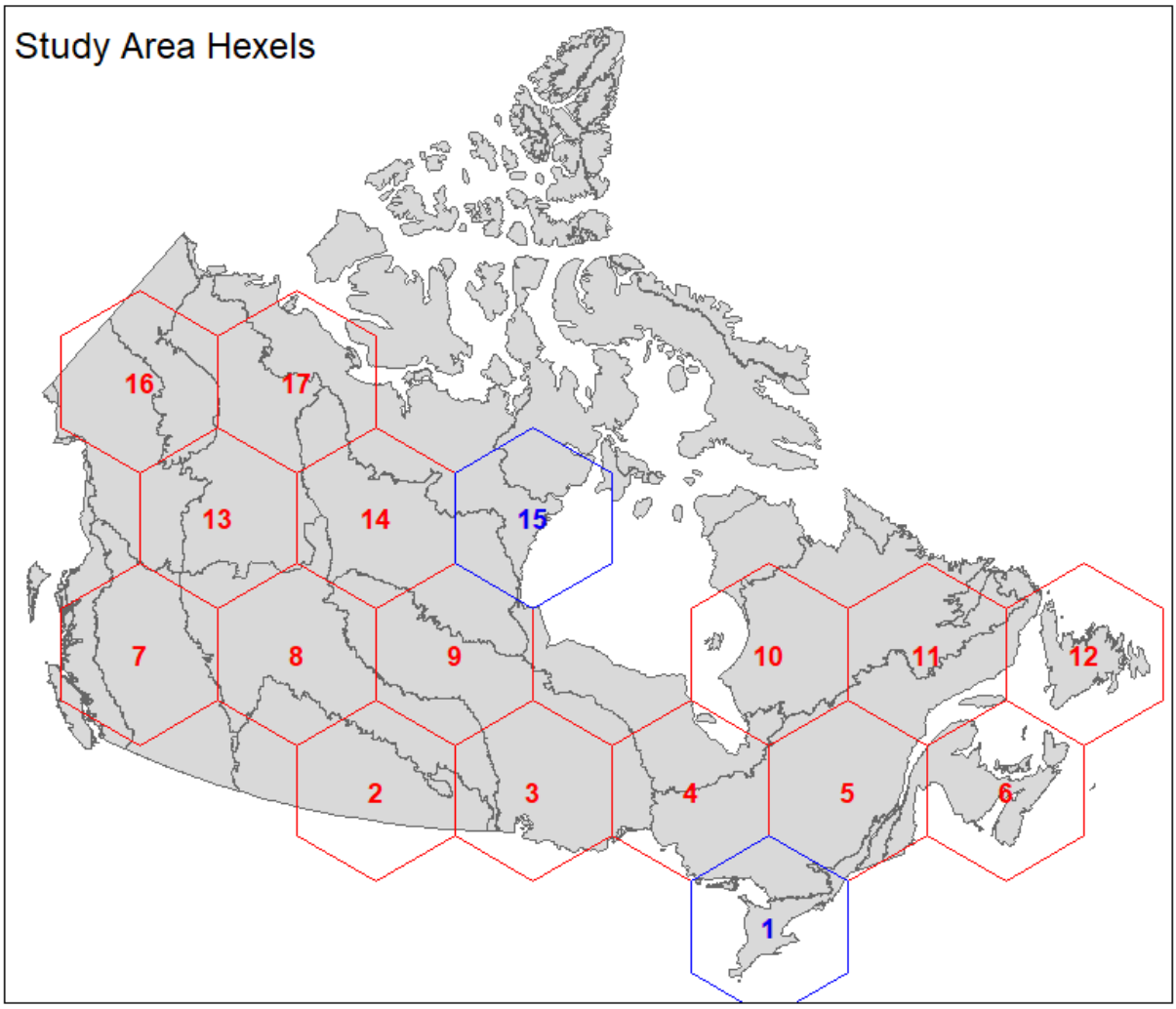


Figure 2.2 The study area of interest was divided into $4.87 \times 10^{11}\ m^2$ or $4.87 \times 10^{5}\ km^2$ hexels across Canada. Hexels one and fifteen are outlined in blue and were removed from the study due to the lack of fire activity within these regions.

## 2.2 Fire Weather Data and Covariates

*Reanalysis Data*

The European Centre for Medium-Range Weather Forecasts (ECMWF) produces ERA5-Land data which is the fifth generation product of an atmospheric reanalysis of the global climate from 1981 to present (Copernicus Climate Change Service (C3S), 2017). Various weather observations from World Meteorological Organization (WMO) satellites and stations are integrated into the global ensemble (Hennerman and Berrisford, 2021). The data is generated at a 0.1 degree resolution which covers the Earth on an approximately 9 km grid and resolves the atmosphere surface level variables. ERA5-Land is dynamically downscaled from the ERA5 reanalysis which is generated at 0.25 degrees resolution. ERA5 produces hourly estimates of various atmospheric climate variables including noon local standard time temperature, 24-hour precipitation, relative humidity, and 10 m wind speeds. Compared to ERA5-interim and other global reanalysis products, ERA5 has shown great improvement to weather observations (Hennerman and Guillory, 2021). The research suggests that advancements in data quality, tropospheric representation, soil moisture accuracy, sea surface temperatures, sea ice detection, and precipitation have led to impressive correlations with observed data. Beck et al. (2019) found that ERA5 performed best when compared with 15 other (non-gauge corrected) precipitation datasets over the contiguous United States. As well, Tarek et al. (2020) found that ERA5 produced significantly lower precipitation and temperature biases in North America than its predecessor. McElhinny et al. (2020) used the available data to calculate FWI System indices from 1979 to 2018 for Canada and validated the results against historical calculations from

Canadian weather stations as provided by Environment and Climate Change Canada (ECCC). Results from the study showed strong agreement with Canadian weather station data (McElhinny et al., 2020). With the advancements made by the ERA5 and ERA5-Land reanalysis models, ERA5-Land was selected as a viable data source for producing Canadian fire weather indices including BUI.

*Build-Up Index*

As mentioned earlier, FWI indices provide information on fuel moisture and expected fire behavior if an ignition occurs. This study uses ERA5-land data from 1981 to 2020 on a 0.1° × 0.1° grid to calculate BUI values according to the same procedure outlined by McElhinny et al. (2020). Weekly BUI values were averaged from the available daily BUI data and aggregated to each hexel by area weighting. Each year is assumed to be 364 days by removing February 29$^{th}$ from leap years and December 31$^{st}$ from remaining years to produce 52 weeks of averaged BUI data. In other words, each year was aggregated into an integer number of weeks for model input. The days that are removed lie outside of the typical fire season and have no impact on forecast results. However, overwintered DC impacts the availability of BUI throughout the year, as DC is used to calculate BUI. Overwintering means that DC calculations begin when the fire season is considered to be active, which is on the third day after the snow has disappeared, and concluded when the fire season is considered to be over, which is when snow covers the ground (Wotton and Flannigan, 1993; Lawson and Armitage, 2008). Consequently, the period for which BUI is calculated at a given location varies each year for regions with winter snow cover. At the beginning of each season, DC is adjusted at startup according to overwinter precipitation values.

Finally, when there is no available data in the winter months, the value is set to zero as the ML algorithm requires the previous 12 weeks of values which are numerical values.

*Teleconnections*

Large scale patterns of ocean-atmosphere pressure and circulation anomalies are called teleconnections. As studied by Byrne and O'Gorman (2018), there is remarkable correlation between ocean and land variables as there is strong evidence that trends in continental temperature and humidity are associated with neighboring ocean regions. Five major teleconnections are known to impact weather patterns in Canada, including El Niño Southern Oscillation (ENSO), Atlantic Multidecadal Oscillation (AMO), Pacific Decadal Oscillation (PDO), Pacific-North American Pattern (PNA), and Arctic Oscillation (AO; Bonsal and Shabbar, 2011). However, it has been suggested that two teleconnections, ENSO and AMO, have a greater impact on Canadian fire weather (Shabbar and Skinner, 2004). Therefore, this study will focus on the influence of these particular teleconnections. ENSO is characterized by two prominent phases: warm El Niño events and cool La Niña events. The phases oscillate every two to seven years and are measured by differences in SSTs and pressure in the equatorial Pacific (McPhaden et al., 2006). Bonsal and Lawford (1999) found El Niño events tend to extend summer drought conditions in the Prairies. As well, Shabbar and Skinner (2004) found that warm El Niño events create a summer moisture deficit in western Canada. Not only did they suggest dry conditions from ENSO, they also determined that the positive phase of AMO is associated with summer dry-spells in the Prairies, lower Great Lakes, and the west coast of Canada. The phases of AMO

modulate over periods of 20-40 years and are characterized by cooling and warming North Atlantic SSTs (Knight et al., 2006).

ENSO is realized by indices that combine oceanic and atmospheric variables from each oscillation. The MEI.v2 index is used to measure ENSO and is calculated for overlapping bi-monthly seasons from 1979 to present, which is useful for understanding intraseasonal variability (Wolter and Timlin, 1993). Monthly ENSO indices are available as tabular datasets through the National Oceanic and Atmospheric Administration ($NOAA_2$, 2022). Moreover, AMO is produced from oceanic SSTs. Similar to ENSO, AMO is described by a single index which is estimated from North Atlantic SSTs and is available through NOAA from 1856 to present. AMO indices are available as raw or detrended datasets through $NOAA_1$ (2022). For this study, raw monthly data was selected for each teleconnection. As weekly averaged forecasts of BUI are the main objective, ENSO and AMO indices were decomposed to the frequency domain using the Fast Fourier Transform (FFT) analysis (Nussbaumer, 1981). In doing this, we are able to interpolate monthly values to 52 weekly values by padding the spectrum in the frequency domain and transforming back to the temporal domain. This serves as a method for resampling data at smaller timesteps, namely weekly values, and to act as a low-pass filter for denoising. While we assume that each year is composed of 52 weeks, data leakage remains minimal because the original data uses a monthly timescale. Often used in geophysical studies as a tool for spectral analysis (Schwarz and Sideris, 1990), the FFT is abundant in various climate- related studies including teleconnections, drought variability, and vegetation and soil (Torrence and Webster, 1999; Dabanl et al., 2017; Azzali and Menenti, 2000).

## 2.3 Long Short-Term Memory Networks

A commonly used method of ML are Artificial Neural Networks (ANN), which are inspired by the human brain and the biological signals that are passed between one neuron to another (McCulloch and Pitts, 1943). ANNs are comprised of node layers including an input layer, one or more hidden layers, and an output layer. Each neuron computes a linear weighted sum of the inputs and applies an activation function to produce an output. As information flows through the network, each node must reach a certain weighted sum threshold for that node to activate and pass information on to the next node. This functions as a cutoff to signals below the threshold and allows for signals above the threshold to pass through. The weights on the connections represent the function parameters, which are fit by optimizing the threshold value. In general, non-linear activation functions such as sigmoid, tanh, and Rectified Linear Unit (ReLU) are used. Two important variants of ANNs are Recurrent Neural Networks (RNNs) and Convolution Neural Networks (CNNs). RNNs are specifically used in solving complex problems involving sequential data or time series data, while CNNs are feedforward networks that do not form a cycle or loop. In CNNs, adjacent nodes convolve to extract spatial information from data. Both networks use training data to learn patterns, but RNNs are suited to temporal problems as they take information from past inputs to influence outputs. In addition, ANNs are an example of a universal function approximator (Hornik et al., 1989) and can be configured to fit the task at hand through adjustments in number of hidden layers, choice of activation function, number of epochs, learning rate, and various other hyperparameters.

Traditional RNNs are well suited to studies involving temporal data as they use back-propagation through time (BPTT; Williams and Zipser, 1995) or real-time recurrent learning (RTRL; Robinson and Fallside, 1987) to store and learn patterns from past inputs. However, these methods have extreme limitations as errors can propagate and grow exponentially. To address this issue, Hochreiter and Schmidhuber (1997) developed the Long Short-Term Memory (LSTM) network, which has become the most common variant of RNNs. LSTMs are designed to drop signals that are not useful and only retain important information. Although, LSTMs are not used extensively in wildland fire research, some advances have been made using LSTMs in combination with CNNs for smoke detection (Cao et al., 2019) and LSTMs in area burned predictions (Liang et al., 2019).

As mentioned earlier, feedforward neural networks and RNNs are variants of DNNs which contain an input layer, hidden layers, and an output layer. In a feedforward neural network, information moves in one direction – from the input layer, through the hidden layers, and to the output layer (Figure 2.3). These networks only consider the immediate and current inputs and cannot remember what was done in past iterations. In an RNN, the information cycles through a loop allowing the network to recall past and present inputs (Figure 2.4). The architecture of LSTMs are similar to RNNs, but contain additional neural network layers to limit error propagation. LSTMs contain three gates that optionally allow information through and are composed of a pointwise multiplication operation and a sigmoid activation function which is shown as:

$$S(x) = \frac{1}{1 - e^{x}}, \quad [Eq. 1]$$

where $e$ is Euler's constant and $x$ is the threshold value. The sigmoid layer outputs a value between zero and one which describes the level to which each new input should influence the cell state. The LSTM forget gate offers protection to the cell state while allowing useful signals through and forgetting signals that do not meet the minimum threshold value (Figure 2.5).

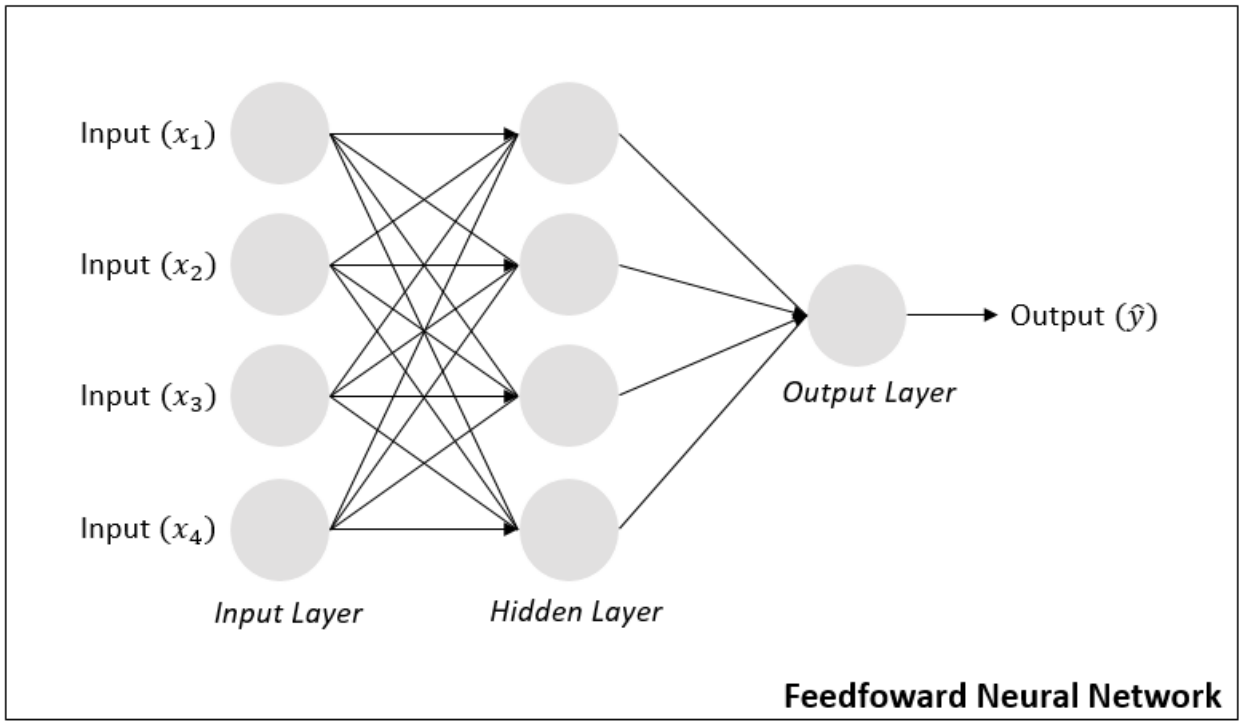


Figure 2.3 Feedforward neural network with an input layer ($x_n$), hidden layer, and output layer ($\hat{y}$). The arrows show connections between nodes in each of the layers. A simple or shallow neural network contains one hidden layer, while DNNs typically contain more than one hidden layer.

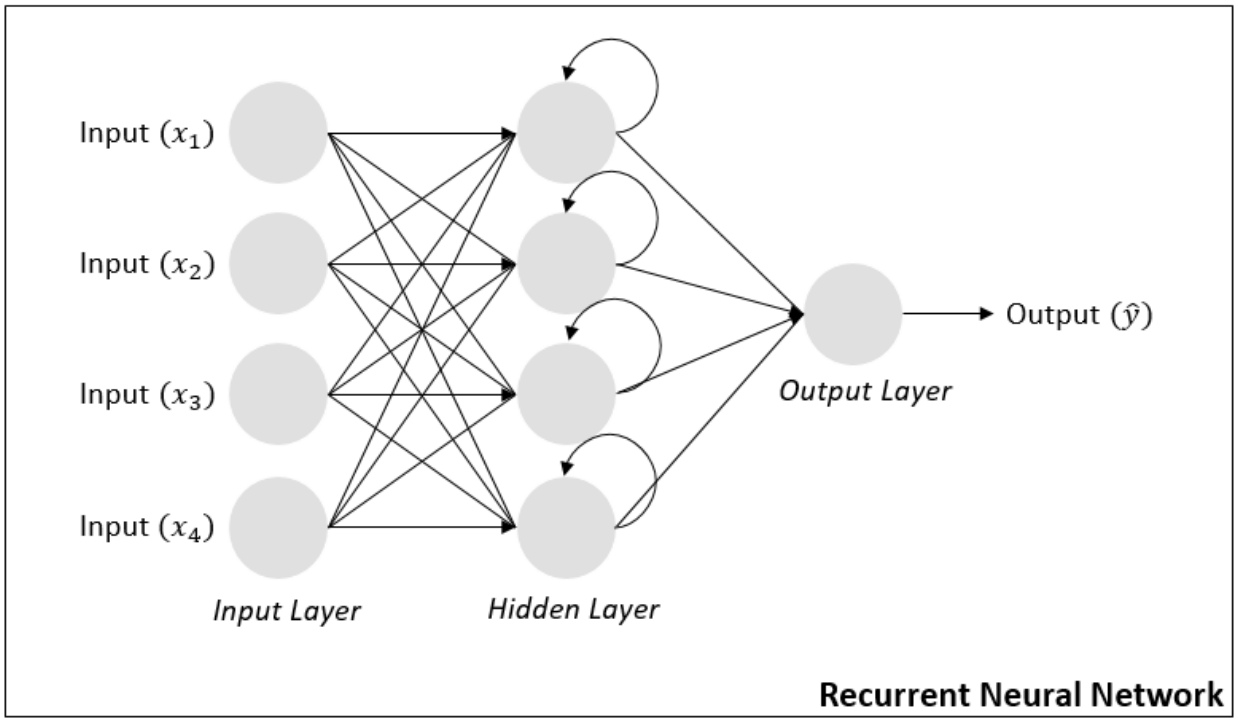


Figure 2.4 RNN architecture with an input layer ($x_n$), hidden layers, and an output layer ($\hat{y}$). The arrows show connections between nodes in each of the layers and between cycles within the hidden layers. The information travels through a loop allowing the network to recall past and present inputs.

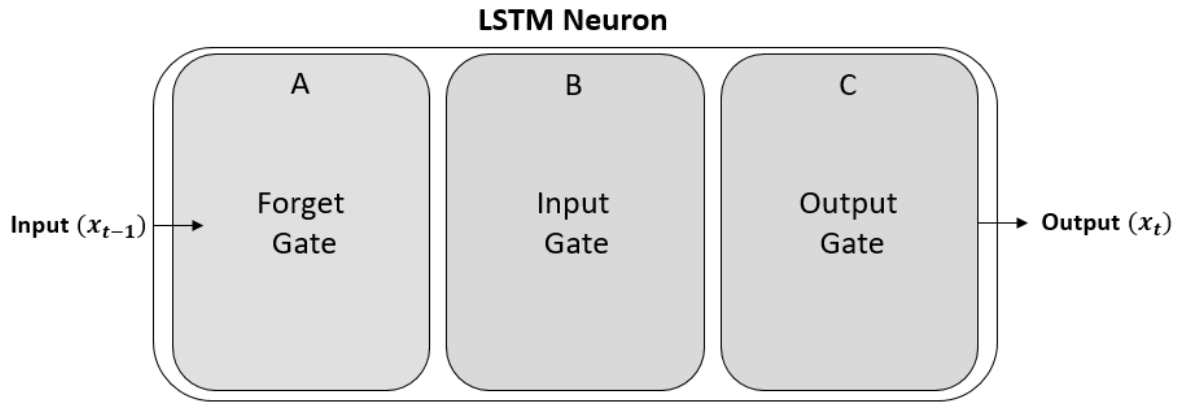


Figure 2.5 Architecture of a simplified LSTM neuron from the hidden layer showing three gates: forget gate, input gate, and output gate. The forget gate forgets irrelevant information, the input gate adds and updates new information, and the output gate passes updated information to the next neuron in the network.

## 2.4 Model Development

Statistical models, including ML models, are designed to relate outcome variables with several independent or dependent variables and define the strength of association (Heinze et al., 2018). ML models may provide insight to relationships between variables and help to gain greater understanding of environmental mechanisms. ML is advantageous since it is able to represent nonlinear relationships and can extract temporal patterns from data. In keeping with these realizations, this study utilizes ML to create weekly BUI forecasts using several covariates including: 12 weeks of past BUI inputs, climatological BUI, and teleconnections.

*Data Preparation and Model Architecture*

This study utilized Keras (Chollet et al., 2015), a deep learning application programming interface (API) that integrates with TensorFlow, which is an infrastructure layer for differentiable programming (Ketkar, 2017). A multivariate, multi-step LSTM model was created using the Python programming language. Four models were created, each followed the same architecture but with differing covariates (see Table 2.1). First, data was separated into training and testing datasets using the "80/20 rule", respectively. Data from 1981 to 2012 was used for training and data from 2013 to 2020 was used for testing. Weekly averaged data from each hexel was compiled into training and testing data frames then normalized by scaling the data to lie between the range of zero to one using Scikit-Learn's preprocessing package (Pedregosa et al., 2011). The first model used the variables: week of the year, previous 12 months of BUI values and BUI climatology. The second model used the variables: week of the year, historical BUI, BUI climatology, and ENSO MEIv2 index. The third model used the variables: week of the year, historical BUI, BUI climatology, and AMO index. Finally, the fourth model used the variables: week of the year, historical BUI, BUI climatology, ENSO MEIv2 index, and AMO index. As the LSTM model learns from past and current inputs to forecast the next values, data must be fed into the model through a moving-window approach. An additional function is created to split the training data into two sequences: model input and expected next values. This function iterates through the training data and uses 12 weeks of inputs to determine the output at a single week. The same moving-window split is applied to the testing data.

*Hyperparameters*

Model optimization and hyperparameter tuning can use one of four basic methodologies: manual tuning, gridded search, randomized search (Bergstra and Bengio, 2012), and Bayesian optimization (Snoek and Larochelle, 2012; Shahriari et al., 2015). Bergstra and Bengio (2012) noted that manual and gridded searches are the most commonly used strategies for hyper-parameter optimization. While random and Bayesian optimization techniques are becoming increasingly popular, this study uses a combination of heuristic and exhaustive manual tuning to minimize training and validation loss curves. Multiple trials of various model hyper-parameter combinations were tested to evaluate and enhance performance for each hexel. Each of the four models used the same final hyper-parameters and general model architecture (Table 2.1).

Model assembly can be very efficient as the Keras library allows for flexible parameter tuning and layer addition. After evaluation of various model architectures, a sequential model with an LSTM layer, dropout layer, and dense layer was selected for this study as it produced the best outcomes in early testing. Each layer is carefully tuned to optimize model results, with a dropout rate of 0.20 which was selected as it prevented overfitting. A dropout rate prevents an RNN from overfitting by randomly dropping out units during training. The LSTM layer has several parameters including 150 LSTM units or LSTM neurons, Rectified Linear Units (ReLU) function activation, and the input shape. The input shape is determined by the number of weeks used for inputs (12 weeks) and number of covariates in the model. ReLU and its derivative are both monotonic (Nair and Hinton, 2010), meaning the function has an output range of zero to infinity and trains much faster than alternative activation functions. This is due to the fact that

the ReLU function is non-saturating as it prunes the negative portion of the function to zero and keeps the positive portion (Jiang et al., 2018). Following the LSTM layer, two dense layers are used to adjust dimensionality of the output to the desired target. Additionally, the model is compiled by defining the loss function using the Root Mean Square Error (RMSE) and the Adam optimizer. Adam optimization is a variant of stochastic gradient descent adapted for ML (Kingma and Ba, 2014). Next, the model is fit to the training data and validated against the testing data with 25 epochs to minimize the training and validation loss. More specifically, the LSTM will use the training data for 25 cycles. Finally, the model is used to predict the next values in the sequence using the testing data set as inputs.

Table 2.1 Hyper-parameter combinations used in the development of four different LSTM models with Keras API.

| | **Model 1** | **Model 2** | **Model 3** | **Model 4** |
|---|---|---|---|---|
| Covariates | Week of year, Historical BUI, BUI Climato-logy | Week of Year, Historical BUI, BUI Climato-logy, ENSO MEIv2 Index | Week of Year, Historical BUI, BUI Climato-logy, AMO Index | Week of Year, Historical BUI, BUI Climato-logy, ENSO MEIv2 Index, AMO Index |
| Model Layers | Dropout (rate = 0.20), LSTM (nodes = 150), Dense (nodes = 5), Dense (nodes = 5) | Dropout (rate = 0.20), LSTM (nodes = 150), Dense (nodes = 5), Dense (nodes = 5) | Dropout (rate = 0.20), LSTM (nodes = 150), Dense (nodes = 5), Dense (nodes = 5) | Dropout (rate = 0.20), LSTM (nodes = 150), Dense (nodes = 5), Dense (nodes = 5) |
| Dropout Rate | 0.20 | 0.20 | 0.20 | 0.20 |
| LSTM Hidden Layer Neurons | 150 | 150 | 150 | 150 |
| Activation Function | ReLU | ReLU | ReLU | ReLU |
| Optimizer | Adam | Adam | Adam | Adam |
| Loss Function | MSE | MSE | MSE | MSE |

| | | | | |
|---|---|---|---|---|
| Epochs | 25 | 25 | 25 | 25 |
| Learning Rate | 0.00005 | 0.00005 | 0.00005 | 0.00005 |

### 2.5 Model Performance and Evaluation

The performance of each model was evaluated with mean absolute error (MAE) and F1-scores compared to climatology and persistence forecasts for each hexel. MAE is used as a metric to evaluate continuous data, whereas F1-scores are used to evaluate categorical data. Climatology and persistence provide baseline forecasts for which to compare our ML model against. A climatology forecast is defined by using the mean seasonal values for each week of the year from 1981 to 2020 to forecast future values. A persistence forecast assumes the forecast value of the current week is the same as the previous weekly observed value. The MAE is the magnitude of error, which takes the absolute value of the difference between the measured value and the observed value and is calculated as:

$$MAE = \frac{1}{n}\sum_{i=1}^{n}|x_i - x| \ , \quad [Eq.2]$$

where $n$ is the number of evaluation data points, $x_i$ is the observed value, $x$ is the measured value, and $|x_i - x|$ is the absolute error. A confusion matrix was used to calculate the F1-score for each hexel and model by assigning BUI values above the 90$^{th}$ percentile to a value of one and BUI values below the 90$^{th}$ percentile to zero. The 90$^{th}$ percentile was chosen to differentiate between BUI values well above the average values. As well, it is used to evaluate the forecast results of extreme BUI values. More generally, the F1-score is used as a measure of model accuracy by taking the harmonic mean of model precision and recall. Precision is the fraction of true positive values that the model classified as positive values and is calculated as:

$$Precision = \frac{\#\ of\ True\ Positives}{\#\ of\ True\ Positives + \#\ of\ False\ Positives}, \quad [Eq. 3]$$

where true positive is defined as correct model prediction of the value, true negative is correct model prediction of the value, false positive is incorrect model prediction of the value, and false negative is the incorrect model prediction of the value. Recall is the fraction of values classified as positive among the total number of positive values and is calculated as:

$$Recall = \frac{\#\ of\ True\ Positives}{\#\ of\ True\ Positives + \#\ of\ False\ Negatives}, \quad [Eq. 4]$$

and, in other words, states the percentage of total relevant results correctly classified by the model forecast. Therefore, the F1-score is given by

$$F_1 = 2 \times \frac{Precision \times Recall}{Precision + Recall}, \quad [Eq. 5]$$

where a perfect model has an F1-score of one and a model with no skill has an F1-score of zero.

As previously mentioned, one of the most commonly used metrics for evaluating model fit is the consideration of training and validation loss over time. The training loss indicates how well the model fits the training data, while the validation loss indicates how well the model fits testing data. Underfitting is characterized by divergence of both curves in time, overfitting is characterized by coinciding curves to a point then diverging curves following that point, and a good fit is characterized by two decreasing curves that coincide and stabilize over time. As well,

when the training data error loss values are much smaller than the test data error loss, it may be under fitting. In this study, the training and testing curves of each of the LSTM models were evaluated for acceptable fit. Training and testing curves were assessed to minimize instances of overfitting and overtraining.

# Chapter 3 Results

This chapter presents one to five week forecasts of BUI produced by the four LSTM models and for the 15 selected hexels as outlined in the previous chapter. However, to avoid repetition, we initially focus on the results from hexel 8 in great detail. These results are presented in sections 3.1 and 3.2. Hexel 8 is selected as the initial area of focus as it is covers a large portion of the Boreal Plains in Alberta. Following this, the remaining results for all hexels are summarized in section 3.3. All results are compared with climatology and persistence forecasts. The models were produced using four combinations of week of year, historical BUI, BUI climatology, ENSO MEI.v2 index, and AMO index (see Table 2.1). The forecast results are displayed by weeks of the year of BUI, MAE, and F1-score comparisons.

## 3.1 Training and Validation Loss Curves

Training and validation loss curves are used to evaluate model fit to training data. Figure 3.1 presents model training and validation loss curves for hexel 8 as MSE loss versus model training epochs. Four sub-figures are produced to show typical training and validation loss curves for 25 epochs for each model which are calculated from training data (31 years, from 1981 to 2012). Both curves show a decreasing MSE loss that begin to coincide and stabilize at approximately 15 epochs with a learning rate of 0.00005 for all models, which suggests good model fit to training data.

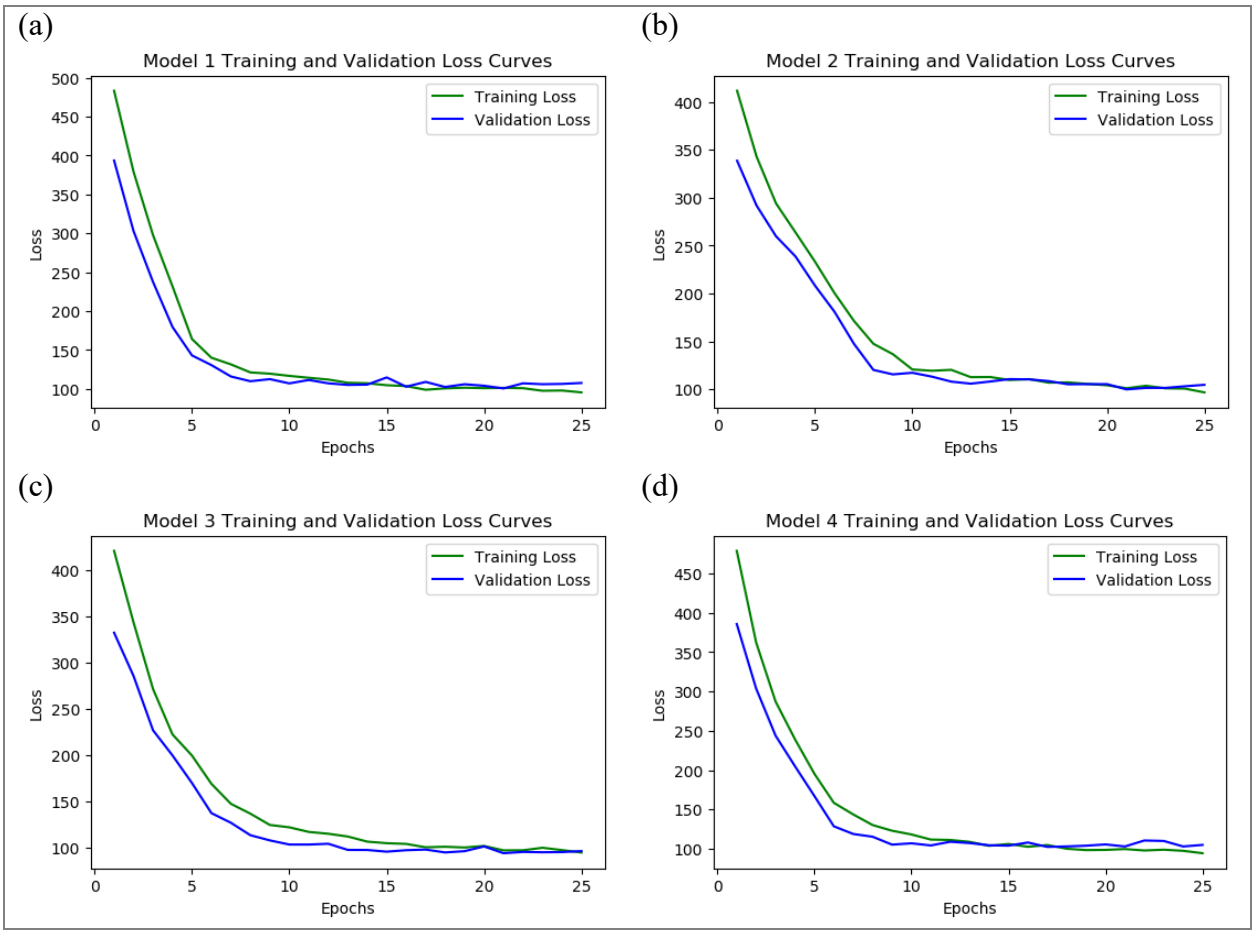


Figure 3.1 Hexel 8 training and validation loss curves shown for each of the four models. Each sub-figure shows MSE loss versus 25 epochs. Green indicates training loss and blue indicates validation loss. Both curves are calculated from model training data from 1981-2012 (31 years).

### 3.2 Build-Up Index Forecast

The 1-5 week forecasts for each of the LSTM models are compared with the seasonal climatology and observed BUI values in Figures 3.2 (Model 1), 3.4 (Model 2), 3.6 (Model 3), and 3.8 (Model 4) for hexel 8. Each year is composed of 52 weekly averaged BUI values, therefore, the hold out data used for testing from 2013 to 2020 is composed of 416 weeks (ie. 52 times 8). Panels (a through e) show 1 to 5 week lead time forecasts of BUI for hexel 8. Due to overwintering of the drought code, specifically inter-annual variability of the spring startup values, zero values start between weeks 39 and 52 and end at the spring startup which begins between weeks 13 and 22. In other words, weekly BUI predictions span the fire season months which begins between March to May and ends between the months of September to October. Blue indicates observed BUI values, red indicates LSTM model forecast of BUI values, and green indicates climatology forecast of BUI values.

Figures 3.3, 3.5, 3.7, and 3.9 show corresponding scatter plots with forecast and observed BUI values; these plots are used as a method of visual inspection to compare differences between predictions and observations. Model BUI, climatology, and persistence forecasts of hexel 8 are compared against observed BUI values for each model. Observed BUI is plotted with the identity line shown by $y = x$. Under perfect conditions, the model forecast and climatology/persistence forecast are expected to be equal and exactly follow the 1:1 identity line. Panels a and b respectively show climatology and persistence compared to the model dataset.

***Hexel 8, Model 1: 1-5 Week Forecasts***

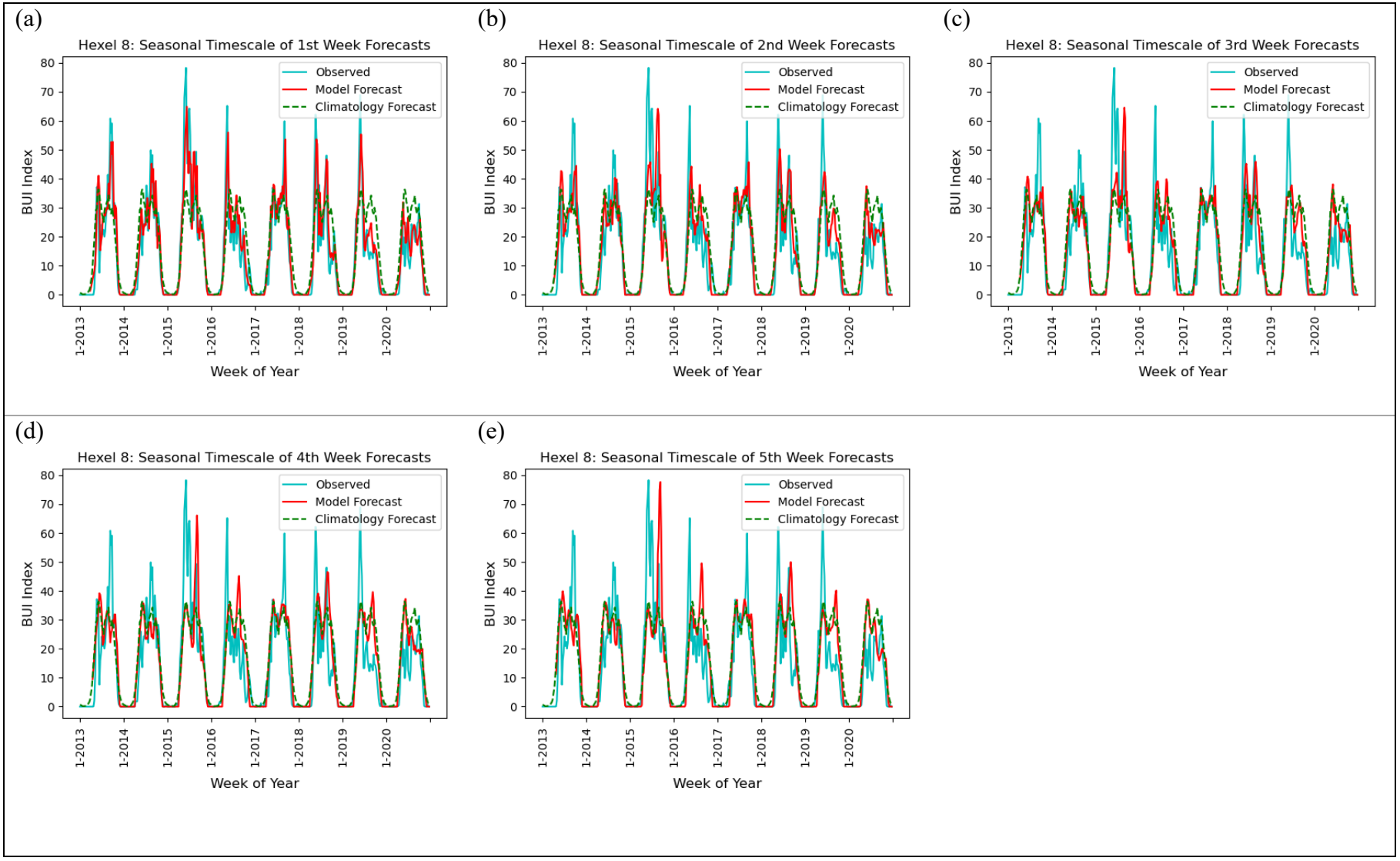


Figure 3.2 Hexel 8 Model 1 comparisons of weekly forecasts for 1 to 5 week lead times (a to e, respectively) for Model 1. Forecasts show weekly averaged BUI values from 2013 to 2020. Each year is composed of 52 weekly averaged values. Blue indicates observed BUI values, red indicates LSTM model forecast of BUI values, and green indicates climatology forecast of BUI values.

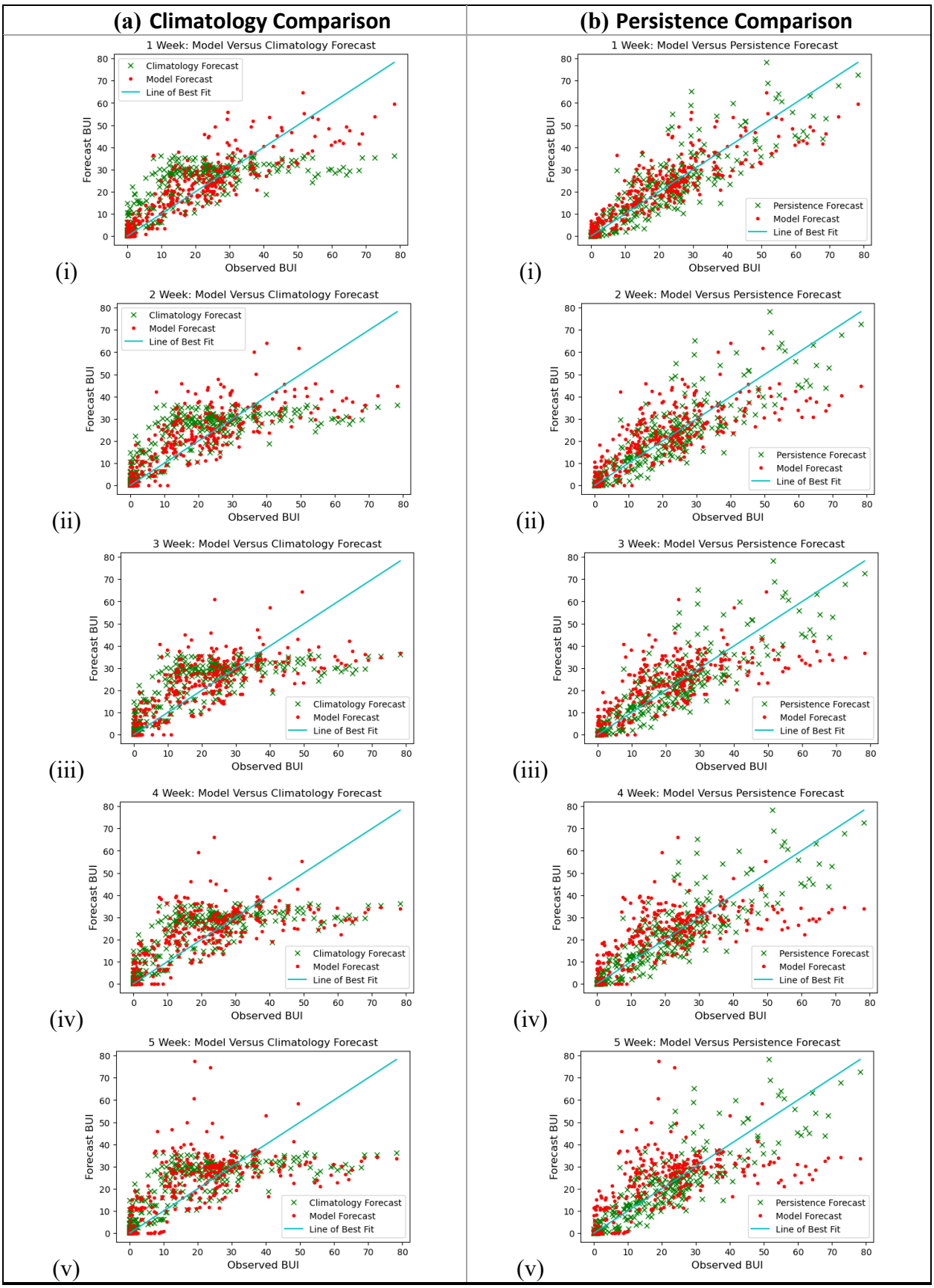


Figure 3.3 Hexel 8 results for weekly forecasts: (a) scatter plot of climatology and Model 1 forecast results, (b) scatter plot of persistence and Model 1 forecast results. Each row (i to v) shows increasing forecast lead times of 1 to 5 weeks. Solid line shows 1:1 relationship denoting perfect model fit. The model forecast is represented by red data points, climatology and persistence are shown in green.

***Hexel 8, Model 2: 1-5 Week Forecasts***

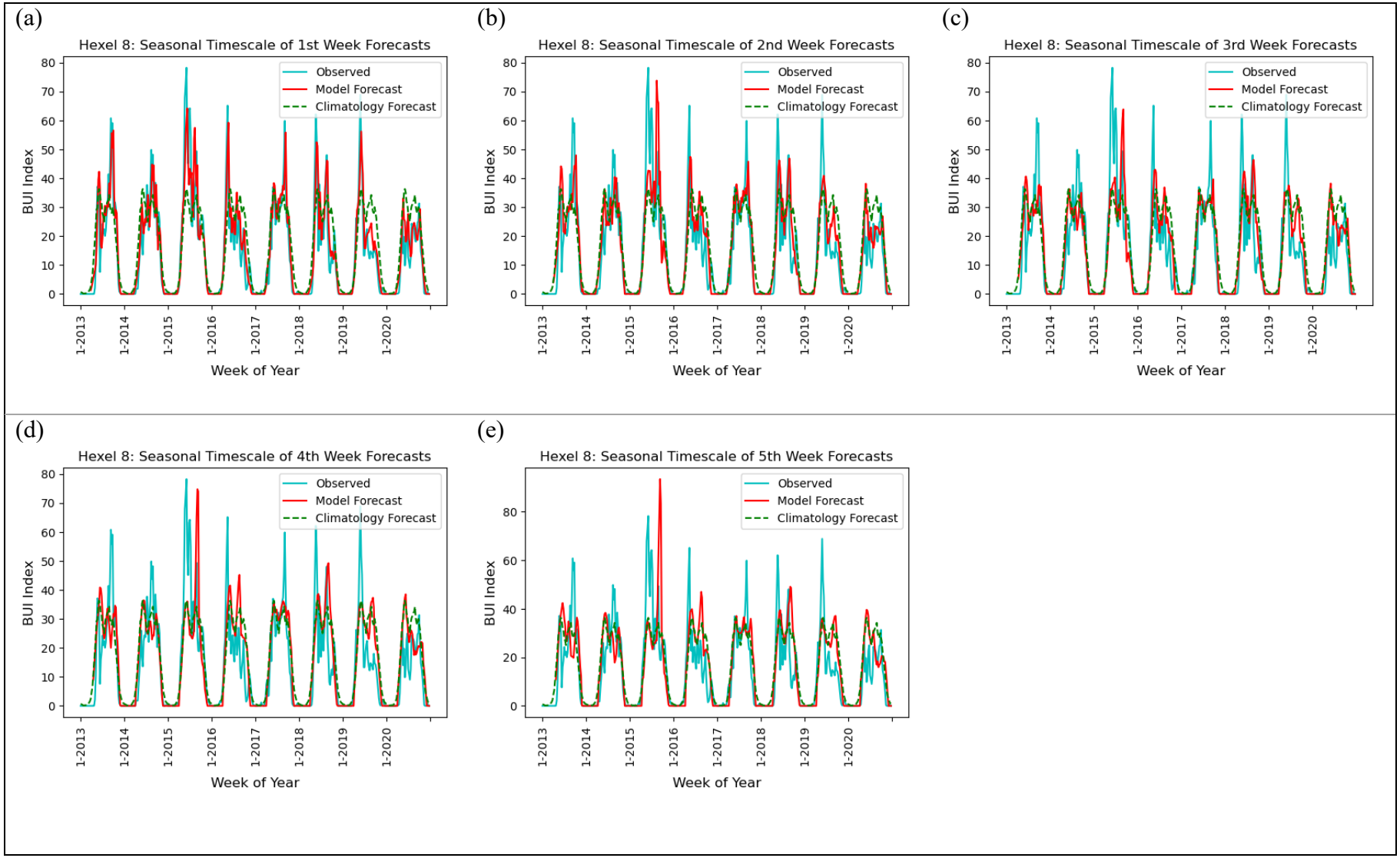


Figure 3.4 Hexel 8 Model 2 comparisons of weekly forecasts for 1 to 5 week lead times (a to e, respectively) for Model 2. Forecasts show weekly averaged BUI values from 2013 to 2020. Each year is composed of 52 weekly averaged values. Blue indicates observed BUI values, red indicates LSTM model forecast of BUI values, and green indicates climatology forecast of BUI values.

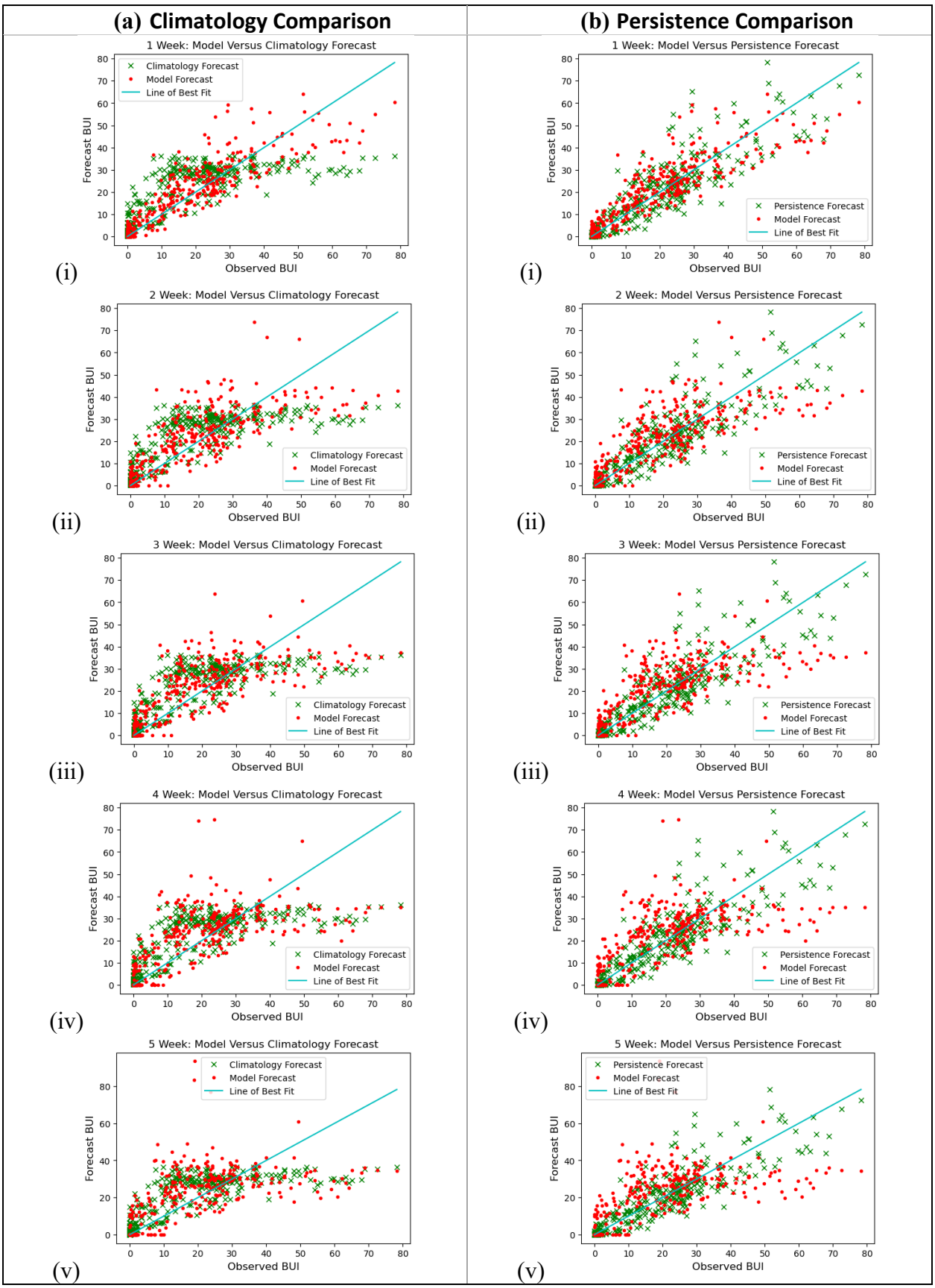


Figure 3.5 Hexel 8 results for weekly forecasts: (a) scatter plot of climatology and Model 2 forecast results, (b) scatter plot of persistence and Model 2 forecast results. Each row (i to v) shows increasing forecast lead times of 1 to 5 weeks. Solid line shows 1:1 relationship denoting perfect model fit. The model forecast is represented by red data points, climatology and persistence are shown in green.

***Hexel 8, Model 3: 1-5 Week Forecasts***

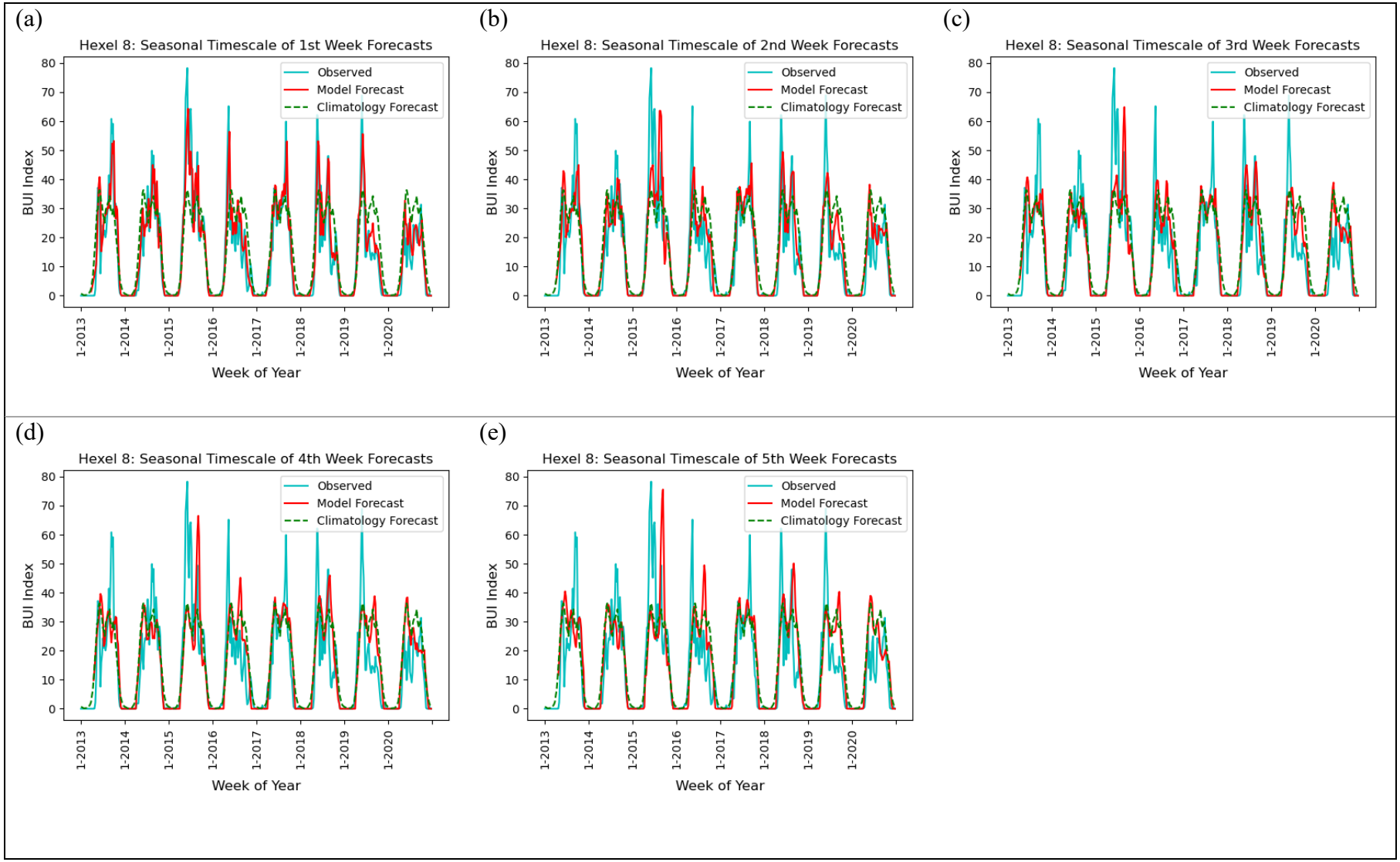


Figure 3.6 Hexel 8 Model 3 comparisons of weekly forecasts for 1 to 5 week lead times (a to e, respectively) for Model 3. Forecasts show weekly averaged BUI values from 2013 to 2020. Each year is composed of 52 weekly averaged values. Blue indicates observed BUI values, red indicates LSTM model forecast of BUI values, and green indicates climatology forecast of BUI values.

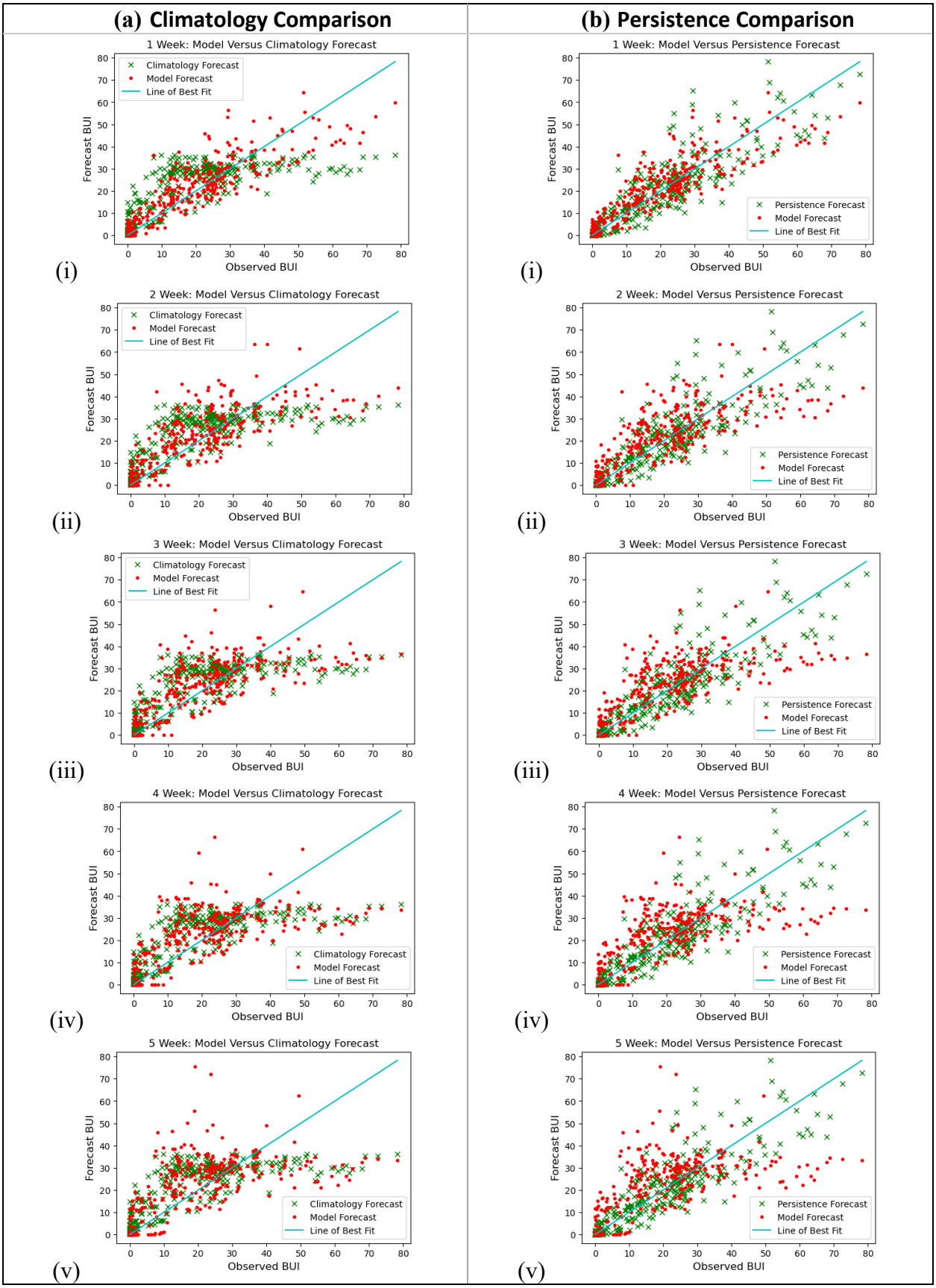


Figure 3.7 Hexel 8 results for weekly forecasts: (a) scatter plot of climatology and Model 3 forecast results, (b) scatter plot of persistence and Model 3 forecast results. Each row (i to v) shows increasing forecast lead times of 1 to 5 weeks. Solid line shows 1:1 relationship denoting perfect model fit. The model forecast is represented by red data points, climatology and persistence are shown in green.

***Hexel 8, Model 4: 1-5 Week Forecasts***

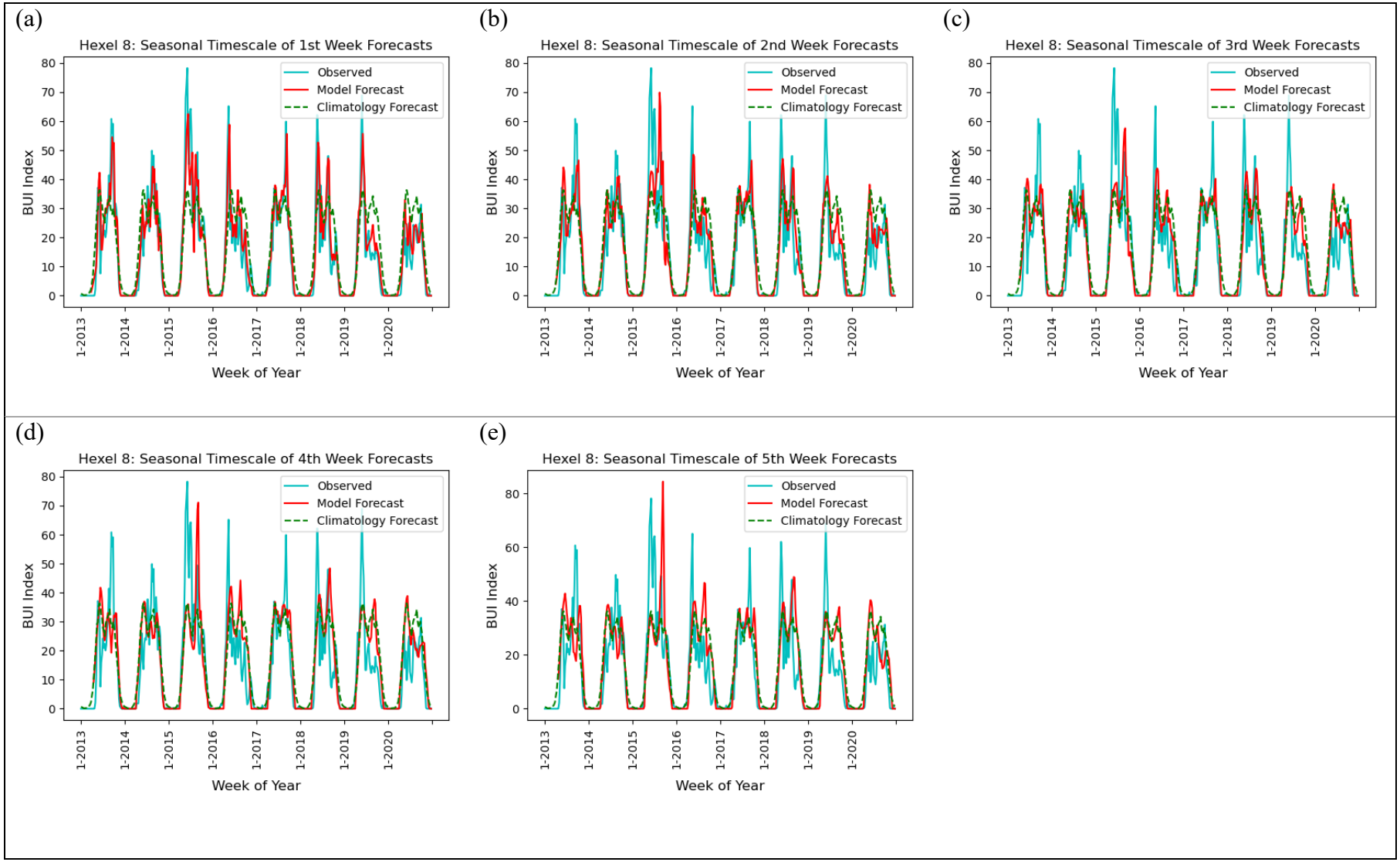


Figure 3.8 Hexel 8 Model 4 comparisons of weekly forecasts for 1 to 5 week lead times (a to e, respectively) for Model 4. Forecasts show weekly averaged BUI values from 2013 to 2020. Each year is composed of 52 weekly averaged values. Blue indicates observed BUI values, red indicates LSTM model forecast of BUI values, and green indicates climatology forecast of BUI values.

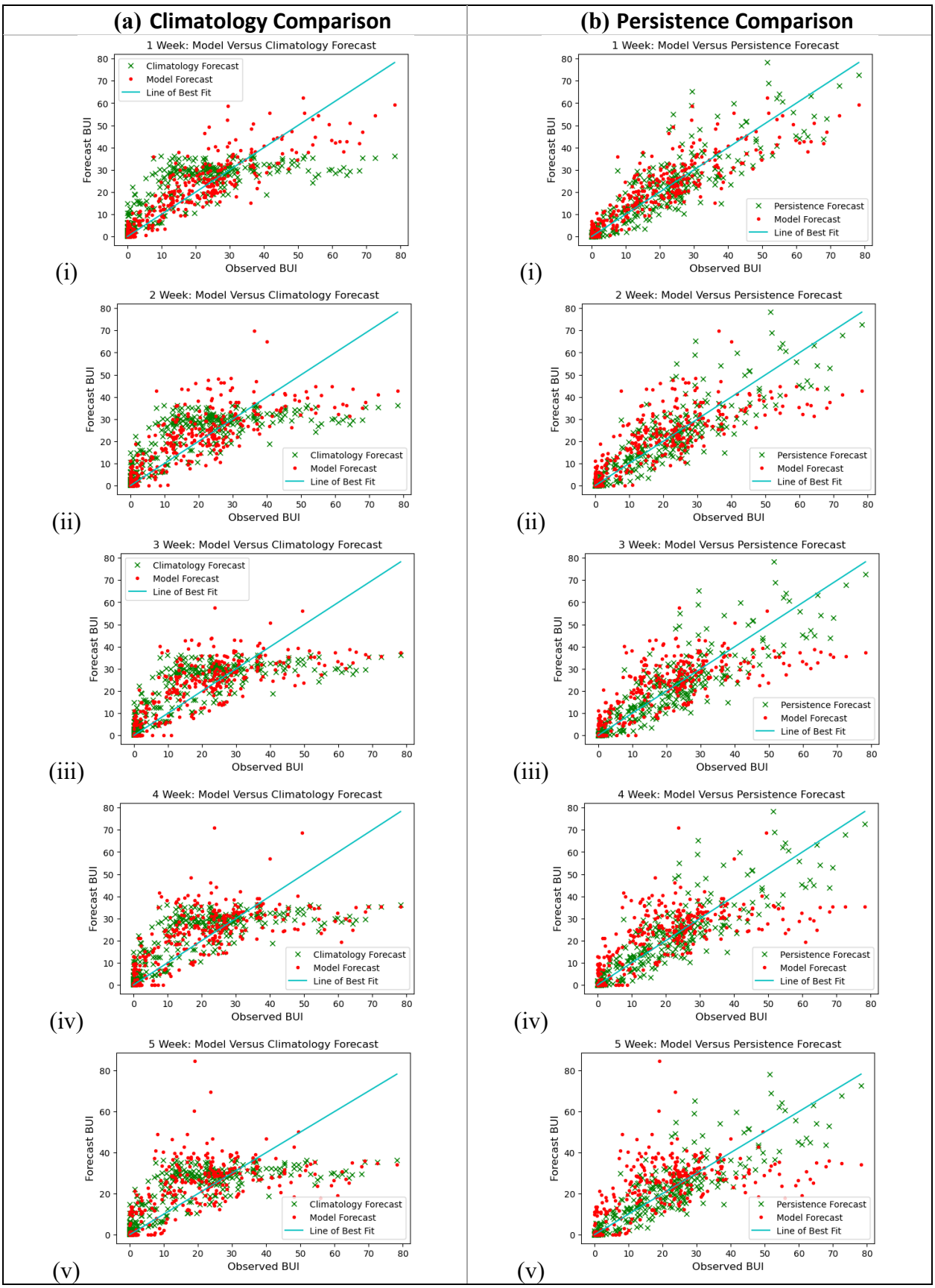


Figure 3.9 Hexel 8 results for weekly forecasts: (a) scatter plot of climatology and Model 4 forecast results, (b) scatter plot of persistence and Model 4 forecast results. Each row (i to v) shows increasing forecast lead times of 1 to 5 weeks. Solid line shows 1:1 relationship denoting perfect model fit. The model forecast is represented by red data points, climatology and persistence are shown in green.

### 3.3 Error Statistics

Hexel 8 MAE results are summarized in Table 3.1. The LSTM model, climatology, and persistence forecast MAE values are shown in columns one to three, respectively. As mentioned previously, the MAE is the absolute value of error in predicted values. Lower MAE values indicate better performing forecast results. In addition, Figure 3.10 shows MAE values for each model as a function of forecast lead time from one to five weeks. In all four instances, persistence outperforms the model and climatology forecasts at a lead time of one week. Similarly, all model forecasts outperform the climatology at a one week lead time. At lead times of two and three weeks, the model forecasts perform better than both the persistence and climatology forecasts. The fourth and fifth week lead time results show climatology performs better than all four models. Full results of MAE scores for all hexels are presented as Figures 6.1-6.15 in Appendix A.

Moreover, MAE for the LSTM model, climatology, and persistence forecasts were calculated for each hexel for one to five week forecast lead times. To summarize these results, the differences between the observed MAE and forecast MAE were plotted as hexel maps for each model (1 to 4) and each forecast lead time (1-5 weeks) as shown in Figures 3.11, 3.12, 3.13, and 3.14. Sub-figures show: ($a$) the difference between model MAE and climatology MAE ($\Delta MAE_{MC}$), ($b$) the difference between model MAE and persistence MAE ($\Delta MAE_{MP}$), and ($c$) the accuracy of model predictions using F1-score. The difference from MAE results gives an indication to which forecast performed best at each lead time for each hexel, and is defined as:

$$\Delta MAE_{MC} = MAE_{Model} - MAE_{Climatology} \qquad [Eq. 6]$$

$$\Delta MAE_{MP} = MAE_{Model} - MAE_{Persistence} \qquad [Eq. 7]$$

where a positive $\Delta MAE$ indicates that the model forecast has larger error and a negative $\Delta MAE$ indicates that the climatology or persistence forecast has larger error. In subplots *a* and *b*, a blue-red colormap is used to show whether the LSTM model forecast or the climatology/persistence forecast perform better. Blue shows a negative $\Delta MAE$, which indicates that the LSTM model forecast is better performing. Red shows a positive $\Delta MAE$, which indicates that the climatology or persistence forecast is better performing. In subplot *c*, F1-scores from the LSTM model forecast is shown across all of the hexels. A higher F1-score, as shown in darker green, indicates better model accuracy. Full results for all LSTM model F1-scores are presented in Appendix Table A1. As well, full results of the F1-scores for the persistence and climatology models are presented in Appendix Table A2 and A3, respectively.

For Models 1 (Figure 3.11a), 2 (Figure 3.12a), and 4 (Figure 3.14a) a negative $\Delta MAE_{MC}$ is shown in some hexels up to a four week lead time. For Model 3 (Figure 3.13a), a negative $\Delta MAE_{MC}$ is shown in some hexels up to a three week lead time. In other words, the model forecasts perform better than the climatology forecast up to a lead time of three or four weeks for some hexels. More specifically, the Model 1 forecast outperformed climatology in hexel 13 up to a lead time of four weeks, in hexels 2, 3, 7, and 8 up to a lead time of three weeks, and in hexels 4, 5, 9, 16, and 17 up to lead time of two weeks. The Model 2 forecast outperformed climatology in hexels 7 and 13 up to a lead time of four weeks, in hexels 2, 3, and 8 up to lead time of three weeks, and in hexels 4, 9, 16, and 17 up to lead time of two weeks. The Model 3 forecast

outperformed climatology in hexels 2, 3, 7, 8, and 13 up to lead time of three weeks and in hexels 4, 5, 9, 16, and 17 up to lead time of two weeks. Finally, the Model 4 forecast outperformed climatology in hexel 7 up to a lead time of four weeks, in hexels 2, 3, 7, 8, and 13 up to lead time of three weeks, and in hexels 4, 9, 16, and 17 up to lead time of two weeks. In general, we find that all models provide improved forecasts for hexels towards the west and west-central regions up to a lead time of three weeks. However, there is some variation in model performance beyond a three week lead time, with Models 1, 2, and 4 showing skill up to four weeks of lead time in few hexels.

The $\Delta MAE_{MC}$ results can be compared to the $\Delta MAE_{MP}$ counterpart. For Models 2 (Figure 3.12b) and 4 (Figure 3.14b), a positive $\Delta MAE_{MP}$ is produced in some hexels up to a lead time of two weeks. In other words, the persistence forecast performs better than the model forecasts up to a lead time of two weeks for some hexels. Beyond a two week lead time, the model forecasts perform better than the persistence forecast in all hexels. For Models 1 (Figure 3.11b) and 3 (Figure 3.13b), a positive $\Delta MAE_{MP}$ is produced in some hexels up to a lead time of one week. Beyond a one week lead time, the model forecasts perform better than the persistence forecast in all hexels.

More specifically, hexels 2, 8, and 9 show a positive $\Delta MAE_{MP}$ and indicate that persistence performed better than Model 1 up to a lead time of one week. However, beyond a lead time of one week, Model 1 performed better than persistence across the country. Persistence performed better than Model 2 up to a lead time of one week in hexels 6, 8, 9, 10, and 12. Beyond a lead time of one week, Model 2 performed better than persistence in all hexels except for hexel 2

which retains skills up to a lead time of two weeks. Persistence performed better than Model 3 up to a lead time of one week in hexels 2, 8, 9, 10, and 12. Beyond a lead time of one week, Model 3 performed better than persistence across the country. Finally, persistence performed better than Model 4 up to a lead time of one week in hexels 6, 8, 9, 10, 11, and 12. Beyond a lead time of one week, Model 4 performed better than persistence in all hexels except for hexel 2 which retains skills up to a lead time of two weeks. In general, we find that all model forecasts perform better than persistence forecasts beyond a two week lead time. Nevertheless, the persistence forecast shows skill in some hexels at a lead time of one week.

Across all four models, the accuracy tends to decreases incrementally in all hexels with increasing lead time (Figure 3.11c, Figure 3.12c, Figure 3.13c, and Figure 3.14c). Similarly, the persistence and climatology forecast accuracy declines with increasing lead time (Table A2 and A3). In general, the model accuracy of west and west-central hexels is slightly higher than eastern hexels.

Table 3.1 Hexel 8 LSTM Model, Climatology, and Persistence MAE for each of the four models at one to five week lead times.

| ***Week*** | ***Model 1 MAE*** | ***Model 2 MAE*** | ***Model 3 MAE*** | ***Model 4 MAE*** | ***Climatology MAE*** | ***Persistence MAE*** |
|---|---|---|---|---|---|---|
| *1* | 4.409 | 4.473 | 4.398 | 4.361 | 6.737 | 4.272 |
| *2* | 5.812 | 5.985 | 5.836 | 6.017 | 6.737 | 6.657 |
| *3* | 6.275 | 6.366 | 6.254 | 6.344 | 6.737 | 8.214 |
| *4* | 6.766 | 7.032 | 6.844 | 6.939 | 6.737 | 9.399 |
| *5* | 7.341 | 7.757 | 7.378 | 7.649 | 6.737 | 10.359 |

***Hexel 8: Model MAE Comparisons***

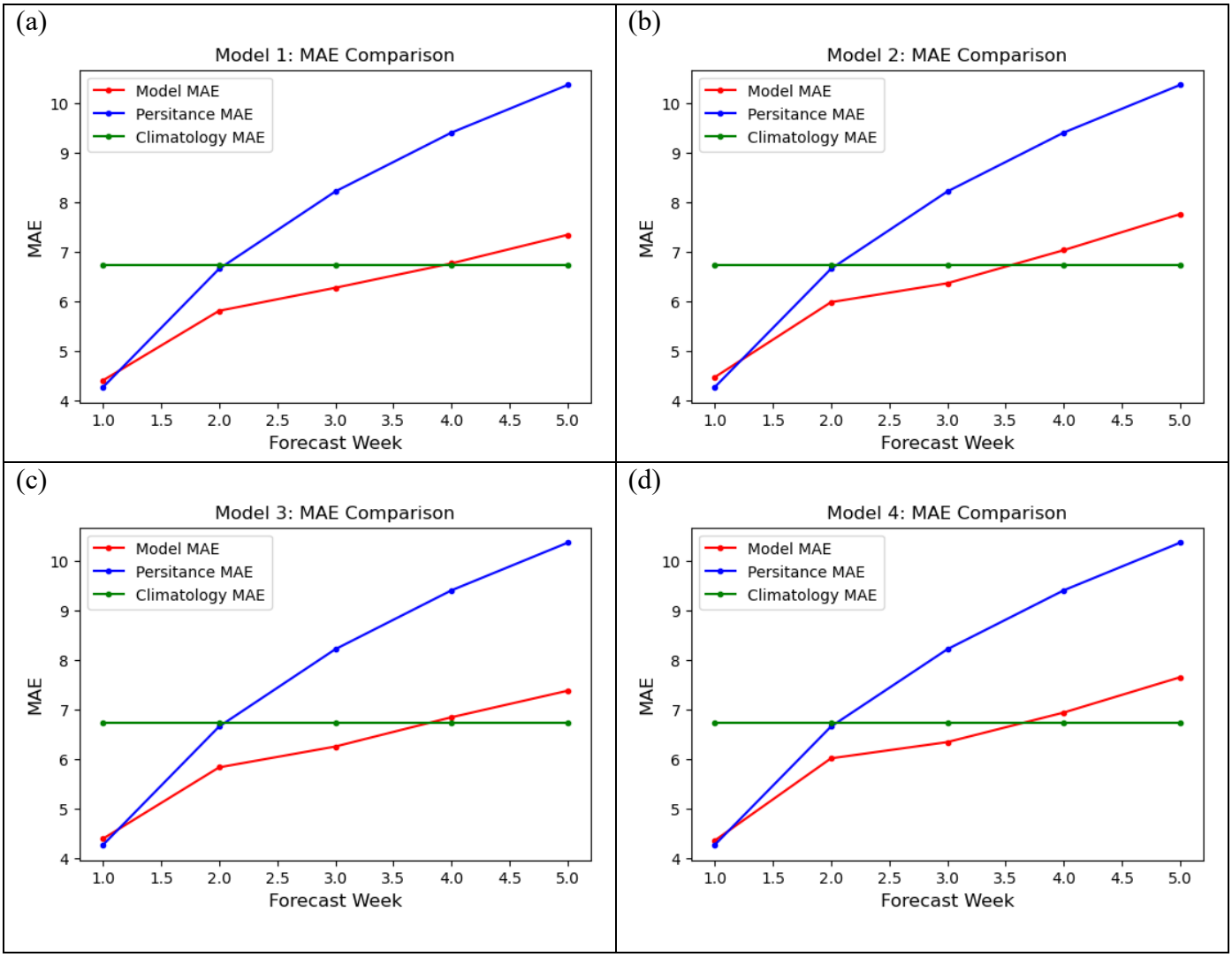


Figure 3.10 Plotted MAE values for Hexel 8 showing Model MAE, Climatology MAE, and Persistence MAE for each of the four models at 1 to 5 week lead times.

*Model 1: Hexel Maps of MAE and Accuracy*

| (a) Model Forecast Vs. Climatology | (b) Model Forecast Vs. Persistence | (c) Accuracy |
|---|---|---|
| (i)<br>**Week 1: MAE Difference of Model Forecast and Climatology**<br> 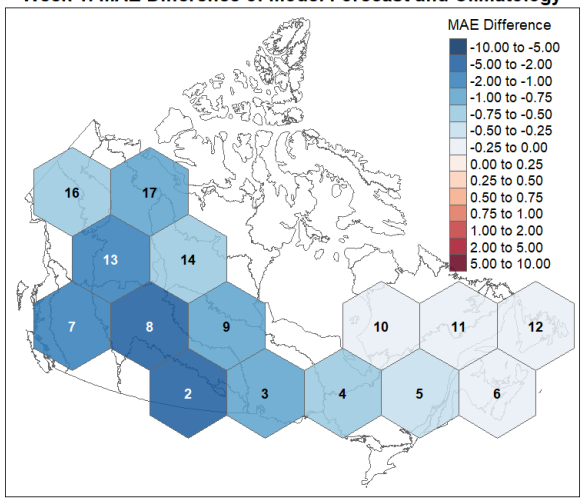 | (i)<br>**Week 1: MAE Difference of Model Forecast and Persistence**<br> 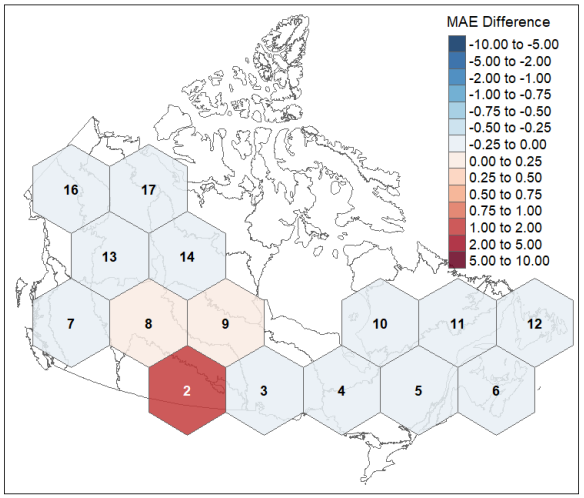 | (i)<br>**Week 1: Accuracy of Model Forecast**<br> 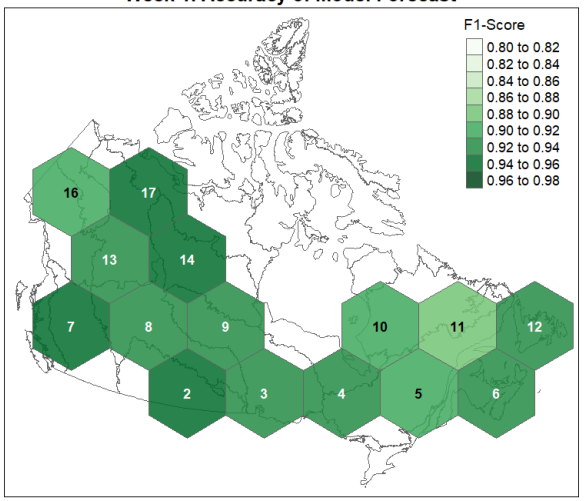 |
| (ii)<br>**Week 2: MAE Difference of Model Forecast and Climatology**<br> 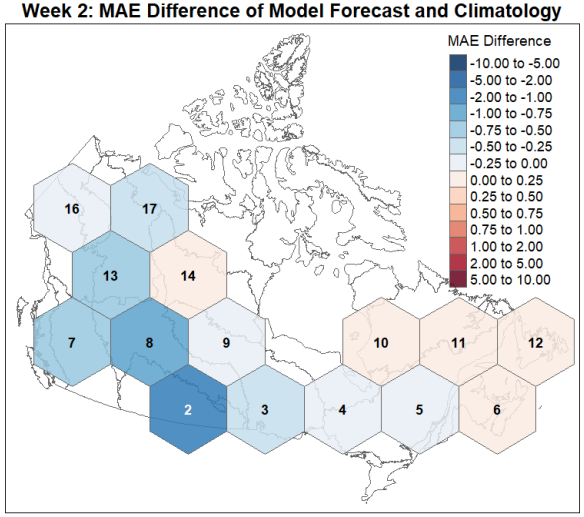 | (ii)<br>**Week 2: MAE Difference of Model Forecast and Persistence**<br> 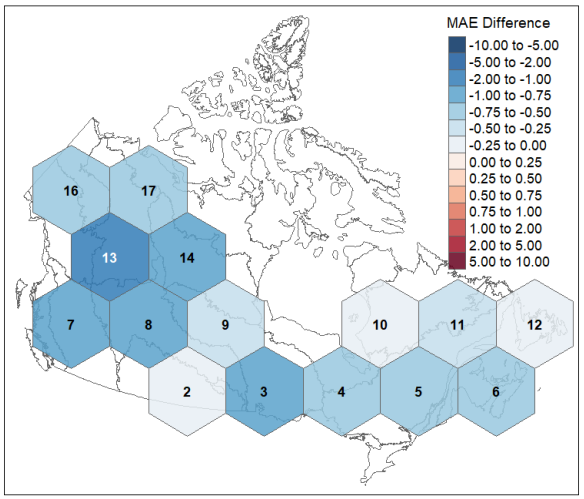 | (ii)<br>**Week 2: Accuracy of Model Forecast**<br> 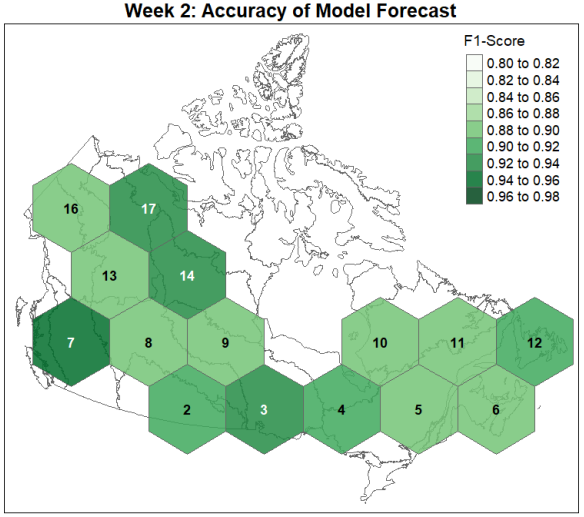 |

(iii)

**Week 3: MAE Difference of Model Forecast and Climatology**

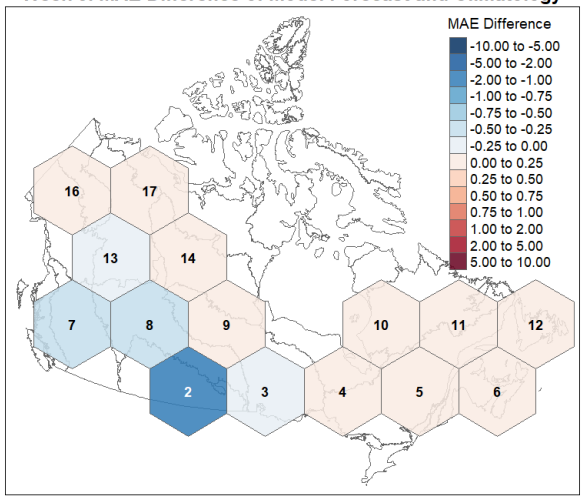


(iii)

**Week 3: MAE Difference of Model Forecast and Persistence**

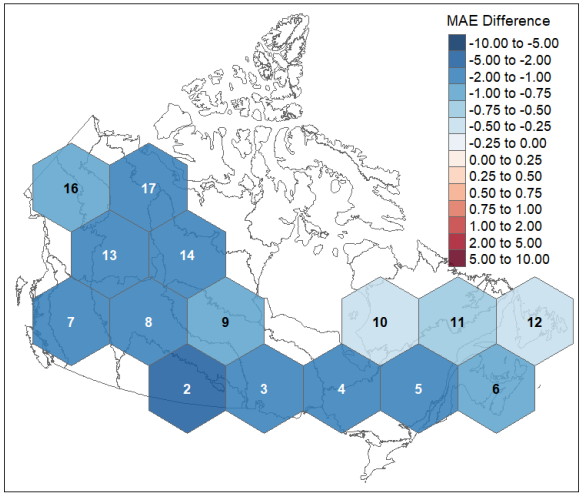


(iii)

**Week 3: Accuracy of Model Forecast**

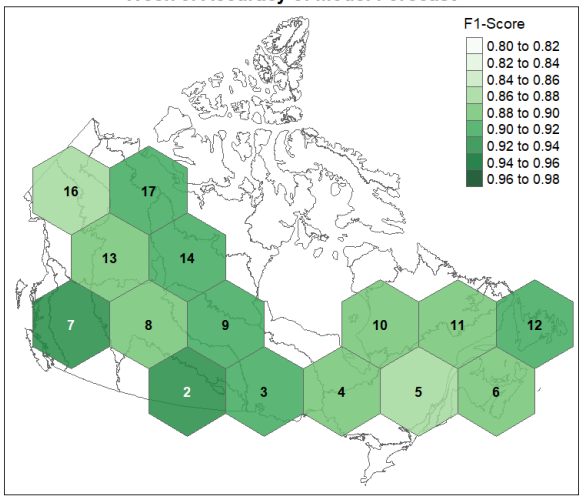


(iv)

**Week 4: MAE Difference of Model Forecast and Climatology**

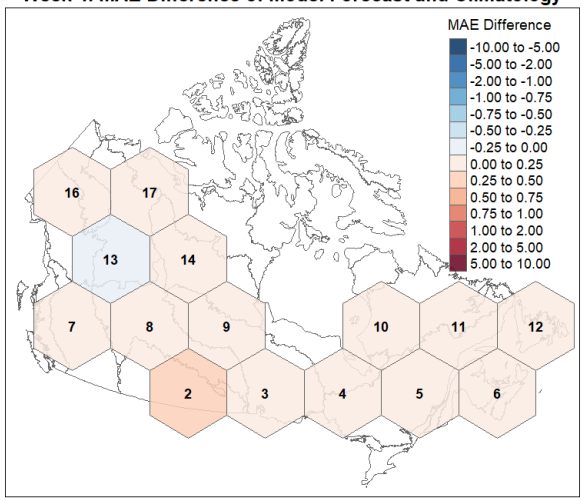


(iv)

**Week 4: MAE Difference of Model Forecast and Persistence**

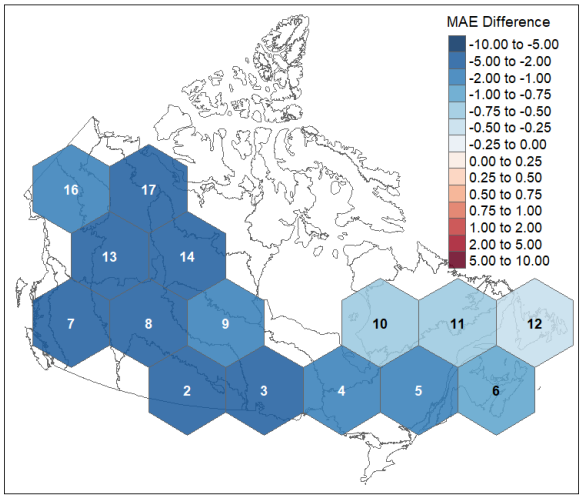


(iv)

**Week 4: Accuracy of Model Forecast**

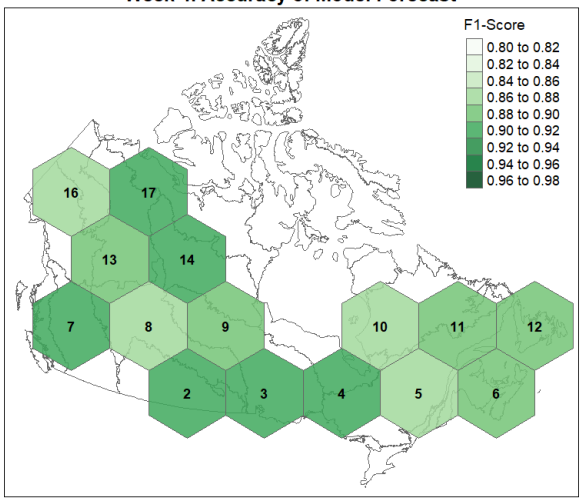

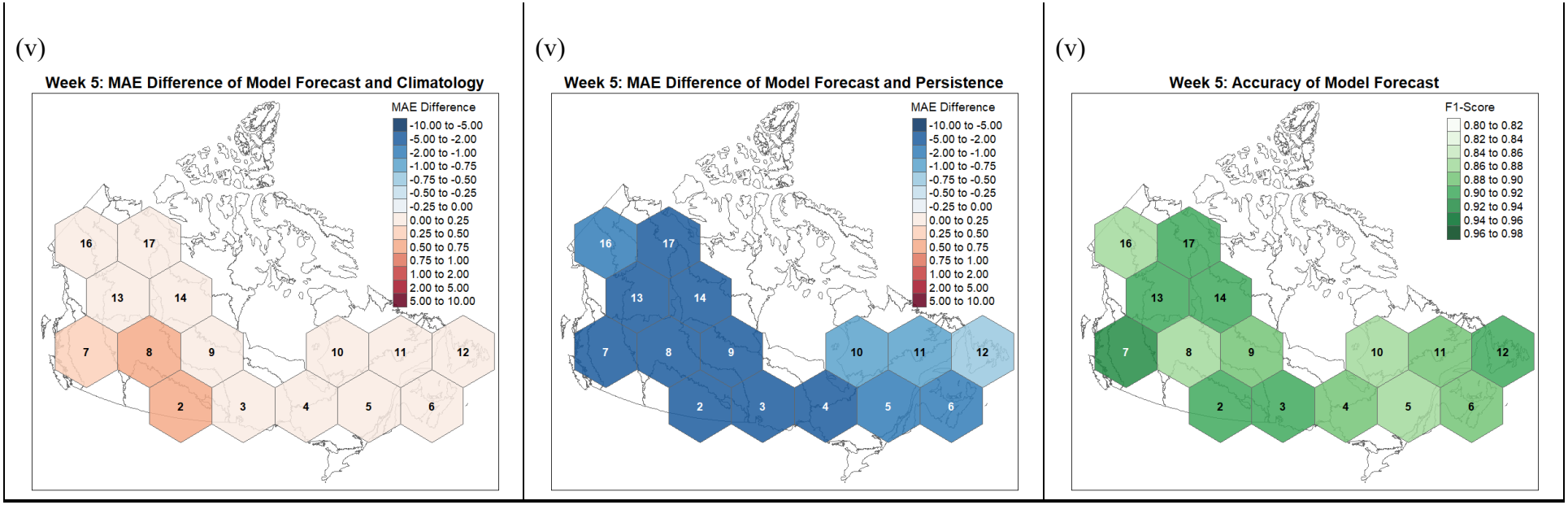


Figure 3.11 Model 1 MAE comparisons of testing data (2013-2020) for LSTM model, climatology, and persistence forecasts for each hexel: (a) the difference between model MAE and climatology MAE, (b) the difference between model MAE and persistence MAE, and (c) the accuracy of model predictions. Blue indicates a negative MAE difference, where the LSTM model forecast is improved. Red indicates a positive MAE difference, where the climatology or persistence forecast is improved. Tones of green represent F1-scores, with darker shades showing higher accuracies.

*Model 2: Hexel Maps of MAE and Accuracy*

| (a) Model Forecast Vs. Climatology | (b) Model Forecast Vs. Persistence | (c) Accuracy |
|---|---|---|
| (i) | (i) | (i) |
| 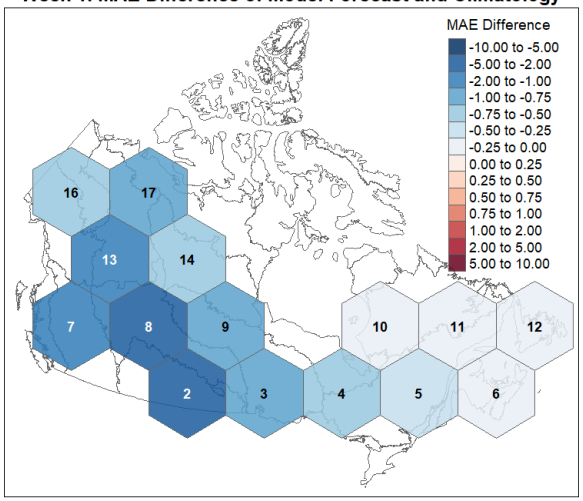 | 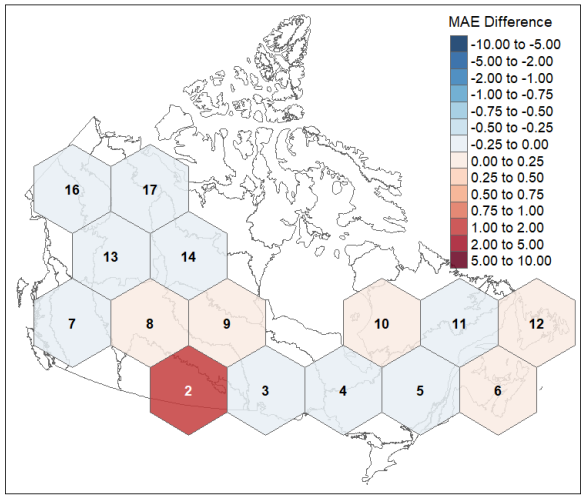 | 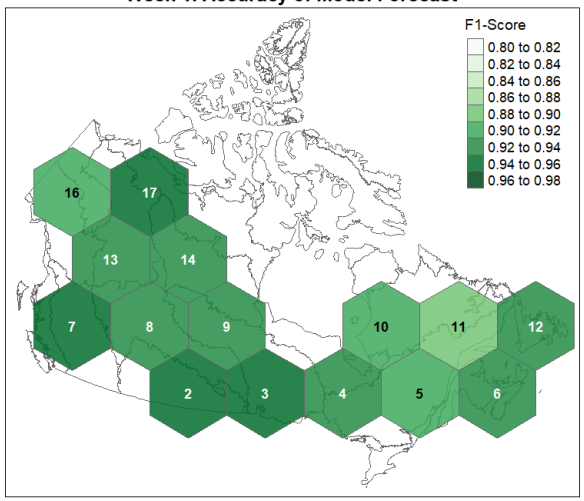 |
| (ii) | (ii) | (ii) |
| 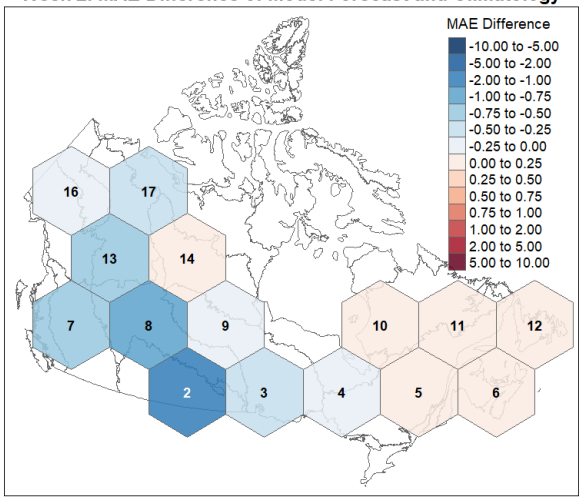 | 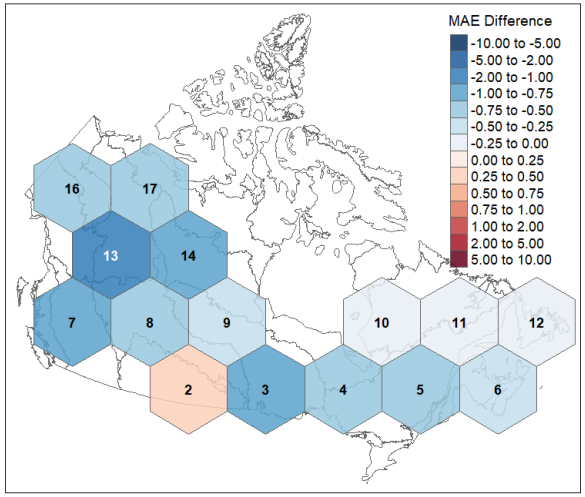 | 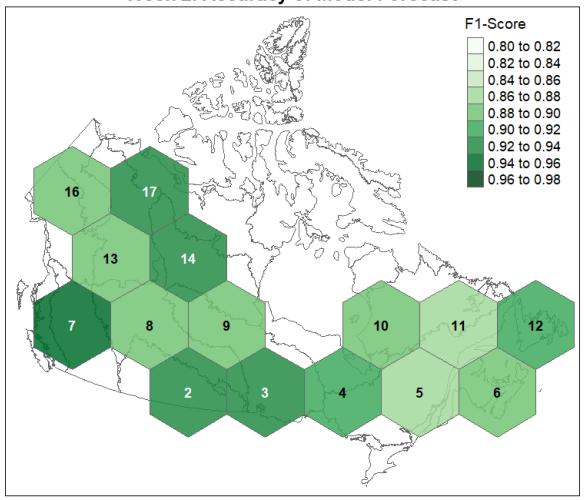 |

(iii)

**Week 3: MAE Difference of Model Forecast and Climatology**

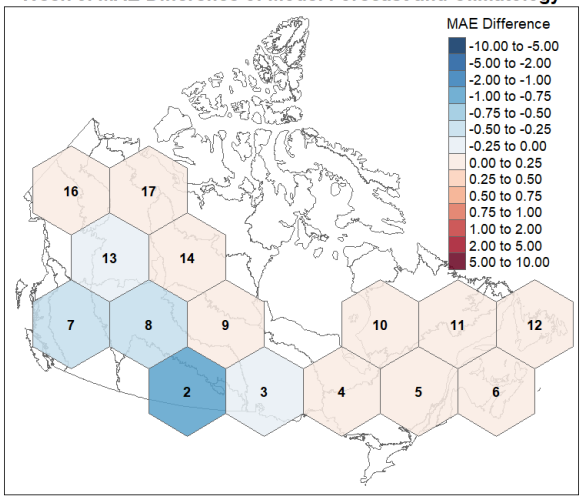


(iii)

**Week 3: MAE Difference of Model Forecast and Persistence**

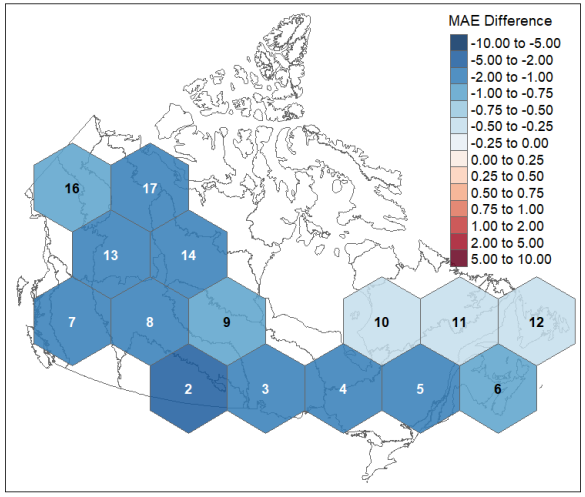


(iii)

**Week 3: Accuracy of Model Forecast**

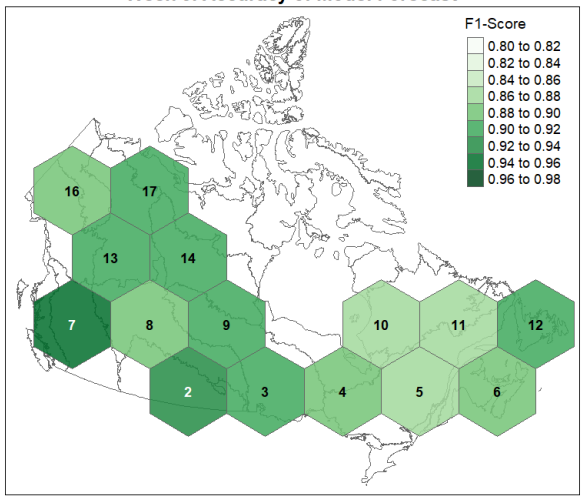


(iv)

**Week 4: MAE Difference of Model Forecast and Climatology**

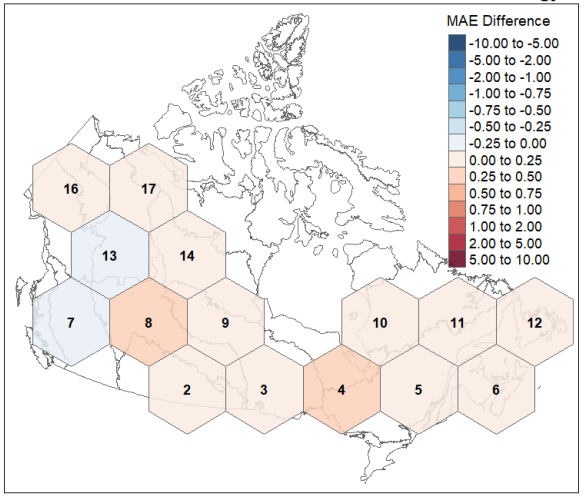


(iv)

**Week 4: MAE Difference of Model Forecast and Persistence**

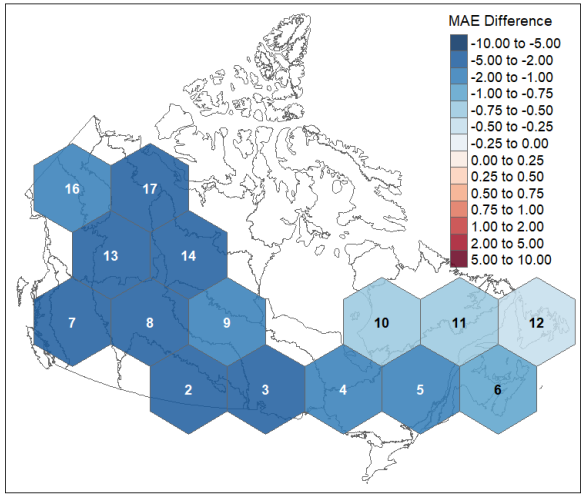


(iv)

**Week 4: Accuracy of Model Forecast**

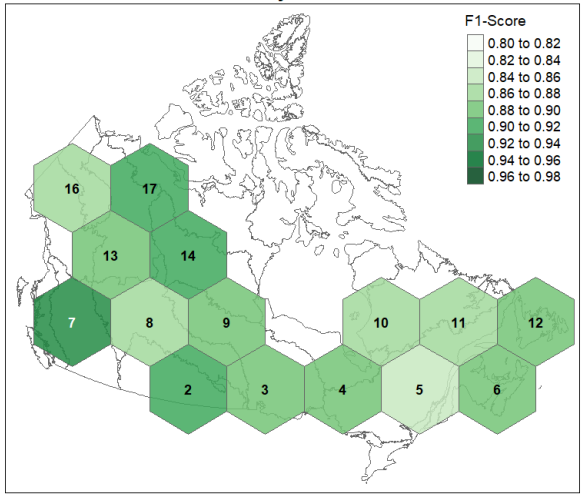

(v)

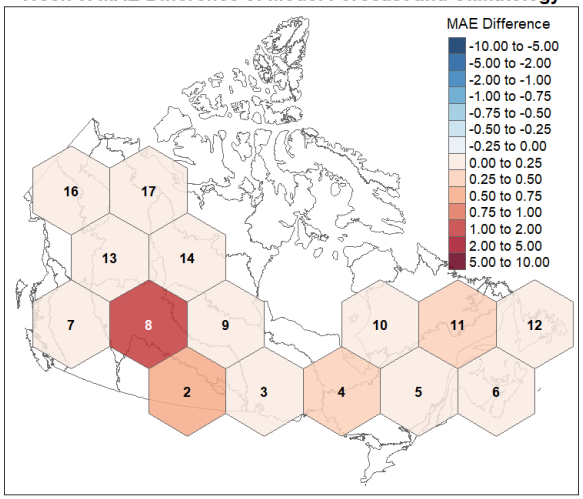


(v)

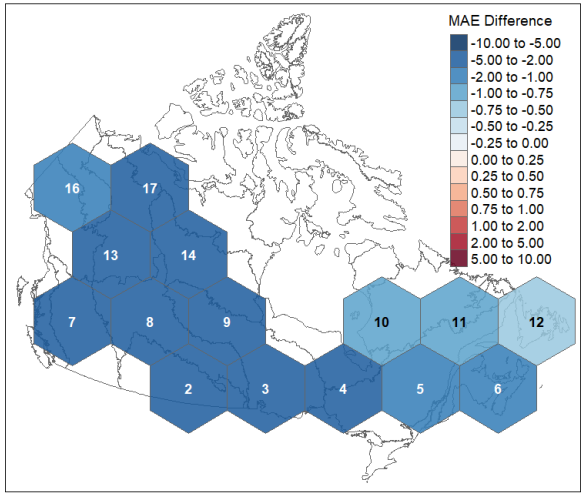


(v)

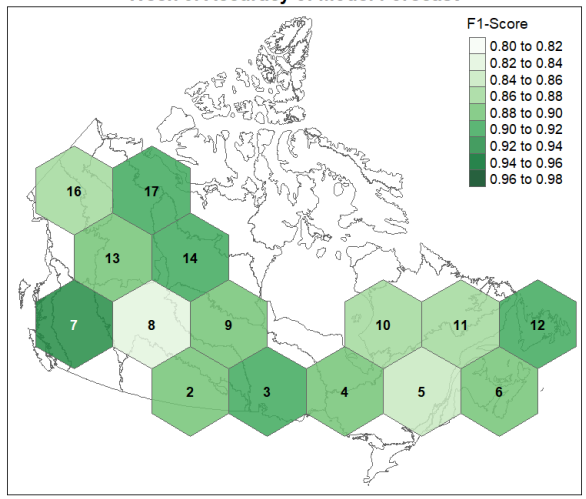


Figure 3.12 Model 2 MAE comparisons of testing data (2013-2020) for LSTM model, climatology, and persistence forecasts for each hexel: (a) the difference between model MAE and climatology MAE, (b) the difference between model MAE and persistence MAE, and (c) the accuracy of model predictions. Blue indicates a negative MAE difference, where the LSTM model forecast is improved. Red indicates a positive MAE difference, where the climatology or persistence forecast is improved. Tones of green represent F1-scores, with darker shades showing higher accuracies.

*Model 3: Hexel Maps of MAE and Accuracy*

| (a) Model Forecast Vs. Climatology | (b) Model Forecast Vs. Persistence | (c) Accuracy |
|---|---|---|
| (i) 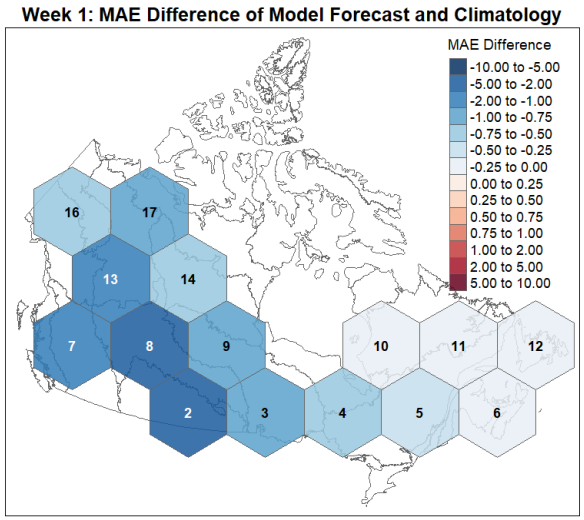  | (i) 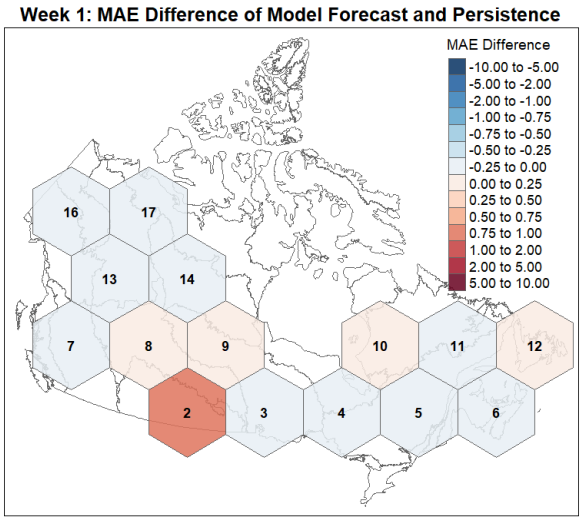  | (i) 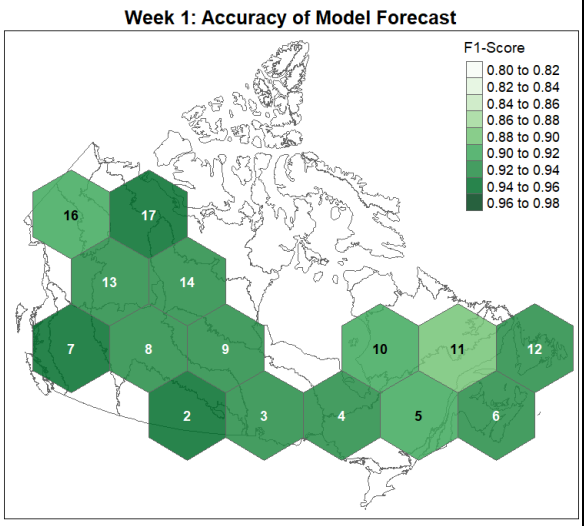  |
| (ii) 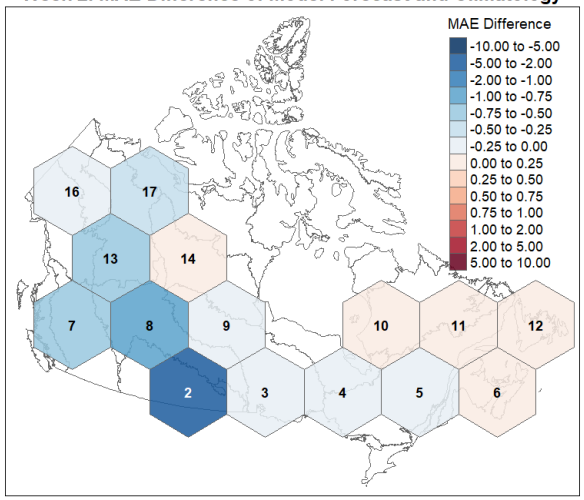  | (ii) 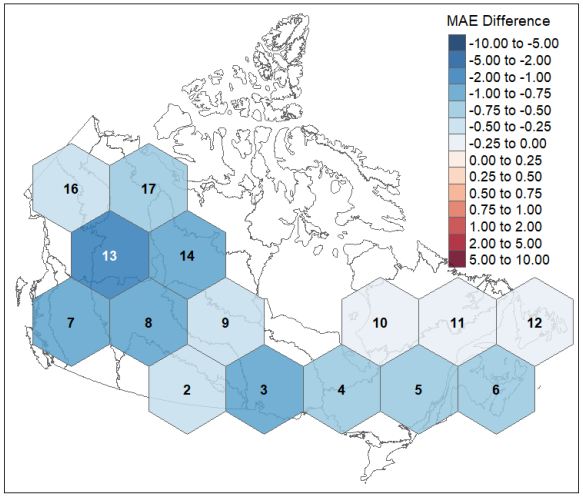  | (ii) 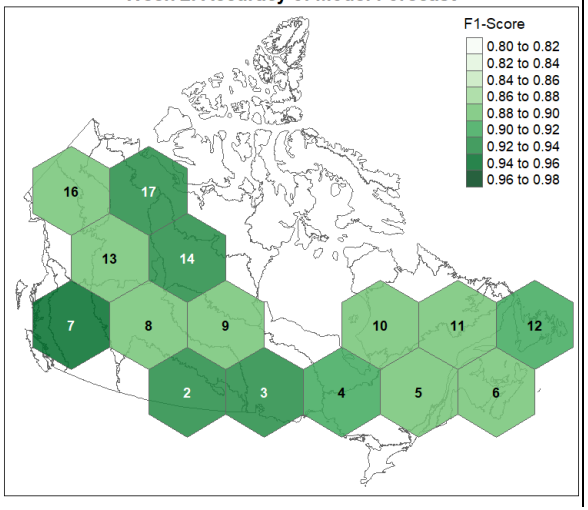  |

(iii)

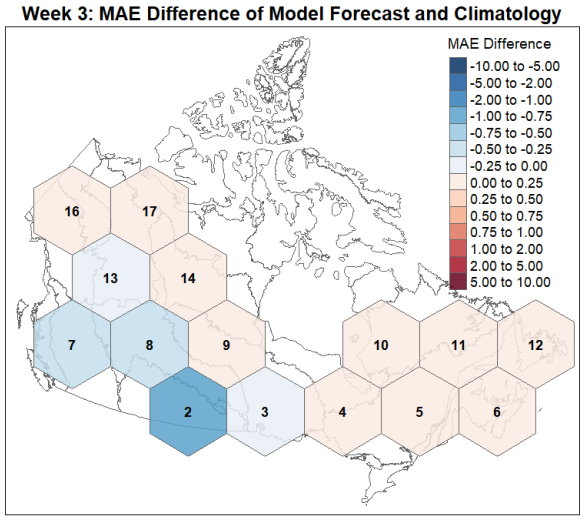


(iii)

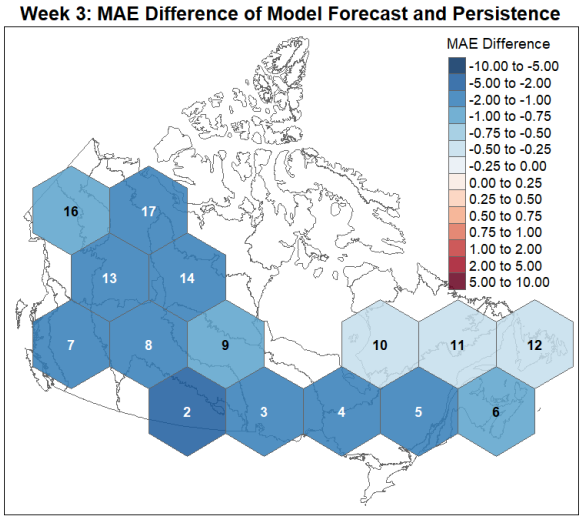


(iii)

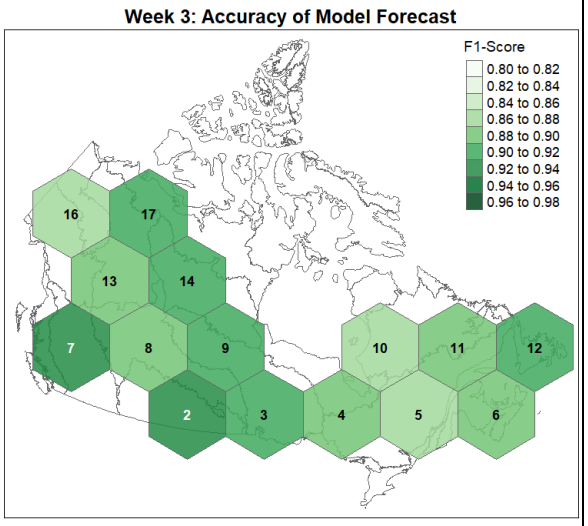


(iv)

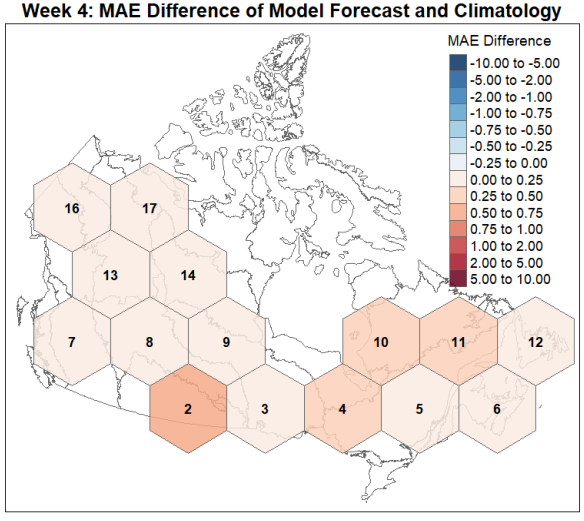


(iv)

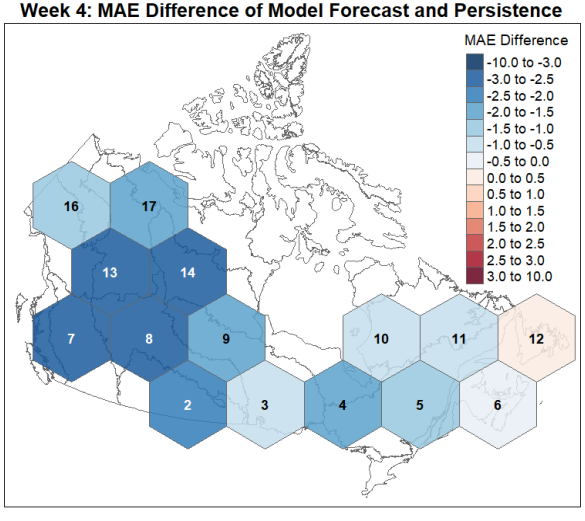


(iv)

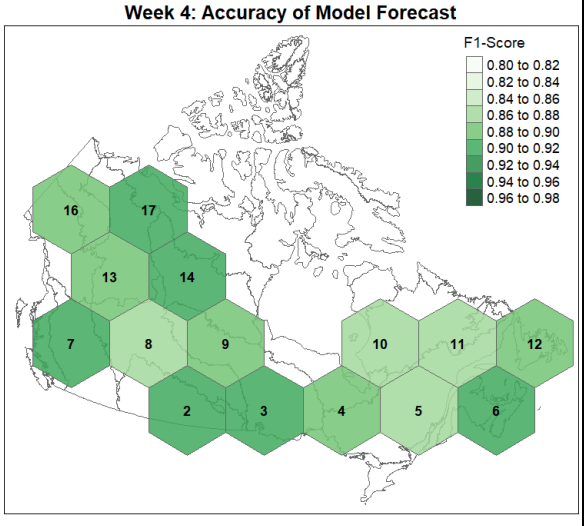

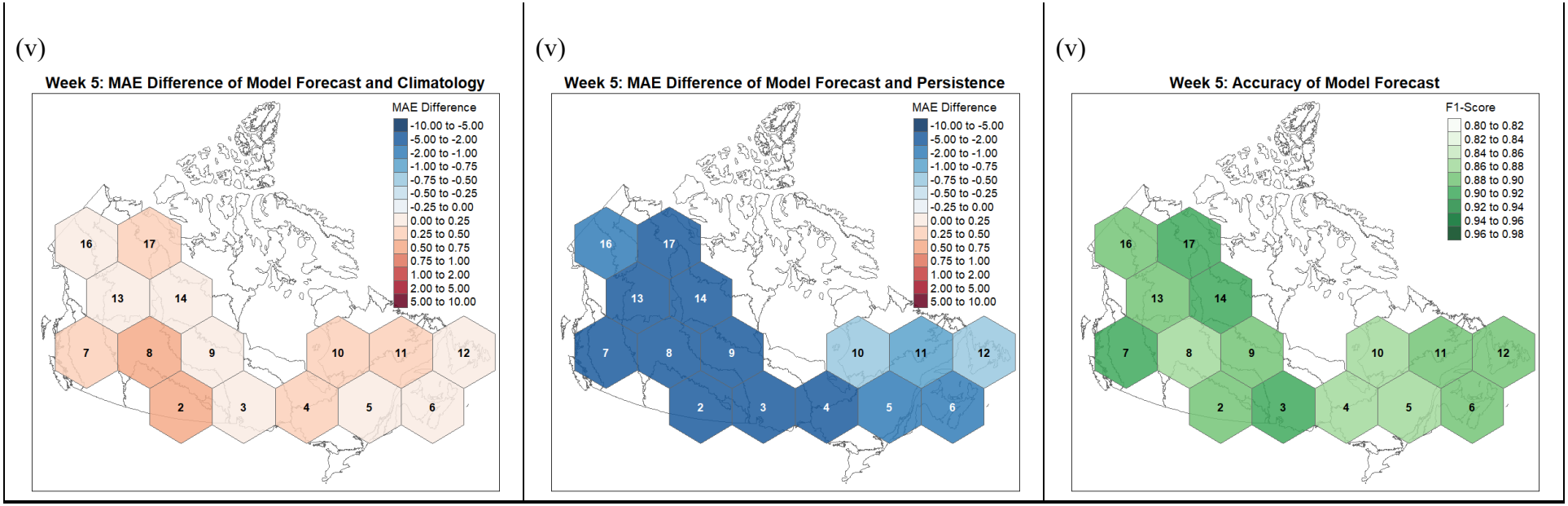


Figure 3.13 Model 3 MAE comparisons of testing data (2013-2020) for LSTM model, climatology, and persistence forecasts for each hexel: (a) the difference between model MAE and climatology MAE, (b) the difference between model MAE and persistence MAE, and (c) the accuracy of model predictions. Blue indicates a negative MAE difference, where the LSTM model forecast is improved. Red indicates a positive MAE difference, where the climatology or persistence forecast is improved. Tones of green represent F1-scores, with darker shades showing higher accuracies.

*Model 4: Hexel Maps of MAE and Accuracy*

| (a) Model Forecast Vs. Climatology | (b) Model Forecast Vs. Persistence | (c) Accuracy |
|---|---|---|
| (i) | (i) | (i) |
| 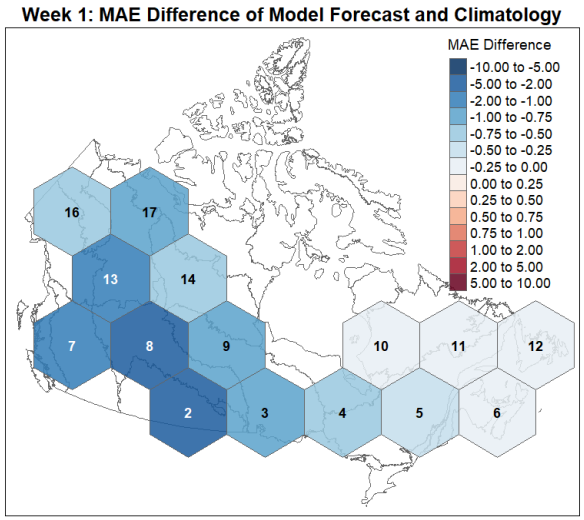 | 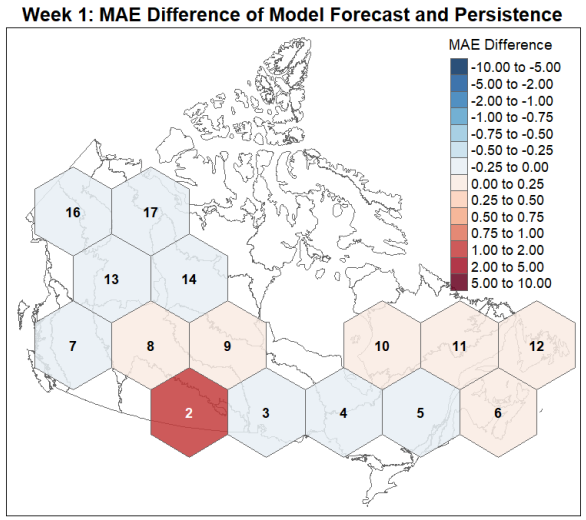 | 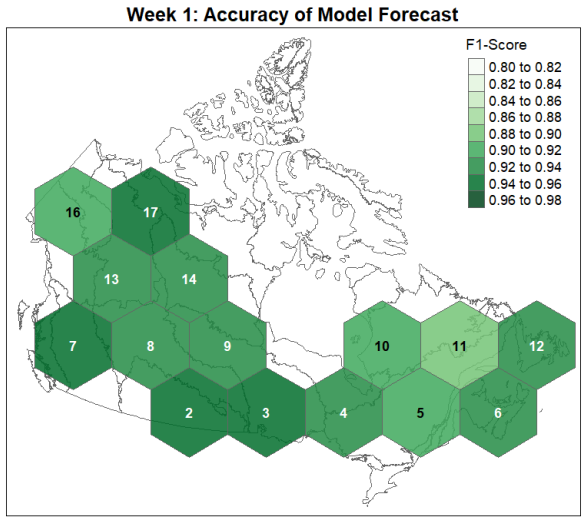 |
| (ii) | (ii) | (ii) |
| 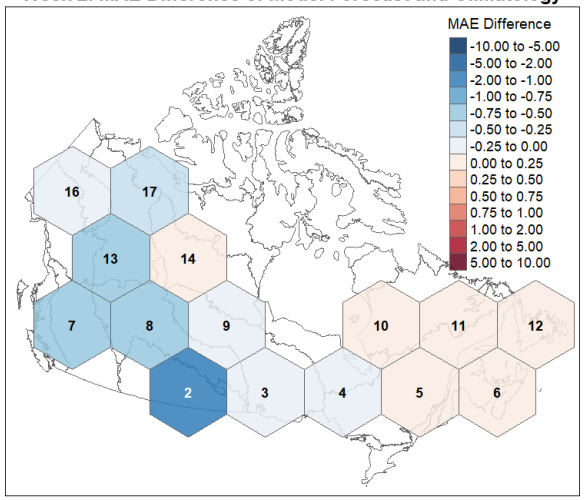 | 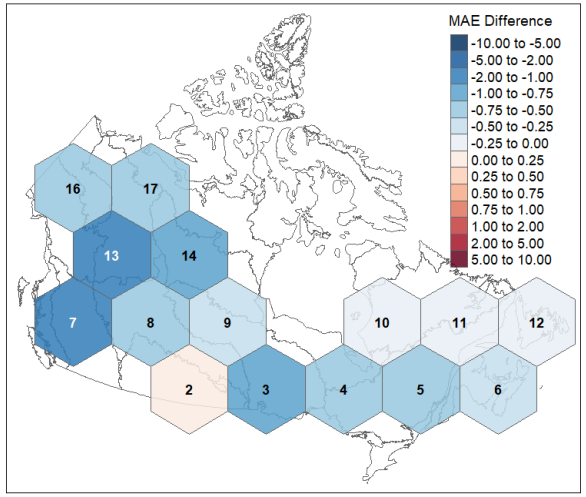 | 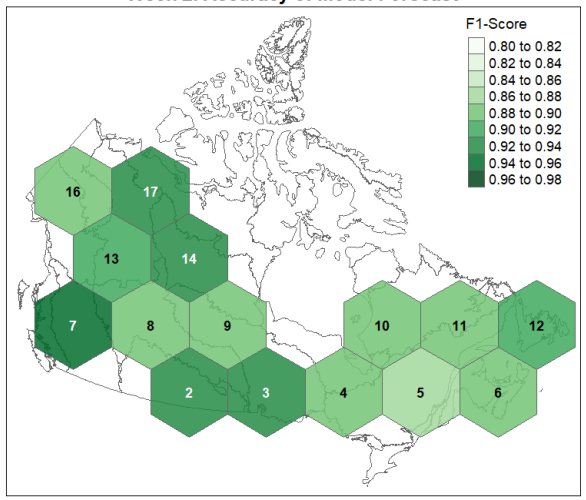 |

(iii)

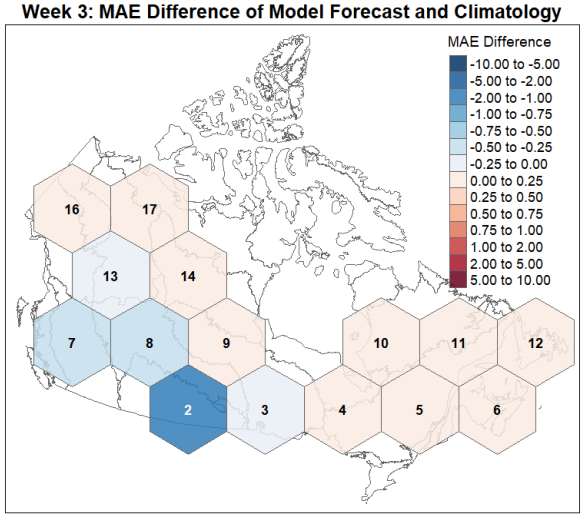


(iii)

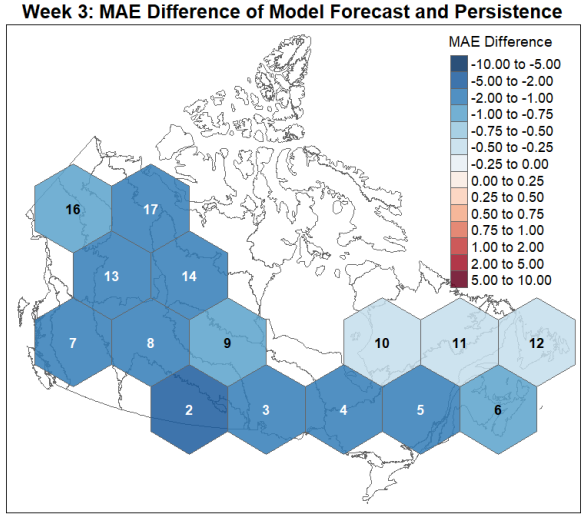


(iii)

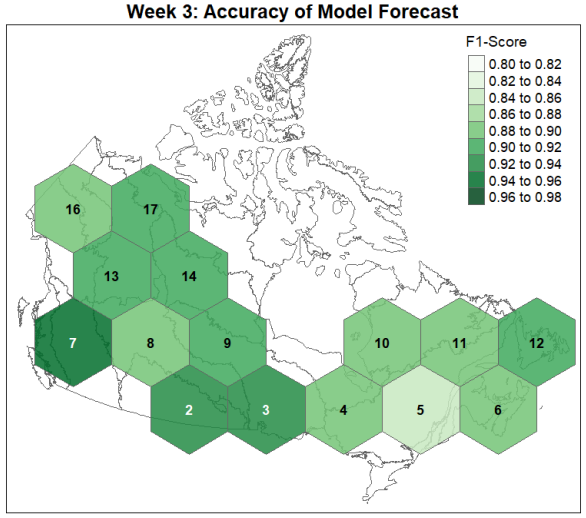


(iv)

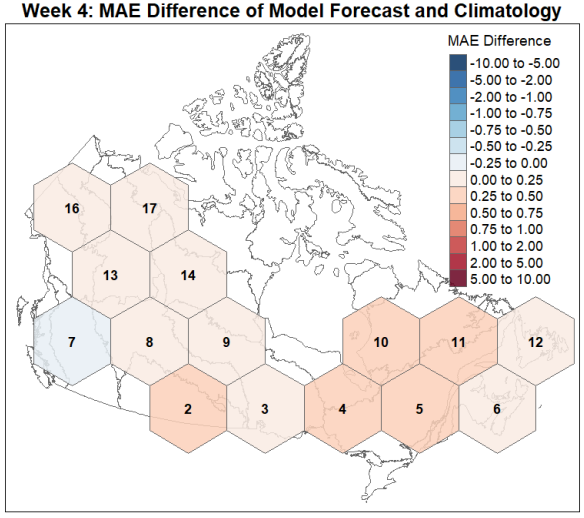


(iv)

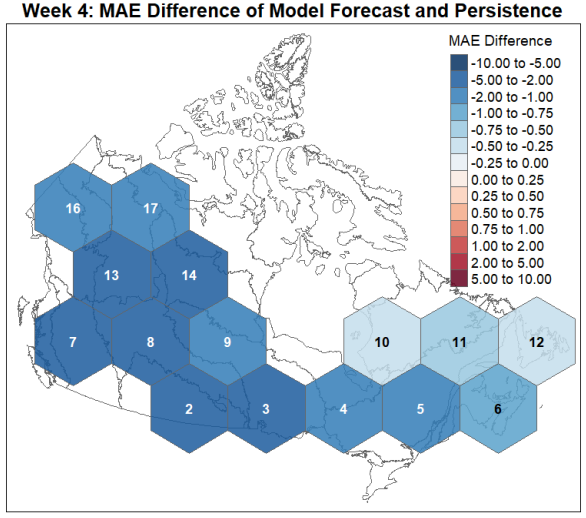


(iv)

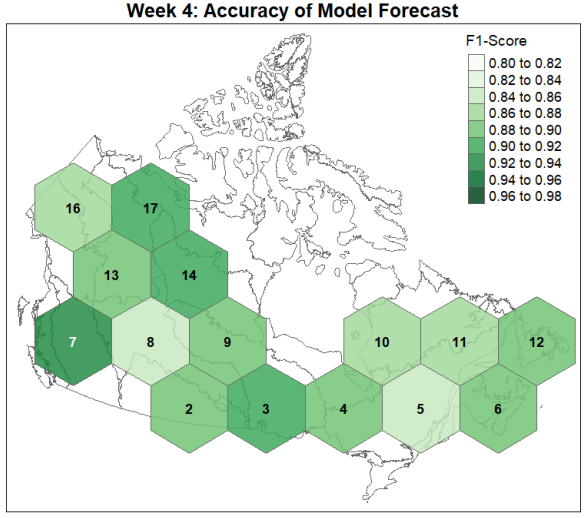

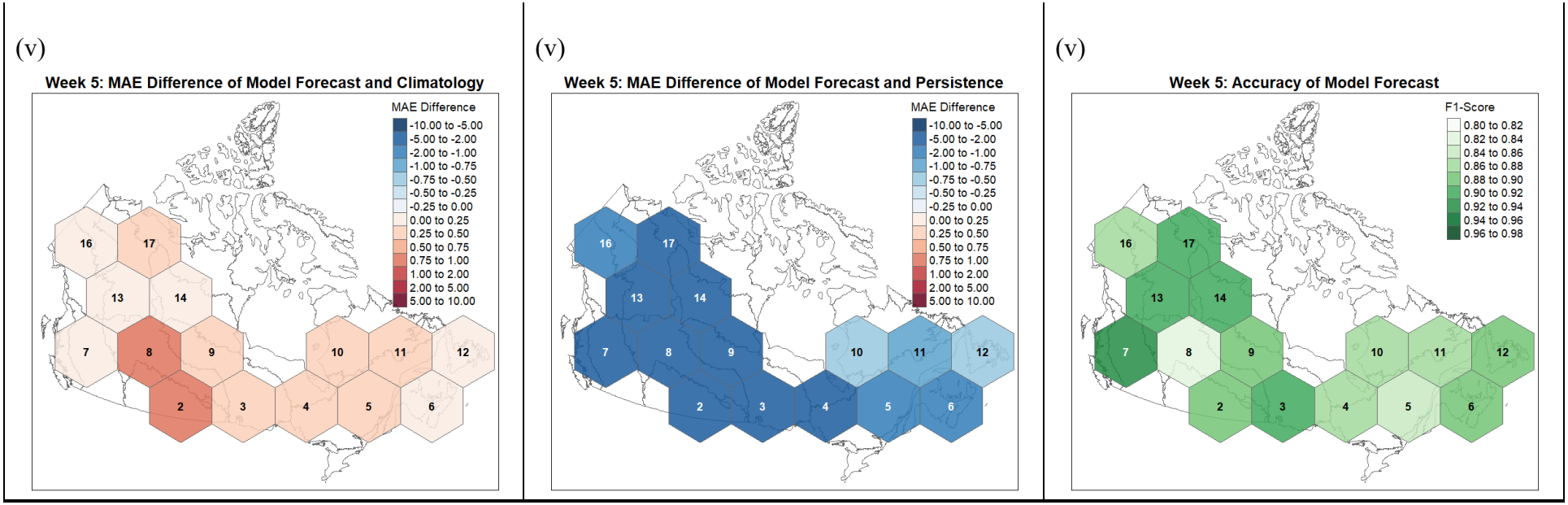


Figure 3.14 Model 4 MAE comparisons of testing data (2013-2020) for LSTM model, climatology, and persistence forecasts for each hexel: (a) the difference between model MAE and climatology MAE, (b) the difference between model MAE and persistence MAE, and (c) the accuracy of model predictions. Blue indicates a negative MAE difference, where the LSTM model forecast is improved. Red indicates a positive MAE difference, where the climatology or persistence forecast is improved. Tones of green represent F1-scores, with darker shades showing higher accuracies.

## Chapter 4 Discussion

In this chapter, the predictive power of using LSTM models to forecast weekly averaged BUI at lead times of one to five weeks is examined in detail. As well, the results from each of the four models considered here is analyzed. Finally, model limitations (including possible sources of error) and suggestions for future research are discussed. Results from this study suggest that ML models used to forecast FWI values may help to extend the time period for skillful forecasts when compared with climatology and persistence. Four LSTM models produced one to five week forecasts of BUI for 15 hexels across Canada. Each model used a different combination of predictive variables which included: week of year, historical BUI, BUI climatology, ENSO MEI.v2 index, and AMO index (see Table 2.1). Each model produced improved forecasting results when compared to climatology and persistence for two to three week forecasting in western Canada. Historically, long term weather prediction and forecasted derivatives of weather (including FWI system indices) has been a significant challenge as modelling at a long-range timescale is very challenging at both small and large scales. Geostationary, polar-orbiting, and deep space satellites monitor and collect global atmospheric data that is used in physics-based forecasting models. More specifically, numerical weather predictions models use atmospheric data, but the forecasts produced have limited success at longer lead times as weather is a chaotic system. Despite major advances made in the field of ML, predicting future weather trends requires identification of both the input and response variables that are appropriate for long range forecasting. Using covariate combinations of historical BUI and teleconnections shows potential for improved FWI forecasts, however, some hexels perform better than others. More specifically,

some hexels show improved predicted BUI when compared with climatology and persistence, while others showed a similar error to those estimates.

### 4.1 Model Performance

Results from this study are compared with the findings of Shabbar and Skinner (2004) who reported that ENSO events usually lead to a summer moisture deficit in western Canada as there is less winter precipitation. In addition, they determined that warm AMO phases tends to be associated with drier conditions in the Prairies, lower Great Lakes, and the west coast of Canada. The extreme BUI values caused by ENSO events in the western extent of Canada may be better forecasted by Model 2 and Model 4 which use ENSO indices as covariate predictors. Whereas drier summer conditions in the Praries, lower Great Lakes, and west coast may be better predicted by Model 3 and Model 4 which use AMO indices as covariate predictors.

As shown in Models 2, 3, and 4, hexels in the west show better results from the LSTM models than climatology and persistence up to three weeks of lead time (Figures 3.15a, 3.16a, and 3.17a). However, the Model 1 forecast at a three week lead time (Figure 3.14a) performs similarly since the same western hexels show improved results when compared to climatology and persistence forecasts. Where Models 2 and 4 differ from Model 1 is demonstrated in hexel 7 at a four week lead time. The addition of ENSO as a covariate gives the models a slight advantage at forecasting BUI in this western hexel. Although Model 2 and 4 show improvements over Model 1 in hexel 7, Model 1 shows similar skill in a neighboring hexel. The Model 1 forecast in hexel 13 shows skill over climatology up to a lead time of four weeks as well.

Moreover, the Model 3 forecast does not show any improvements over the Model 1 forecast up to a lead time of four weeks. In general, all model forecasts perform better than climatology in hexels 2, 3, 7, 8, and 13 up to a lead time of three weeks. As well, all model forecasts perform better than persistence in all hexels beyond two weeks of lead time. These results suggest that the addition of teleconnections as covariates is useful to a certain degree. The efficacy of additional teleconnection covariates on model forecasting skill is not clear without additional research.

Although relationships between teleconnections and FWI values have been explored in this research, there may be limitations in this approach. As stated by Hofman et al. (2017) and Ribeiro et al. (2016), causal features can improve the interpretability of predictive models while correlations only capture the co-occurrence of features (Yu et al., 2020). While Models 2, 3, and 4 contain teleconnections as covariate predictors, the forecasting ability of Model 1 remains on par with these models for up to three weeks of lead time. This suggests that the relationship between BUI, ENSO, and AMO should be explored in further detail to determine whether teleconnections are truly causal predictors and not just correlations.

Despite the uncertainty of teleconnections as casual covariates; week of year, historical BUI, and climatological BUI proved to be useful predictors in the LSTM models. As shown in the identity line plots (Figures 3.3a, 3.6a, 3.9a, and 3.11a), the model forecasts progressively learned the seasonal climatology. At a lead time of five weeks, each model forecast showed similar results to the climatology forecast. Although the models trend towards climatology, the model forecast results outperform the climatology forecast in many western hexels up to a lead time of three weeks. It is important to note that the LSTM models use twelve weeks or three months of

observed covariate values as inputs to forecast up to a five week lead time. This suggests that model skill may be attributed to teleconnection values from up to three months previous, but the most important predictor is observed BUI. This offers an opportunity to improve traditional long term BUI forecasts that rely solely on climatology and short term forecasts that rely on persistence. ML models and teleconnections as covariates may be used as additional predictive tools to validate the climatological BUI forecast and improve forecasting at around three weeks of lead time.

Finally, there is a need for long range forecasts in resource management within fire management zones and between agencies. Fire management operations may use long range forecasts of BUI to provide even earlier warning signs to relative potential for fire, as the BUI gives an indication of how much fuel is available for combustion. In addition to this, using BUI as the main predictor may capture the effects of both the DC and DMC in forecasts result. Both DC and DMC have been used to forecast several fire related events, including lightning-ignited wildfires (Flannigan and Wotton, 1991). As well, with improved methods for long range fire weather forecasts, fire management agencies can allocate resources and anticipate provincial and territorial firefighting needs. Fire fighters and government officials can be deployed in high fire danger zones to apply mitigation techniques, preventative treatments, or to give early warning to communities. This research presents an opportunity for improved early warning systems that have the potential to prevent the spread of unwanted fires.

### 4.2 Limitations and Sources of Error

There are a number of limitations and possible sources of errors within this study. Firstly, ML models require robust input data to produce accurate results. Missing data or inconsistent records may reduce learning and pattern detection of the LSTM model. Namely, overwintered DC values result in various start and end points for BUI data throughout the record. The interannual variability in the fire season startup may provide valuable information to the model. As well, prediction and interpretation of hexel 2 climate is limited by extremely high BUI values. Most of hexel 2 lies within the Canadian Prairies which can be described as a semi-arid grassland and agricultural farmland during the fire season.

While data quality and consistency is important to consider, choice of model variables and hyperparameters can largely dictate the success of an ML model. As mentioned earlier, covariate selection based on casual inference is commonly used in ML forecasting models (eg. Guyon et al., 2007). In this study, it was assumed that ENSO and AMO have a causal influence on BUI as teleconnections have a demonstrated effect on global weather systems up to a 3 month lead time (Bonsal and Shabbar, 2011; Girardin et al., 2006; Johnson and Wowchuk, 1993; Schoennagle, 2005; Skinner et al., 2006; Simard et al. 1985; Chu et al. 2002; Westerling and Swetnam 2003). In other words, teleconnections may increase model predictive power for up to 3 months of lead time. However, despite this assumption, the explicit relationship between teleconnections and FWI system indices in Canada have not been fully explored. Current research has focused on the effect of teleconnections on temperature and precipitation separately, however, it would be beneficial to examine the relationship specifically to fire weather. This presents a limitation to

this study, but offers an opportunity to study the influence of teleconnections on the FWI system in future research. As well, the model presented in this research uses teleconnections data from the previous 12 weeks (approximately 3 months), however, longer timescales may allow for increased predictive power.

Moreover, hyperparameter selection used a combination of heuristic and exhaustive manual tuning to minimize training and validation loss curves. While an extensive combination of hyperparameters were tested to optimize model results, automation of this process may offer alternate configurations that produce better results. As stated previously, hyperparameter tuning can be done using manual tuning, gridded searches, randomized searches (Bergstra and Bengio, 2012), or Bayesian optimization (Snoek and Larochelle, 2012; Shahriari et al., 2015). Exploring these methods may expose optimal hyperparameters that were previously overlooked.

Potential covariates were omitted from this study to preserve a simplistic model architecture. Potential covariates included FWI system indices and weather variables that are used to produce BUI and other teleconnections that impact North American weather. For example, Jain and Flannigan (2021) study the relationship between variability of the polar jet stream with extreme wildfire activity, showing jet stream patterns correlated with observed wildfires in North America. This suggests that the use of synoptic weather patterns at the scale of the polar jet stream may provide further predictive power for days up to weeks in advance. This is important as numerical weather prediction (NWP) models are better at forecasting upper air patterns when compared to surface variables. As well, Skinner et al. (2006) state that the PDO results in drier conditions in western, northwestern, and areas of northeastern Canada. Johnson and Wowchuk

(1993) suggest that PNA is associated with blocking ridges in eastern North America that lead to increased fire severity. Finally, Macias Fauria and Johnson (2006) suggest that interactions of PDO, ENSO, and AO with Canadian fire weather can explain the increase of fire frequency in the early twentieth century. Although some weather variables, like wind speed, were not considered in this study, they play a factor in Canadian fire weather and present an opportunity for further research.

Another potential avenue for further work is to vary the spatial resolution of the study area. While this study focuses on time-series forecasting of set hexel sizes, each hexel individually represents a non-spatial model. The size of the modeling unit may have implications on model accuracy and forecast lead times as atmosphere-land dynamics are coupled and exhibit spatial and temporal covariance. In future work, it may be beneficial to reduce the size of the hexels to produce more models. Alternatively, Liu et al. (2017) combined the ML architectures, CNN and LSTM to extract spatial-temporal data through one deep learning model, called Conv-LSTM. A full spatiotemporal model using Conv-LSTM or similar models may be considered for future research.

Finally, the results of this study are compared with climatology and persistence forecasts only. Although comparisons to NWP model forecasts are out of the scope of this study, analyzing the results of an ML model forecast against NWP models would be an integral part of any future work. As completed in a study by Boychuk et al. (2020), forecasts of FWI are quantitatively verified against results from the NAEFS forecast. More generally, NWP forecasts of fire weather could also provide valuable covariates to further improve LSTM model forecasts.

# Chapter 5 Conclusion

Weather plays in integral role in determining wildfire risk and it can be used as part of an early warning system for fire management agencies. Currently, fire weather can be forecasted using observed surface and upper air weather and numerical weather prediction systems. However, such models may lead to uncertainties at large lead times which can cause low predictive skill for FWI system indices. With the development of recurrent neural networks, BUI – a measure of available fuels for combustion - can be forecasted on a sub-seasonal time scale of one to five weeks. This study provides an opportunity to use ML models as an additional predictive tool to validate the climatological BUI forecast and to improve forecasting around three weeks of lead time.

Four LSTM model variations were evaluated to determine whether ML is a viable tool for forecasting BUI. Weekly averages of BUI were calculated using the fifth version of the European Centre for Medium-Range Weather Forecasts Reanalysis (ERA5-Land) data. The ERA5 data was aggregated onto $4.87 \times 10^5\ m^2$ hexels across Canada and active fire season data from April to October was split into training and testing datasets which span 80% of the data (1981 – 2012) and 20% (2013 - 2020) respectively. Moreover, the climate teleconnections ENSO and AMO were used as covariates in the models to enhance model predictive ability.

The results presented here indicate that ML models are suitable as additional tools for forecasting BUI values. ML models may be used in conjunction with climatological and persistence forecasts to provide insight at longer time periods. In particular, this study finds that ML models

outperform climatology in the western half of the country including areas of the Pacific Maritime, Montane Cordillera, Boreal Plains, Boreal Shield West, Boreal Cordillera, Taiga Plains, and the Prairies and for up to a three week lead time. The results of BUI forecasts at four and five week lead times are model dependent and spatially dependent. In addition, the use of ENSO and AMO as covariates shows limited improvement to LSTM forecasting ability, as Model 1 forecast skill remains on par with Model 2, 3, and 4. This suggests an opportunity to further explore the causality between fire weather and various teleconnections.

The methods presented in this research provide an opportunity to assist fire management agencies and operations across the country and internationally. As this study shows improved forecasting ability up to 3 weeks in advance, this may offer additional time for provincial fire management agencies to assemble firefighting resources that typically require weeks to months of planning. As well, having prior knowledge of regions that are more susceptible to fire conducive conditions may allow agencies to allocate resources more efficiently. This is due to the limited supply of firefighting equipment, trained personnel, and government funding. Additionally, the provinces that are predicted to have less active fire seasons may share resources more effectively with high fire risk areas. In Canada, national preparedness levels are used to dictate the state of emergency. At levels of 4 and 5, fire management agencies may organize large-scale resource sharing to assist with wildfire mitigation domestically or internationally. High level planning is needed to coordinate these efforts and can be done efficiently with longer range forecasts that allow for more time.

## References


Albert-Green, A., Dean, C.B., Martell, D.L. and Woolford, D.G., 2013. A methodology for investigating trends in changes in the timing of the fire season with applications to lightning-caused forest fires in Alberta and Ontario, Canada. *Canadian Journal of Forest Research*, *43*(1), pp.39-45.

Amiro, B.D., Logan, K.A., Wotton, B.M., Flannigan, M.D., Todd, J.B., Stocks, B.J. and Martell, D.L., 2004. Fire weather index system components for large fires in the Canadian boreal forest. *International Journal of Wildland Fire*, *13*(4), pp.391-400.

Anderson, K.R.; Englefield, P.; Carr, R. 2007. Predicting fire-weather severity using seasonal forecasts**.** In 7th Symposium on Fire and Forest Meteorology, Bar Harbor, ME, 23–25 October 2007. Am. Meteorol. Soc., Boston, MA

Azzali, S. and Menenti, M., 2000. Mapping vegetation-soil-climate complexes in southern Africa using temporal Fourier analysis of NOAA-AVHRR NDVI data. *International Journal of Remote Sensing*, *21*(5), pp.973-996.

Bauer, P., Thorpe, A. and Brunet, G., 2015. The quiet revolution of numerical weather prediction. *Nature*, *525*(7567), pp.47-55.

Beck, H.E., Pan, M., Roy, T., Weedon, G.P., Pappenberger, F., Van Dijk, A.I., Huffman, G.J., Adler, R.F. and Wood, E.F., 2019. Daily evaluation of 26 precipitation datasets using Stage-IV gauge-radar data for the CONUS. *Hydrology and Earth System Sciences*, *23*(1), pp.207-224.

Bergstra, J. and Bengio, Y., 2012. Random search for hyper-parameter optimization. *Journal of machine learning research*, *13*(2).

Birch, Colin P.D., Oom, Sander P., and Beecham, Jonathan A. Rectangular and hexagonal grids used for observation, experiment, and simulation in ecology. *Ecological Modelling*, Vol. 206, No. 3–4. (August 2007), pp. 347–359.

Bond, W.J. and Keeley, J.E., 2005. Fire as a global 'herbivore': the ecology and evolution of flammable ecosystems. *Trends in ecology & evolution*, *20*(7), pp.387-394.

Bonsal, B.R. and Lawford, R.G., 1999. Teleconnections between El Niño and La Niña events and summer extended dry spells on the Canadian Prairies. *International Journal of Climatology: A Journal of the Royal Meteorological Society*, *19*(13), pp.1445-1458.

Bonsal, B. and Shabbar, A., 2011. *Large-scale climate oscillations influencing Canada, 1900-2008*. Montreal, QC, Canada: Canadian Councils of Resource Ministers.

Bose, I. and Mahapatra, R.K., 2001. Business data mining—a machine learning

perspective. *Information & management*, *39*(3), pp.211-225.

Boychuk, D., McFayden, C.B., Evens, J., Shields, J., Stacey, A., Woolford, D.G., Wotton, M., Johnston, D., Leonard, D. and McLarty, D., 2020. Assembling and customizing multiple fire weather forecasts for burn probability and other fire management applications in Ontario, Canada. *Fire*, *3*(2), p.16.

Brandt, J.P., Flannigan, M.D., Maynard, D.G., Thompson, I.D. and Volney, W.J.A., 2013. An introduction to Canada's boreal zone: ecosystem processes, health, sustainability, and environmental issues. *Environmental Reviews*, *21*(4), pp.207-226.

Byrne, M.P. and O'Gorman, P.A., 2018. Trends in continental temperature and humidity directly linked to ocean warming. *Proceedings of the National Academy of Sciences*, *115*(19), pp.4863-4868.

Cao, Y., Yang, F., Tang, Q. and Lu, X., 2019. An attention enhanced bidirectional LSTM for early forest fire smoke recognition. *IEEE Access*, *7*, pp.154732-154742.

Cardil, A., Rodrigues, M., Tapia, M., Barbero, R., Ramírez, J., Stoof, C.R., Silva, C.A., Mohan, M. and de-Miguel, S., 2023. Climate teleconnections modulate global burned area. Nature Communications, 14(1), p.427.

Carleo, G., Cirac, I., Cranmer, K., Daudet, L., Schuld, M., Tishby, N., Vogt-Maranto, L. and Zdeborová, L., 2019. Machine learning and the physical sciences. *Reviews of Modern Physics*, *91*(4), p.045002.

Cary, G.J., Keane, R.E., Gardner, R.H., Lavorel, S., Flannigan, M.D., Davies, I.D., Li, C., Lenihan, J.M., Rupp, T.S. and Mouillot, F., 2006. Comparison of the sensitivity of landscape-fire-succession models to variation in terrain, fuel pattern, climate and weather. *Landscape ecology*, *21*(1), pp.121-137.

Chollet, F. & others, 2015. Keras. Available at: https://github.com/fchollet/keras.

Chu, P.S., Yan, W. and Fujioka, F., 2002. Fire-climate relationships and long-lead seasonal wildfire prediction for Hawaii. *International Journal of Wildland Fire*, *11*(1), pp.25-31.

Coogan, S.C., Robinne, F.N., Jain, P. and Flannigan, M.D., 2019. Scientists' warning on wildfire—a Canadian perspective. *Canadian Journal of Forest Research*, *49*(9), pp.1015-1023.

Copernicus Climate Change Service (C3S). 2017, https://climate.copernicus.eu/CopernicusESC. Accessed 20 August 2019.

Côté, J., S. Gravel, A. Méthot, A. Patoine, M. Roch, and A. Staniforth, 1998: The operational CMC-MRB Global Environmental Multiscale (GEM) model: Part I - Design considerations and formulation, Mon. Wea. Rev. 126, 1373-1395.

Crisci, C., Ghattas, B. and Perera, G., 2012. A review of supervised machine learning algorithms and their applications to ecological data. *Ecological Modelling*, *240*, pp.113-122.

Dabanl, İ., Mishra, A.K. and Şen, Z., 2017. Long-term spatio-temporal drought variability in Turkey. *Journal of Hydrology*, *552*, pp.779-792.

Diaz, H.F., Hoerling, M.P. and Eischeid, J.K., 2001. ENSO variability, teleconnections and climate change. *International Journal of Climatology: A Journal of the Royal Meteorological Society*, *21*(15), pp.1845-1862.

Domeisen, D.I., Garfinkel, C.I. and Butler, A.H., 2019. The teleconnection of El Niño Southern Oscillation to the stratosphere. *Reviews of Geophysics*, *57*(1), pp.5-47.

Ecological Stratification Working Group (1995) 'A national ecologi-cal framework for Canada.' (Agri-food Canada Research Branch,Environment Canada: Ottawa/Hull)

Environment and Climate Change Canada (2022). *North American Ensemble Forecast* (NAEFS).
Retrieved April 2, 2022, from https://weather.gc.ca/ensemble/naefs/index_e.html

Flannigan, M.D. and Harrington, J.B., 1988. A study of the relation of meteorological variables to monthly provincial area burned by wildfire in Canada (1953–80). *Journal of Applied Meteorology and Climatology*, *27*(4), pp.441-452.

Flannigan, M.D. and Wotton, B.M., 1991. Lightning-ignited forest fires in northwestern Ontario. *Canadian Journal of Forest Research*, *21*(3), pp.277-287.

Flannigan, M.D., Logan, K.A., Amiro, B.D., Skinner, W.R. and Stocks, B.J., 2005. Future area burned in Canada. *Climatic change*, *72*(1), pp.1-16.

Flannigan, M.D., Krawchuk, M.A., de Groot, W.J., Wotton, B.M. and Gowman, L.M., 2009. Implications of changing climate for global wildland fire. *International journal of wildland fire*, *18*(5), pp.483-507.

Flannigan, M. D., Wotton, B. M., Marshall, G. A., De Groot, W. J., Johnston, J., Jurko, N., & Cantin, A. S. (2016). Fuel moisture sensitivity to temperature and precipitation: climate change implications. *Climatic Change*, *134*(1), 59-71.

Gillett, N.P., Weaver, A.J., Zwiers, F.W. and Flannigan, M.D., 2004. Detecting the effect of climate change on Canadian forest fires. *Geophysical Research Letters*, *31*(18).

Girardin, M.P., Tardif, J.C., Flannigan, M.D. and Bergeron, Y., 2006. Synoptic-scale atmospheric circulation and boreal Canada summer drought variability of the past three centuries. *Journal of Climate*, *19*(10), pp.1922-1947.

González, M.E. and Veblen, T.T., 2006. Climatic influences on fire in Araucaria araucana–Nothofagus forests in the Andean cordillera of south-central Chile. *Ecoscience*, *13*(3), pp.342-350.

Guyon, I. and Aliferis, C., 2007. Causal feature selection. In *Computational methods of feature selection* (pp. 79-102). Chapman and Hall/CRC.

Hanes, C.C.; Wang, X.; Jain, P.; Parisien, M.-P.; Little, J.M.; Flannigan, M.D. 2019. Fire-regime changes in Canada over the last half century. Canadian Journal of Forest Research 49: 256-269. doi: 10.1139/cjfr-2018-0293

Heinze, G., Wallisch, C. and Dunkler, D., 2018. Variable selection–a review and recommendations for the practicing statistician. *Biometrical journal*, *60*(3), pp.431-449.

Hennerman, K. and Berrisford, P.: ERA5 data documentation, available at: https://confluence.ecmwf.int/display/CKB/ERA5+data+documentation, last access: 15 January 2021.

Hennerman, K. and Guillory, A.: What are the changes from ERA-Interim to ERA5, available at: https://confluence.ecmwf.int/pages/viewpage.action?pageId=74764925, last access: 15 January 2021.

Hessilt, T.D., Abatzoglou, J.T., Chen, Y., Randerson, J.T., Scholten, R.C., Van Der Werf, G. and Veraverbeke, S., 2022. Future increases in lightning ignition efficiency and wildfire occurrence expected from drier fuels in boreal forest ecosystems of western North America. *Environmental Research Letters*, *17*(5), p.054008.

Hochreiter, S. and Schmidhuber, J., 1997. Long short-term memory. *Neural computation*, *9*(8), pp.1735-1780.

Hofman, J.M., Sharma, A. and Watts, D.J., 2017. Prediction and explanation in social systems. *Science*, *355*(6324), pp.486-488.

Hornik, K., Stinchcombe, M. and White, H., 1989. Multilayer feedforward networks are universal approximators. *Neural networks*, *2*(5), pp.359-366.

Jain, P., Coogan, S.C., Subramanian, S.G., Crowley, M., Taylor, S. and Flannigan, M.D., 2020. A review of machine learning applications in wildfire science and management. *Environmental Reviews*, *28*(4), pp.478-505.

Jain, P. and Flannigan, M., 2021. The relationship between the polar jet stream and extreme wildfire events in North America. *Journal of Climate*, *34*(15), pp.6247-6265.

Jia, Y. and Ma, J., 2017. What can machine learning do for seismic data processing? An interpolation application. *Geophysics*, *82*(3), pp.V163-V177.

Jiang, X., Pang, Y., Li, X., Pan, J. and Xie, Y., 2018. Deep neural networks with elastic rectified linear units for object recognition. *Neurocomputing*, *275*, pp.1132-1139.

Johnson, E.A. and Wowchuk, D.R., 1993. Wildfires in the southern Canadian Rocky Mountains and their relationship to mid-tropospheric anomalies. *Canadian Journal of Forest Research*, *23*(6), pp.1213-1222.

Ketkar, N., 2017. Introduction to keras. In *Deep learning with Python* (pp. 97-111). Apress, Berkeley, CA.

Kingma, D.P. and Ba, J., 2014. Adam: A method for stochastic optimization. *arXiv preprint arXiv:1412.6980*.

Kirchmeier-Young, Megan C., Francis W. Zwiers, Nathan P. Gillett, and Alex J. Cannon. "Attributing extreme fire risk in Western Canada to human emissions." *Climatic Change* 144, no. 2 (2017): 365-379.

Kitzberger, T., Brown, P.M., Heyerdahl, E.K., Swetnam, T.W. and Veblen, T.T., 2007. Contingent Pacific–Atlantic Ocean influence on multicentury wildfire synchrony over western North America. *Proceedings of the National Academy of Sciences*, *104*(2), pp.543-548.

Knight, J.R., Folland, C.K. and Scaife, A.A., 2006. Climate impacts of the Atlantic multidecadal oscillation. *Geophysical Research Letters*, *33*(17)

Krasnopolsky, V.M. and Fox-Rabinovitz, M.S., 2006. Complex hybrid models combining deterministic and machine learning components for numerical climate modeling and weather prediction. *Neural Networks*, *19*(2), pp.122-134.

Lawson, B.D. and Armitage, O.B., 2008. Weather guide for the Canadian forest fire danger rating system.

Liang, H., Zhang, M. and Wang, H., 2019. A neural network model for wildfire scale prediction using meteorological factors. *IEEE Access*, *7*, pp.176746-176755.

Liu, Y., Zheng, H., Feng, X. and Chen, Z., 2017, October. Short-term traffic flow prediction with Conv-LSTM. In *2017 9th International Conference on Wireless Communications and Signal Processing (WCSP)* (pp. 1-6). IEEE.

Liu, Z., Peng, C., Work, T., Candau, J.N., DesRochers, A. and Kneeshaw, D., 2018. Application of machine-learning methods in forest ecology: recent progress and future challenges. *Environmental Reviews*, *26*(4), pp.339-350.

Macias Fauria, M. and Johnson, E.A., 2006. Large-scale climatic patterns control large lightning fire occurrence in Canada and Alaska forest regions. *Journal of Geophysical Research: Biogeosciences*, *111*(G4).

Martell, D.L., 2001. Forest fire management. In *Forest Fires* (pp. 527-583). Academic Press.

Maxwell, A.E., Warner, T.A. and Fang, F., 2018. Implementation of machine-learning classification in remote sensing: An applied review. *International Journal of Remote Sensing*, *39*(9), pp.2784-2817.

McCollor, Doug; Stull, Roland. *Weather & Forecasting.* Feb2009, Vol. 24 Issue 1, p3-17. 15p. 2 Charts, 13 Graphs, 1 Map. DOI: 10.1175/2008WAF2222130.1.

McCulloch, W.S. and Pitts, W., 1943. A logical calculus of the ideas immanent in nervous activity. *The bulletin of mathematical biophysics*, *5*(4), pp.115-133.

McElhinny, M., Beckers, J. F., Hanes, C., Flannigan, M., and Jain, P.: A high-resolution reanalysis of global fire weather from 1979 to 2018 – overwintering the Drought Code, Earth Syst. Sci. Data, 12, 1823–1833, https://doi.org/10.5194/essd-12-1823-2020, 2020.

McGovern, A., Elmore, K.L., Gagne, D.J., Haupt, S.E., Karstens, C.D., Lagerquist, R., Smith, T. and Williams, J.K., 2017. Using artificial intelligence to improve real-time decision-making for high-impact weather. *Bulletin of the American Meteorological Society*, *98*(10), pp.2073-2090.

McGovern, A., Lagerquist, R., Gagne, D.J., Jergensen, G.E., Elmore, K.L., Homeyer, C.R. and Smith, T., 2019. Making the black box more transparent: Understanding the physical implications of machine learning. *Bulletin of the American Meteorological Society*, *100*(11), pp.2175-2199.

McPhaden, M.J., Zebiak, S.E. and Glantz, M.H., 2006. ENSO as an integrating concept in earth science. *science*, *314*(5806), pp.1740-1745.

Mitchell, T.M. and Mitchell, T.M., 1997. *Machine learning* (Vol. 1, No. 9). New York: McGraw-hill.

Moritz, M.A., Batllori, E., Bradstock, R.A., Gill, A.M., Handmer, J., Hessburg, P.F., Leonard, J., McCaffrey, S., Odion, D.C., Schoennagel, T. and Syphard, A.D., 2014. Learning to coexist with wildfire. *Nature*, *515*(7525), pp.58-66.

Mosavi, A., Ozturk, P. and Chau, K.W., 2018. Flood prediction using machine learning models: Literature review. *Water*, *10*(11), p.1536.

Murphy, K.P., 2012. Machine learning: a probabilistic perspective. MIT press.

Nair, V. and Hinton, G.E., 2010, January. Rectified linear units improve restricted boltzmann machines. In *Icml*.

Natural Resources Canada, 2022. State of Canada's Forests: Annual Report 2022. (ISSN 1488-

2736). Retrieved December 18, 2023, from https://natural-resources.canada.ca/our-natural-resources/forests/state-canadas-forests-report/16496

NOAA$_1$ (2022) *Climate Timeseries AMO (Atlantic Multidecadal Oscillation) Index*. Available at: https://psl.noaa.gov/data/timeseries/AMO/ (Accessed: 1 September 2021).

NOAA$_2$ (2022) *Multivariate ENSO Index Version 2 (MEI.v2)*. Available at: https://psl.noaa.gov/enso/mei/ (Accessed: 1 September 2021).

Nussbaumer, H.J., 1981. The fast Fourier transform. In *Fast Fourier Transform and Convolution Algorithms* (pp. 80-111). Springer, Berlin, Heidelberg.

Olden, J.D., Lawler, J.J. and Poff, N.L., 2008. Machine learning methods without tears: a primer for ecologists. *The Quarterly review of biology*, *83*(2), pp.171-193.

Pedregosa, F., Varoquaux, G., Gramfort, A., Michel, V., Thirion, B., Grisel, O., Blondel, M., Prettenhofer, P., Weiss, R., Dubourg, V. and Vanderplas, J., 2011. Scikit-learn: Machine learning in Python. *the Journal of machine Learning research*, *12*, pp.2825-2830.

Poole, D.L. and Mackworth, A.K., 2010. *Artificial Intelligence: foundations of computational agents*. Cambridge University Press.

Price, C. and Rind, D., 1994. The impact of a 2× CO 2 climate on lightning-caused fires. *Journal of Climate*, *7*(10), pp.1484-1494.

Rajkomar, A., Dean, J. and Kohane, I., 2019. Machine learning in medicine. *New England Journal of Medicine*, *380*(14), pp.1347-1358.

Reich, Y. and Barai, S.V., 1999. Evaluating machine learning models for engineering problems. *Artificial Intelligence in Engineering*, *13*(3), pp.257-272.

Ribeiro, M.T., Singh, S. and Guestrin, C., 2016. "Why should I trust you?" Explaining the predictions of any classifier. *Proceedings of the 22nd ACM SIGKDD international conference on knowledge discovery and data mining*, pp.1135-1144.

Robinson, A.J. and Fallside, F., 1987. *The utility driven dynamic error propagation network*. Cambridge: University of Cambridge Department of Engineering.

Rodriguez-Galiano, V., Sanchez-Castillo, M., Chica-Olmo, M. and Chica-Rivas, M.J.O.G.R., 2015. Machine learning predictive models for mineral prospectivity: An evaluation of neural networks, random forest, regression trees and support vector machines. *Ore Geology Reviews*, *71*, pp.804-818.

Romps, D.M., Seeley, J.T., Vollaro, D. and Molinari, J., 2014. Projected increase in lightning strikes in the United States due to global warming. *Science*, *346*(6211), pp.851-854.

Roulet, N., Moore, T.I.M., Bubier, J. and Lafleur, P., 1992. Northern fens: methane flux and climatic change. *Tellus B*, *44*(2), pp.100-105.

Sanabria, L.A., Qin, X., Li, J., Cechet, R.P. and Lucas, C., 2013. Spatial interpolation of McArthur's forest fire danger index across Australia: observational study. *Environmental modelling & software*, *50*, pp.37-50.

San-Miguel-Ayanz, J., Schulte, E., Schmuck, G., Camia, A., Strobl, P., Liberta, G., Giovando, C., Boca, R., Sedano, F., Kempeneers, P. and McInerney, D., 2012. Comprehensive monitoring of wildfires in Europe: the European forest fire information system (EFFIS). In *Approaches to managing disaster-Assessing hazards, emergencies and disaster impacts*. IntechOpen.

Schmoldt, D.L., 2001. Application of artificial intelligence to risk analysis for forested ecosystems. In *Risk analysis in forest management* (pp. 49-74). Springer, Dordrecht.

Schoennagel, T., Veblen, T.T., Romme, W.H., Sibold, J.S. and Cook, E.R., 2005. ENSO and PDO variability affect drought-induced fire occurrence in Rocky Mountain subalpine forests. *Ecological Applications*, *15*(6), pp.2000-2014.

Schwarz, K.P., Sideris, M.G. and Forsberg, R., 1990. The use of FFT techniques in physical geodesy. *Geophysical Journal International*, *100*(3), pp.485-514.

Shabbar, A. and Skinner, W., 2004. Summer drought patterns in Canada and the relationship Toglobal sea surface temperatures. *Journal of Climate*, *17*(14), pp.2866-2880.

Shahriari, B., Swersky, K., Wang, Z., Adams, R.P. and De Freitas, N., 2015. Taking the human out of the loop: A review of Bayesian optimization. *Proceedings of the IEEE*, *104*(1), pp.148-175.

Sharma, A.R., Jain, P., Abatzoglou, J.T. and Flannigan, M., 2022. Persistent Positive Anomalies in Geopotential Heights Promote Wildfires in Western North America. Journal of Climate, 35(19), pp.6469-6486.

Simard, A.J., Haines, D.A. and Main, W.A., 1985. Relations between El Niño/Southern Oscillation anomalies and wildland fire activity in the United States. *Agricultural and Forest Meteorology*, *36*(2), pp.93-104.

Skinner, W.R., Stocks, B.J., Martell, D.L., Bonsal, B. and Shabbar, A., 1999. The association between circulation anomaliesin the mid-troposphere and area burnedby wildland fire in Canada. *Theoretical and Applied Climatology*, *63*(1), pp.89-105.

Skinner, W.R., Shabbar, A., Flannigan, M.D. and Logan, K., 2006. Large forest fires in Canada and the relationship to global sea surface temperatures. *Journal of Geophysical Research: Atmospheres*, *111*(D14).

Snoek, J., Larochelle, H. and Adams, R.P., 2012. Practical bayesian optimization of machine learning algorithms. *Advances in neural information processing systems*, *25*.

Stocks, B.J., Lawson, B.D., Alexander, M.E., Wagner, C.V., McAlpine, R.S., Lynham, T.J. and Dube, D.E., 1989. The Canadian forest fire danger rating system: an overview. *The Forestry Chronicle*, *65*(6), pp.450-457.

Stocks, B.J., Mason, J.A., Todd, J.B., Bosch, E.M., Wotton, B.M., Amiro, B.D., Flannigan, M.D., Hirsch, K.G., Logan, K.A., Martell, D.L. and Skinner, W.R., 2002. Large forest fires in Canada, 1959–1997. *Journal of Geophysical Research: Atmospheres*, *107*(D1), pp.FFR-5.

Stocks, B.J., and Martell, D.L. 2016. Forest fire management expenditures in Canada: 1970–2013. For. Chron. 92: 298–306. doi:10.5558/tfc2016-056.

Surden, H., 2014. Machine learning and law. *Wash. L. Rev.*, *89*, p.87.

Tahmasebi, P., Kamrava, S., Bai, T., & Sahimi, M., 2020. Machine learning in geo-and environmental sciences: From small to large scale. *Advances in Water Resources*, *142*, 103619.

Tarek, M., Brissette, F.P. and Arsenault, R., 2020. Evaluation of the ERA5 reanalysis as a potential reference dataset for hydrological modelling over North America. *Hydrology and Earth System Sciences*, *24*(5), pp.2527-2544.

Torrence, C. and Webster, P.J., 1998. The annual cycle of persistence in the El Nño/Southern Oscillation. *Quarterly Journal of the Royal Meteorological Society*, *124*(550), pp.1985-2004.

Toth,Z., and Coauthors, 2006: The North American Ensemble Forecast System (NAEFS). Preprints, 18th Conf. on Probability and Statistics in the Atmospheric Sciences, Atlanta, GA, Amer.Meteor. Soc., 4.1. [Available online at http://ams.confex. com/ams/pdfpapers/102588.pdf.]

Trouet, V., Taylor, A.H., Carleton, A.M. and Skinner, C.N., 2009. Interannual variations in fire weather, fire extent, and synoptic-scale circulation patterns in northern California and Oregon. *Theoretical and Applied Climatology*, *95*(3), pp.349-360.

Troup, A.J., 1965. The 'southern oscillation'. *Quarterly Journal of the Royal Meteorological Society*, *91*(390), pp.490-506.

Turner, J.A.; Lawson, B.D. 1978. Weather in the Canadian Forest Fire Danger Rating System. A user guide to national standards and practices. Environment Canada, Pacific Forest Research Centre, Victoria, BC. BC-X-177.

Van Wagner, C.V., 1977. Conditions for the start and spread of crown fire. *Canadian Journal of*

*Forest Research*, *7*(1), pp.23-34.

Van Wagner, C.E., 1987. Development and structure of the Canadian forest fire weather index system (Vol. 35).

Verdon, D.C., Kiem, A.S. and Franks, S.W., 2004. Multi-decadal variability of forest fire risk—Eastern Australia. *International Journal of Wildland Fire*, *13*(2), pp.165-171.

Vitart, F. and Robertson, A.W., 2018. The sub-seasonal to seasonal prediction project (S2S) and the prediction of extreme events. *npj Climate and Atmospheric Science*, *1*(1), p.3.

Wang, X., Thompson, D.K., Marshall, G.A., Tymstra, C., Carr, R. and Flannigan, M.D., 2015. Increasing frequency of extreme fire weather in Canada with climate change. *Climatic Change*, *130*(4), pp.573-586.

Williams, R.J. and Zipser, D., 1995. Gradient-based learning algorithms for recurrent. *Backpropagation: Theory, architectures, and applications*, *433*, p.17.

Westerling, A.L. and Swetnam, T.W., 2003. Interannual to decadal drought and wildfire in the western United States. *EOS, Transactions American Geophysical Union*, *84*(49), pp.545-555.

Westerling, A.L., Hidalgo, H.G., Cayan, D.R. and Swetnam, T.W., 2006. Warming and earlier spring increase western US forest wildfire activity. *science*, *313*(5789), pp.940-943.

Wolter, K., 1993. Monitoring ENSO in COADS with a seasonally adjusted principal component index. In *Proc. of the 17th Climate Diagnostics Workshop, 1993*.

Wotton, B.M. and Flannigan, M.D., 1993. Length of the fire season in a changing climate. *The Forestry Chronicle*, *69*(2), pp.187-192.

Yu, K., Guo, X., Liu, L., Li, J., Wang, H., Ling, Z. and Wu, X., 2020. Causality-based feature selection: Methods and evaluations. *ACM Computing Surveys (CSUR)*, *53*(5), pp.1-36.

Zhang, Y., Wallace, J.M. and Battisti, D.S., 1997. ENSO-like interdecadal variability: 1900–93. *Journal of climate*, *10*(5), pp.1004-1020.

## Appendix A

Table A.1) LSTM Model F1-Scores for each of the four models at one to five week lead times for all hexels.

| *Week* | *Model 1* | *Model 2* | *Model 3* | *Model 4* |
|---|---|---|---|---|
| ***Hexel 2*** | | | | |
| *1* | 0.947115 | 0.947115 | 0.944712 | 0.942308 |
| *2* | 0.918269 | 0.939904 | 0.923077 | 0.935096 |
| *3* | 0.927885 | 0.932692 | 0.927885 | 0.935096 |
| *4* | 0.906259 | 0.906250 | 0.903846 | 0.894231 |
| *5* | 0.901442 | 0.894231 | 0.899038 | 0.887019 |
| ***Hexel 3*** | | | | |
| *1* | 0.939904 | 0.944712 | 0.93750 | 0.944712 |
| *2* | 0.923077 | 0.923077 | 0.925481 | 0.920673 |
| *3* | 0.915865 | 0.915865 | 0.918269 | 0.920673 |
| *4* | 0.906250 | 0.899038 | 0.906250 | 0.906250 |
| *5* | 0.901442 | 0.906250 | 0.901442 | 0.906250 |
| ***Hexel 4*** | | | | |
| *1* | 0.932692 | 0.932692 | 0.927885 | 0.932692 |
| *2* | 0.903846 | 0.903846 | 0.903846 | 0.899038 |
| *3* | 0.894231 | 0.894231 | 0.899038 | 0.891827 |
| *4* | 0.903846 | 0.887019 | 0.884615 | 0.884615 |
| *5* | 0.894231 | 0.894231 | 0.879808 | 0.870192 |
| ***Hexel 5*** | | | | |
| *1* | 0.915865 | 0.911058 | 0.913462 | 0.908654 |
| *2* | 0.891827 | 0.867788 | 0.887019 | 0.870192 |
| *3* | 0.877404 | 0.867788 | 0.865385 | 0.850962 |
| *4* | 0.870192 | 0.858173 | 0.870192 | 0.858173 |
| *5* | 0.870192 | 0.858173 | 0.867788 | 0.843750 |
| ***Hexel 6*** | | | | |
| *1* | 0.923077 | 0.920673 | 0.923077 | 0.923077 |
| *2* | 0.896635 | 0.896635 | 0.899038 | 0.899038 |
| *3* | 0.899038 | 0.899038 | 0.899038 | 0.899038 |
| *4* | 0.899038 | 0.899038 | 0.901442 | 0.899038 |
| *5* | 0.899038 | 0.899038 | 0.899038 | 0.899038 |
| ***Hexel 7*** | | | | |
| *1* | 0.951923 | 0.944712 | 0.954327 | 0.947115 |
| *2* | 0.947115 | 0.949519 | 0.949519 | 0.947115 |
| *3* | 0.939904 | 0.942308 | 0.939904 | 0.944712 |
| *4* | 0.918269 | 0.925481 | 0.913462 | 0.923077 |
| *5* | 0.920673 | 0.925481 | 0.918269 | 0.923077 |
| ***Hexel 8*** | | | | |
| *1* | 0.923077 | 0.925481 | 0.925481 | 0.932692 |
| *2* | 0.894231 | 0.894231 | 0.894231 | 0.884615 |
| *3* | 0.887019 | 0.882212 | 0.884615 | 0.882212 |
| *4* | 0.870192 | 0.860577 | 0.872596 | 0.858173 |
| *5* | 0.865385 | 0.838942 | 0.860577 | 0.831731 |
| ***Hexel 9*** | | | | |
| *1* | 0.925481 | 0.927885 | 0.927885 | 0.930288 |
| *2* | 0.894231 | 0.894231 | 0.894231 | 0.896635 |

| | | | | |
|---|---|---|---|---|
| *3* | 0.901442 | 0.906250 | 0.903846 | 0.903846 |
| *4* | 0.882212 | 0.884615 | 0.887019 | 0.887019 |
| *5* | 0.891827 | 0.891827 | 0.891827 | 0.889423 |
| ***Hexel 10*** | | | | |
| *1* | 0.903846 | 0.901442 | 0.903846 | 0.901442 |
| *2* | 0.891827 | 0.887019 | 0.882212 | 0.884615 |
| *3* | 0.884615 | 0.877404 | 0.879808 | 0.882212 |
| *4* | 0.870192 | 0.872596 | 0.862981 | 0.870192 |
| *5* | 0.867788 | 0.867788 | 0.862981 | 0.865385 |
| ***Hexel 11*** | | | | |
| *1* | 0.896635 | 0.899038 | 0.891827 | 0.896635 |
| *2* | 0.891827 | 0.877404 | 0.884615 | 0.882212 |
| *3* | 0.884615 | 0.879808 | 0.884615 | 0.882212 |
| *4* | 0.882212 | 0.877404 | 0.8750 | 0.872596 |
| *5* | 0.882212 | 0.879808 | 0.882212 | 0.877404 |
| ***Hexel 12*** | | | | |
| *1* | 0.939904 | 0.935096 | 0.939904 | 0.935096 |
| *2* | 0.911058 | 0.911058 | 0.911058 | 0.915865 |
| *3* | 0.913462 | 0.906250 | 0.913462 | 0.913462 |
| *4* | 0.896635 | 0.899038 | 0.894231 | 0.894231 |
| *5* | 0.901442 | 0.903846 | 0.896635 | 0.899038 |
| ***Hexel 13*** | | | | |
| *1* | 0.932692 | 0.93750 | 0.925481 | 0.935096 |
| *2* | 0.896635 | 0.899038 | 0.896635 | 0.901442 |
| *3* | 0.899038 | 0.906250 | 0.899038 | 0.906250 |
| *4* | 0.894231 | 0.896635 | 0.894231 | 0.896635 |
| *5* | 0.901442 | 0.899038 | 0.899038 | 0.901442 |
| ***Hexel 14*** | | | | |
| *1* | 0.942308 | 0.93750 | 0.93750 | 0.93750 |
| *2* | 0.925481 | 0.925481 | 0.920673 | 0.920673 |
| *3* | 0.918269 | 0.913462 | 0.915865 | 0.913462 |
| *4* | 0.908654 | 0.911058 | 0.911058 | 0.915865 |
| *5* | 0.911058 | 0.913462 | 0.908654 | 0.913462 |
| ***Hexel 16*** | | | | |
| *1* | 0.911058 | 0.913462 | 0.911058 | 0.918269 |
| *2* | 0.884615 | 0.889423 | 0.887019 | 0.896635 |
| *3* | 0.877404 | 0.882212 | 0.877404 | 0.884615 |
| *4* | 0.877404 | 0.877404 | 0.882212 | 0.8750 |
| *5* | 0.872596 | 0.8750 | 0.882212 | 0.879808 |
| ***Hexel 17*** | | | | |
| *1* | 0.959135 | 0.959135 | 0.959135 | 0.959135 |
| *2* | 0.932692 | 0.930288 | 0.930288 | 0.927885 |
| *3* | 0.913462 | 0.913462 | 0.911058 | 0.903846 |
| *4* | 0.908654 | 0.908654 | 0.908654 | 0.908654 |
| *5* | 0.901442 | 0.903846 | 0.901442 | 0.903846 |

Table A.2) Persistence Model F1-Scores for each of the four models at one to five week lead times for all hexels.

| *Week* | *Persistence F1-Scores* |
|---|---|
| ***Hexel 2*** | |
| *1* | 0.961538 |
| *2* | 0.927885 |
| *3* | 0.903846 |
| *4* | 0.889423 |
| *5* | 0.876545 |
| ***Hexel 3*** | |
| *1* | 0.932692 |
| *2* | 0.899038 |
| *3* | 0.889423 |
| *4* | 0.884615 |
| *5* | 0.875423 |
| ***Hexel 4*** | |
| *1* | 0.918269 |
| *2* | 0.879808 |
| *3* | 0.860577 |
| *4* | 0.860577 |
| *5* | 0.855413 |
| ***Hexel 5*** | |
| *1* | 0.913462 |
| *2* | 0.879808 |
| *3* | 0.855769 |
| *4* | 0.831731 |
| *5* | 0.830561 |
| ***Hexel 6*** | |
| *1* | 0.923077 |
| *2* | 0.8750 |
| *3* | 0.846154 |
| *4* | 0.841346 |
| *5* | 0.836543 |
| ***Hexel 7*** | |
| *1* | 0.93750 |
| *2* | 0.913462 |
| *3* | 0.903846 |
| *4* | 0.879808 |
| *5* | 0.862456 |
| ***Hexel 8*** | |
| *1* | 0.927885 |
| *2* | 0.894231 |
| *3* | 0.865385 |
| *4* | 0.841346 |
| *5* | 0.834623 |
| ***Hexel 9*** | |
| *1* | 0.942308 |
| *2* | 0.913462 |
| *3* | 0.889423 |

| | |
|---|---|
| *4* | 0.889423 |
| *5* | 0.876212 |
| ***Hexel 10*** | |
| *1* | 0.894231 |
| *2* | 0.879808 |
| *3* | 0.879808 |
| *4* | 0.870192 |
| *5* | 0.865973 |
| ***Hexel 11*** | |
| *1* | 0.918269 |
| *2* | 0.884615 |
| *3* | 0.889423 |
| *4* | 0.870192 |
| *5* | 0.863543 |
| ***Hexel 12*** | |
| *1* | 0.927885 |
| *2* | 0.894231 |
| *3* | 0.8750 |
| *4* | 0.850962 |
| *5* | 0.846543 |
| ***Hexel 13*** | |
| *1* | 0.93750 |
| *2* | 0.903846 |
| *3* | 0.889423 |
| *4* | 0.870192 |
| *5* | 0.861354 |
| ***Hexel 14*** | |
| *1* | 0.942308 |
| *2* | 0.913462 |
| *3* | 0.889423 |
| *4* | 0.870192 |
| *5* | 0.864328 |
| ***Hexel 16*** | |
| *1* | 0.918269 |
| *2* | 0.8750 |
| *3* | 0.8750 |
| *4* | 0.860577 |
| *5* | 0.854326 |
| ***Hexel 17*** | |
| *1* | 0.956731 |
| *2* | 0.923077 |
| *3* | 0.899038 |
| *4* | 0.879808 |
| *5* | 0.871354 |

Table A.3) Climatology Model F1-Scores for each of the four models at one to five week lead times for all hexels.

| *Week* | *Climatology F1-Scores* |
|---|---|
| ***Hexel 2*** | |
| *1* | 0.899038 |
| *2* | 0.899038 |
| *3* | 0.899038 |
| *4* | 0.899038 |
| *5* | 0.899038 |
| ***Hexel 3*** | |
| *1* | 0.899038 |
| *2* | 0.899038 |
| *3* | 0.899038 |
| *4* | 0.899038 |
| *5* | 0.899038 |
| ***Hexel 4*** | |
| *1* | 0.879807 |
| *2* | 0.879807 |
| *3* | 0.879807 |
| *4* | 0.879807 |
| *5* | 0.879807 |
| ***Hexel 5*** | |
| *1* | 0.884615 |
| *2* | 0.884615 |
| *3* | 0.884615 |
| *4* | 0.884615 |
| *5* | 0.884615 |
| ***Hexel 6*** | |
| *1* | 0.899038 |
| *2* | 0.899038 |
| *3* | 0.899038 |
| *4* | 0.899038 |
| *5* | 0.899038 |
| ***Hexel 7*** | |
| *1* | 0.918269 |
| *2* | 0.918269 |
| *3* | 0.918269 |
| *4* | 0.918269 |
| *5* | 0.918269 |
| ***Hexel 8*** | |
| *1* | 0.899038 |
| *2* | 0.899038 |
| *3* | 0.899038 |
| *4* | 0.899038 |
| *5* | 0.899038 |
| ***Hexel 9*** | |
| *1* | 0.899038 |
| *2* | 0.899038 |
| *3* | 0.899038 |

| | |
|---|---|
| *4* | 0.899038 |
| *5* | 0.899038 |
| ***Hexel 10*** | |
| *1* | 0.870192 |
| *2* | 0.870192 |
| *3* | 0.870192 |
| *4* | 0.870192 |
| *5* | 0.870192 |
| ***Hexel 11*** | |
| *1* | 0.884615 |
| *2* | 0.884615 |
| *3* | 0.884615 |
| *4* | 0.884615 |
| *5* | 0.884615 |
| ***Hexel 12*** | |
| *1* | 0.889423 |
| *2* | 0.889423 |
| *3* | 0.889423 |
| *4* | 0.889423 |
| *5* | 0.889423 |
| ***Hexel 13*** | |
| *1* | 0.899038 |
| *2* | 0.899038 |
| *3* | 0.899038 |
| *4* | 0.899038 |
| *5* | 0.899038 |
| ***Hexel 14*** | |
| *1* | 0.913461 |
| *2* | 0.913461 |
| *3* | 0.913461 |
| *4* | 0.913461 |
| *5* | 0.913461 |
| ***Hexel 16*** | |
| *1* | 0.8750 |
| *2* | 0.8750 |
| *3* | 0.8750 |
| *4* | 0.8750 |
| *5* | 0.8750 |
| ***Hexel 17*** | |
| *1* | 0.899038 |
| *2* | 0.899038 |
| *3* | 0.899038 |
| *4* | 0.899038 |
| *5* | 0.899038 |

***Hexel 2: Model MAE Comparisons***

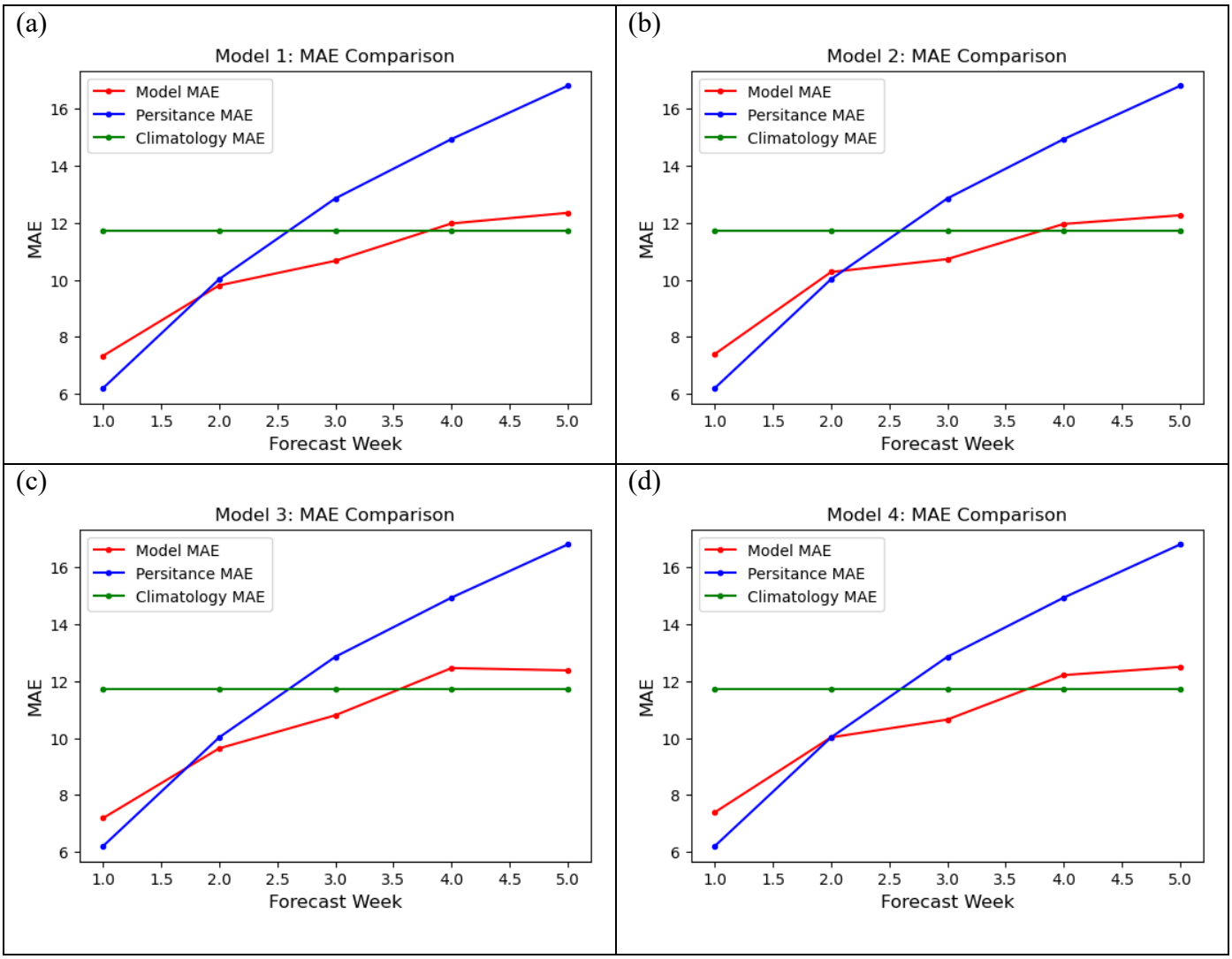


Figure A.1) Plotted MAE values for Hexel 2 showing Model MAE, Climatology MAE, and Persistence MAE for each of the four models (a to d) at one to five week lead times.

***Hexel 3: Model MAE Comparisons***

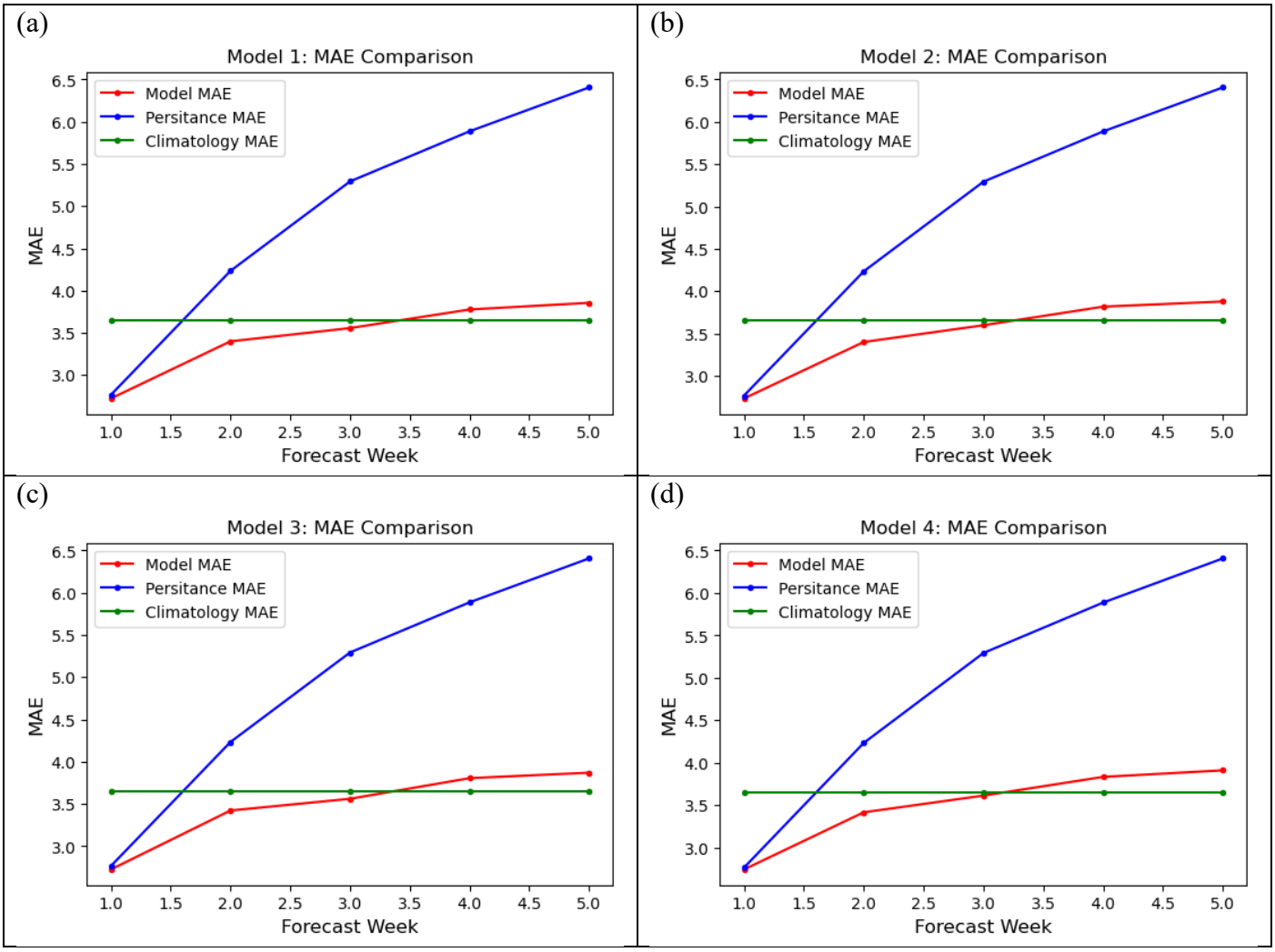


Figure A.2) Plotted MAE values for Hexel 3 showing Model MAE, Climatology MAE, and Persistence MAE for each of the four models (a to d) at one to five week lead times.

***Hexel 4: Model MAE Comparisons***

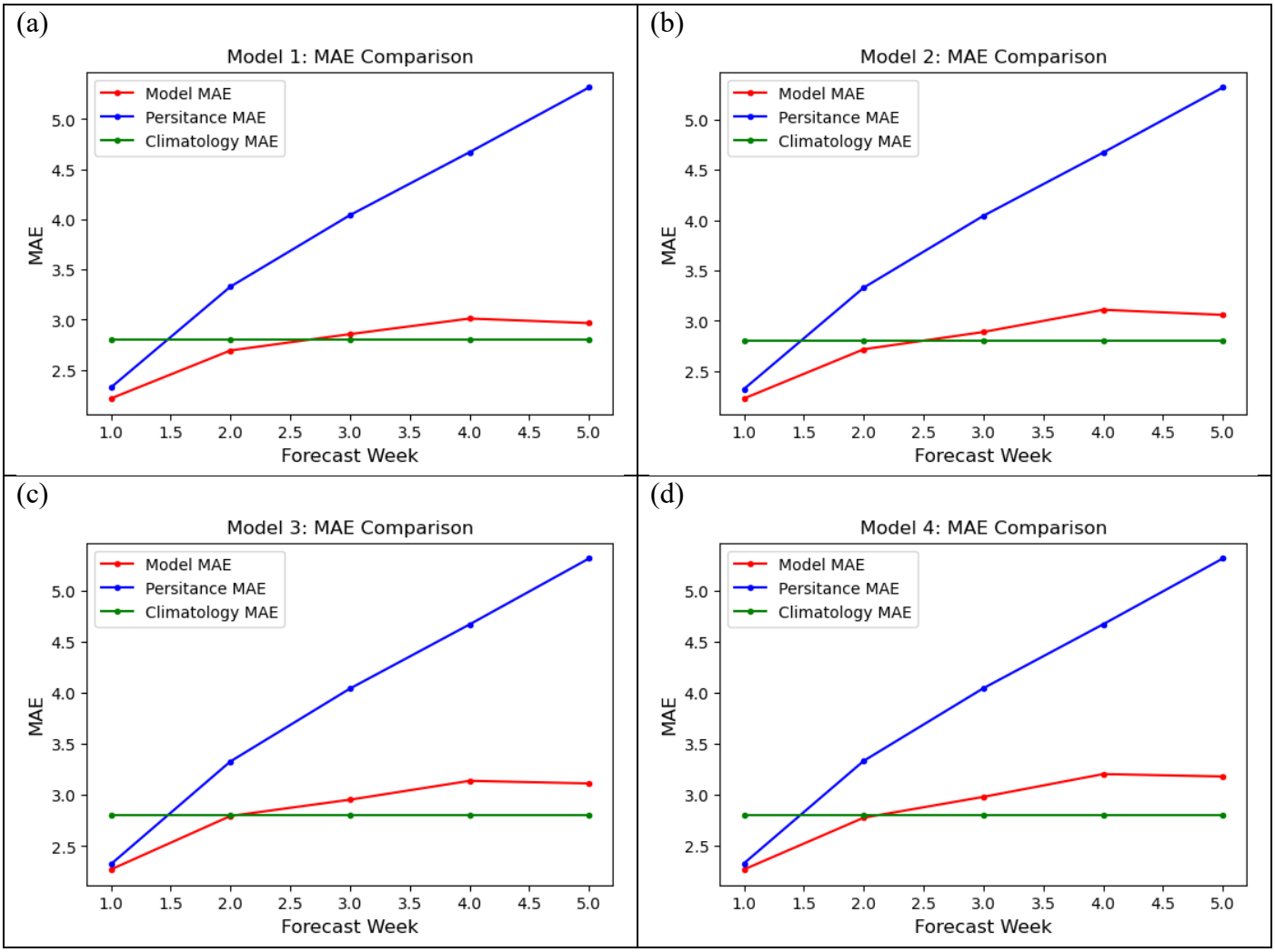


Figure A.3) Plotted MAE values for Hexel 4 showing Model MAE, Climatology MAE, and Persistence MAE for each of the four models (a to d) at one to five week lead times.

***Hexel 5: Model MAE Comparisons***

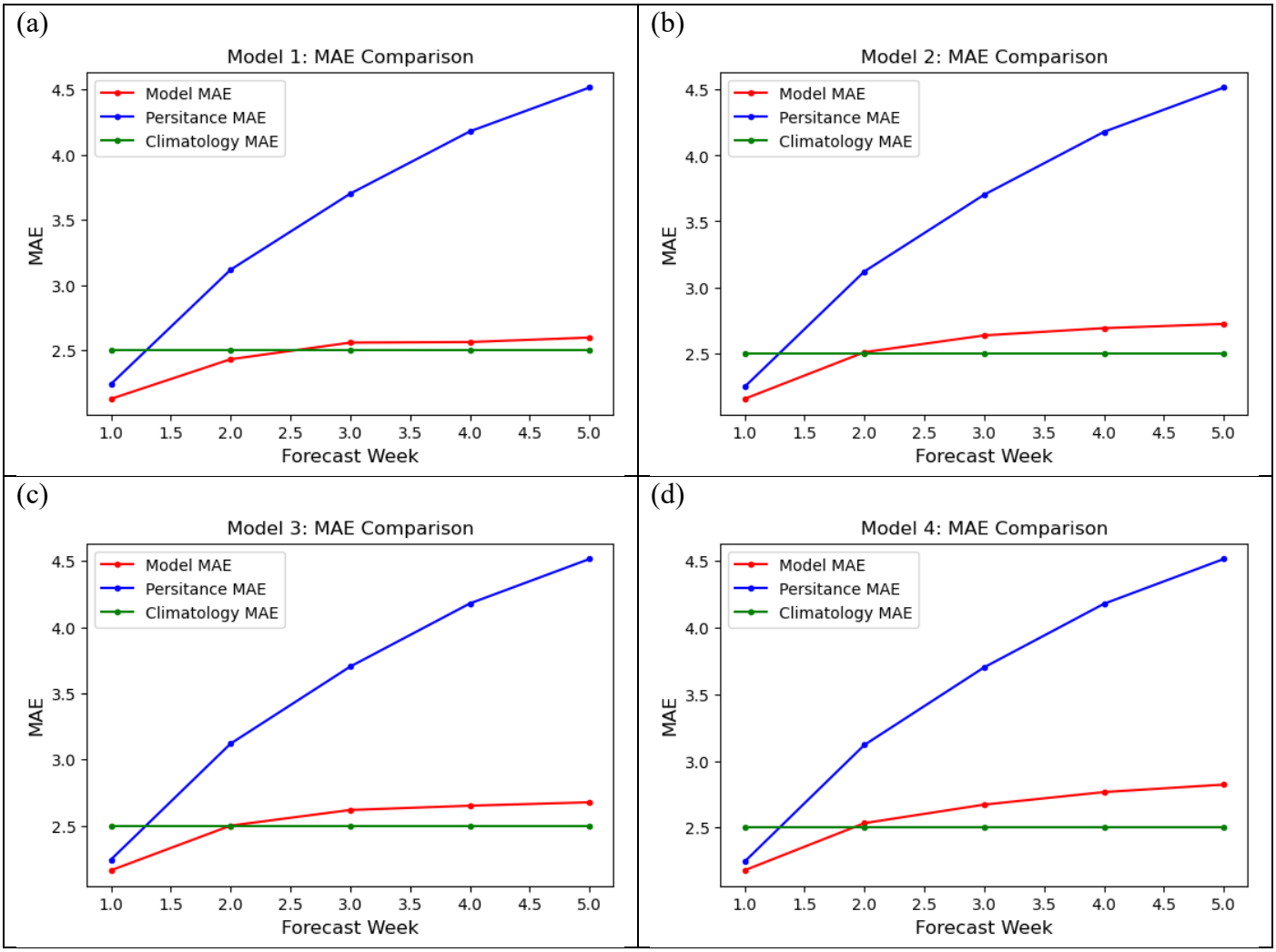


Figure A.4) Plotted MAE values for Hexel 5 showing Model MAE, Climatology MAE, and Persistence MAE for each of the four models (a to d) at one to five week lead times.

***Hexel 6: Model MAE Comparisons***

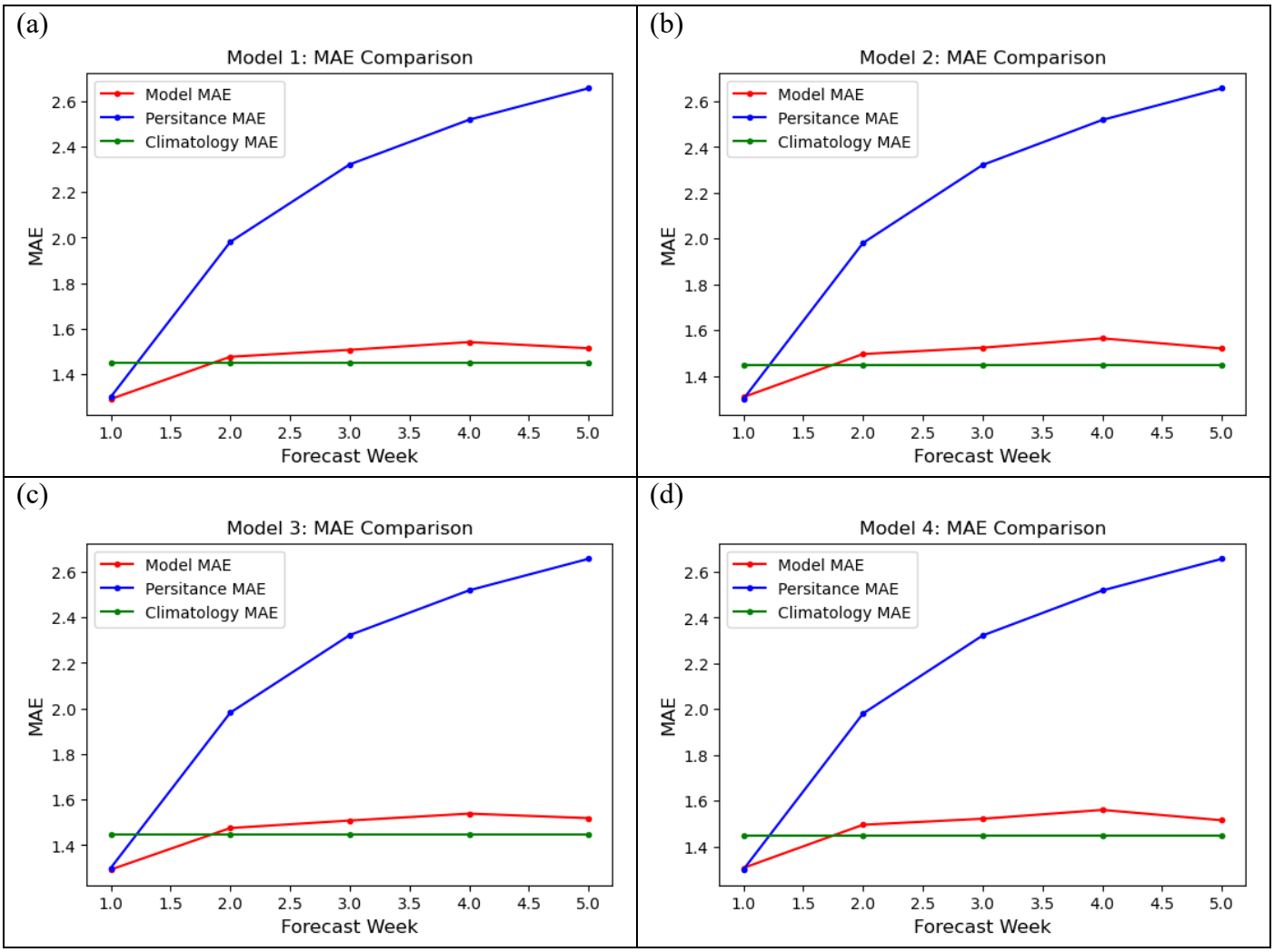


Figure A.5) Plotted MAE values for Hexel 6 showing Model MAE, Climatology MAE, and Persistence MAE for each of the four models (a to d) at one to five week lead times.

***Hexel 7: Model MAE Comparisons***

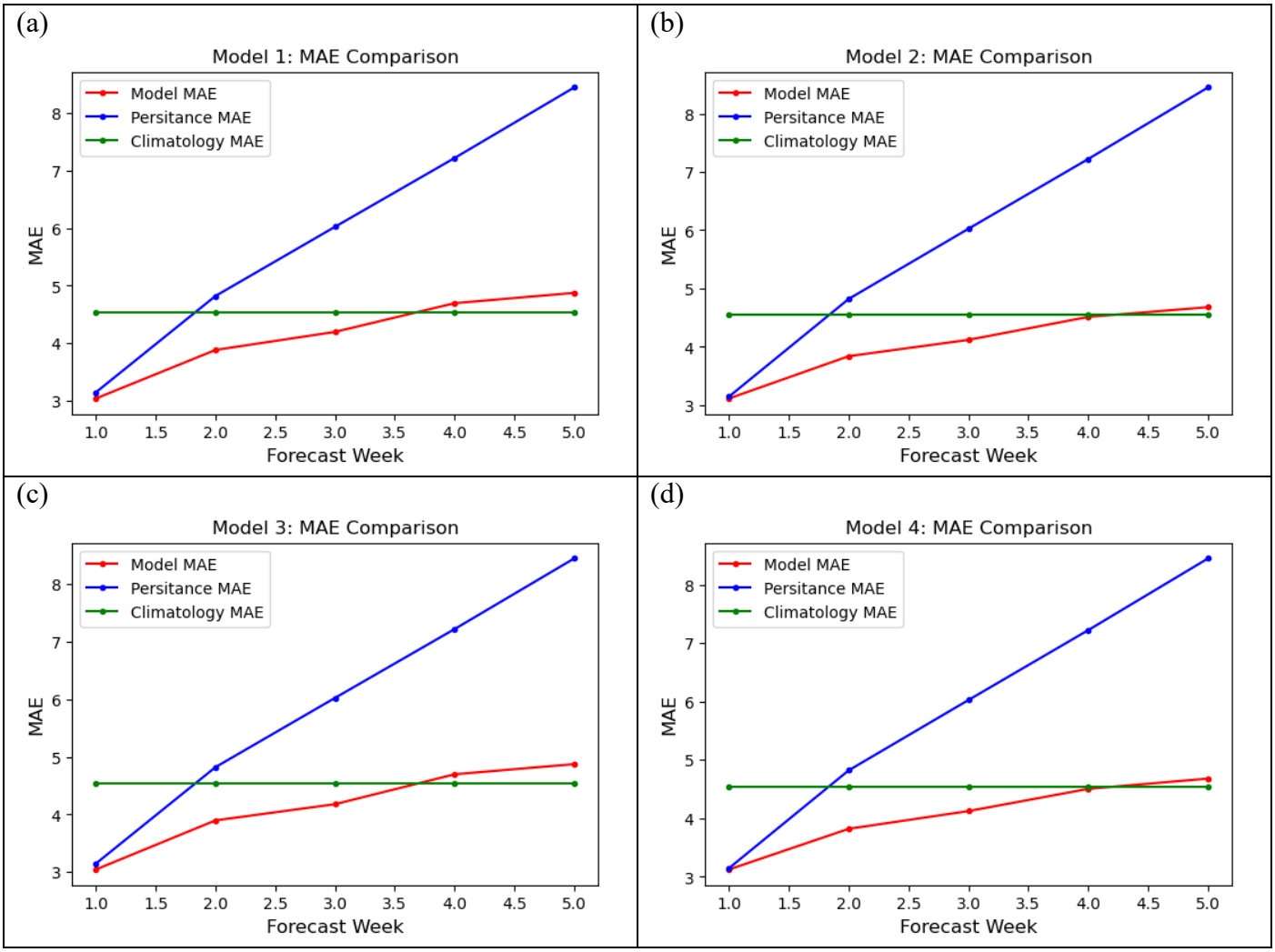


Figure A.6) Plotted MAE values for Hexel 7 showing Model MAE, Climatology MAE, and Persistence MAE for each of the four models (a to d) at one to five week lead times.

***Hexel 8: Model MAE Comparisons***

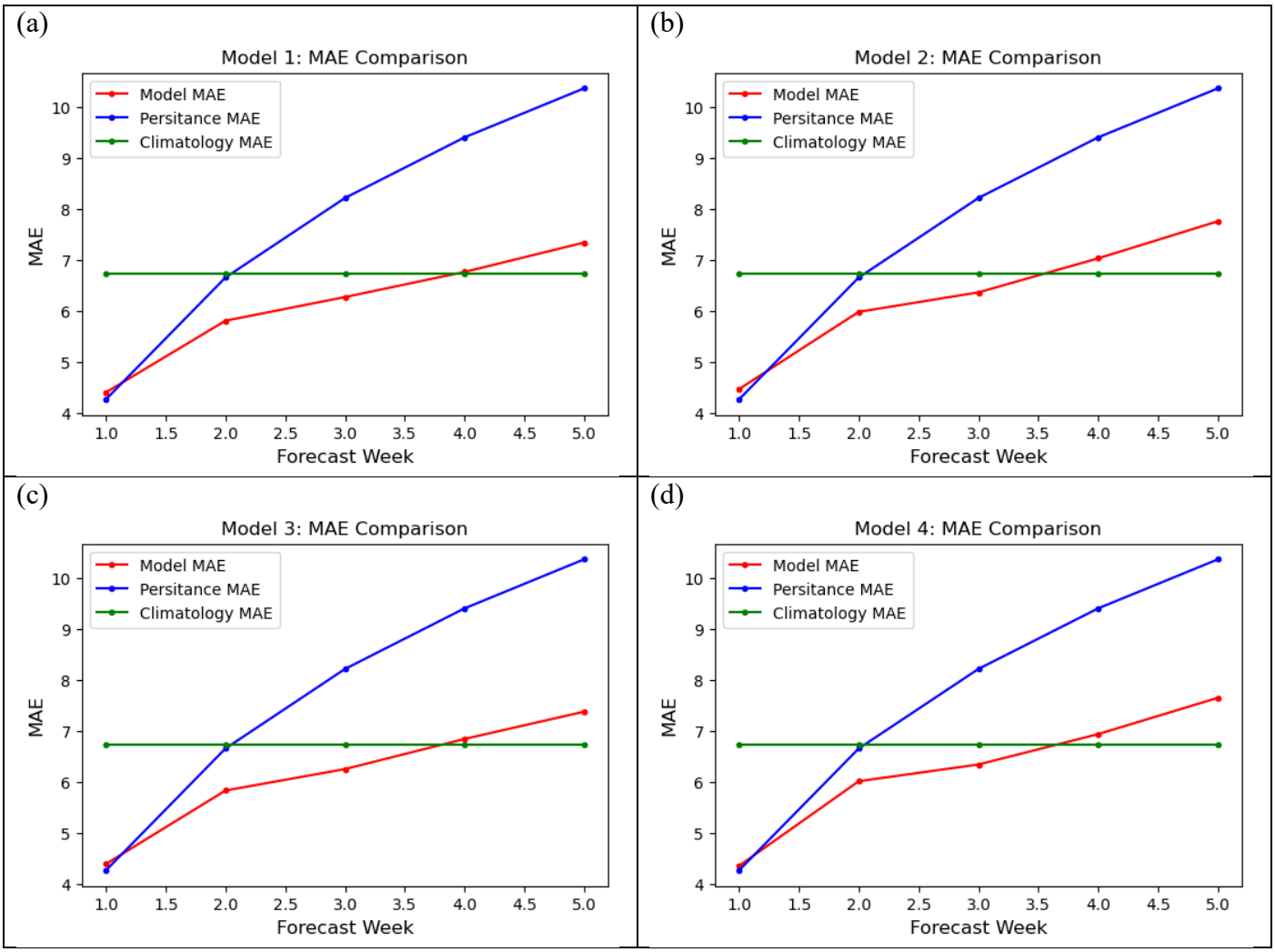


Figure A.7) Plotted MAE values for Hexel 8 showing Model MAE, Climatology MAE, and Persistence MAE for each of the four models (a to d) at one to five week lead times.

***Hexel 9: Model MAE Comparisons***

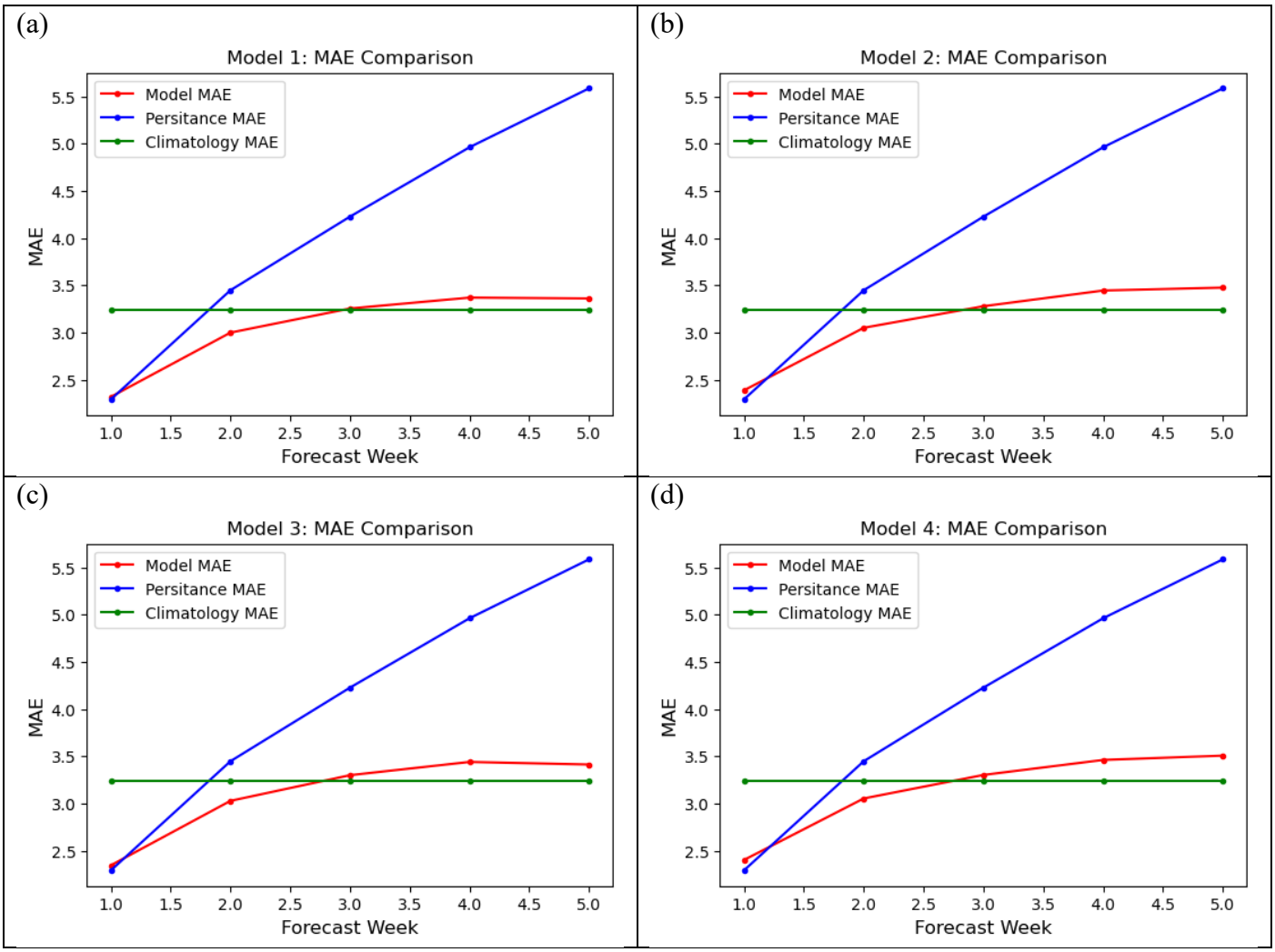


Figure A.8) Plotted MAE values for Hexel 9 showing Model MAE, Climatology MAE, and Persistence MAE for each of the four models (a to d) at one to five week lead times.

## *Hexel 10: Model MAE Comparisons*

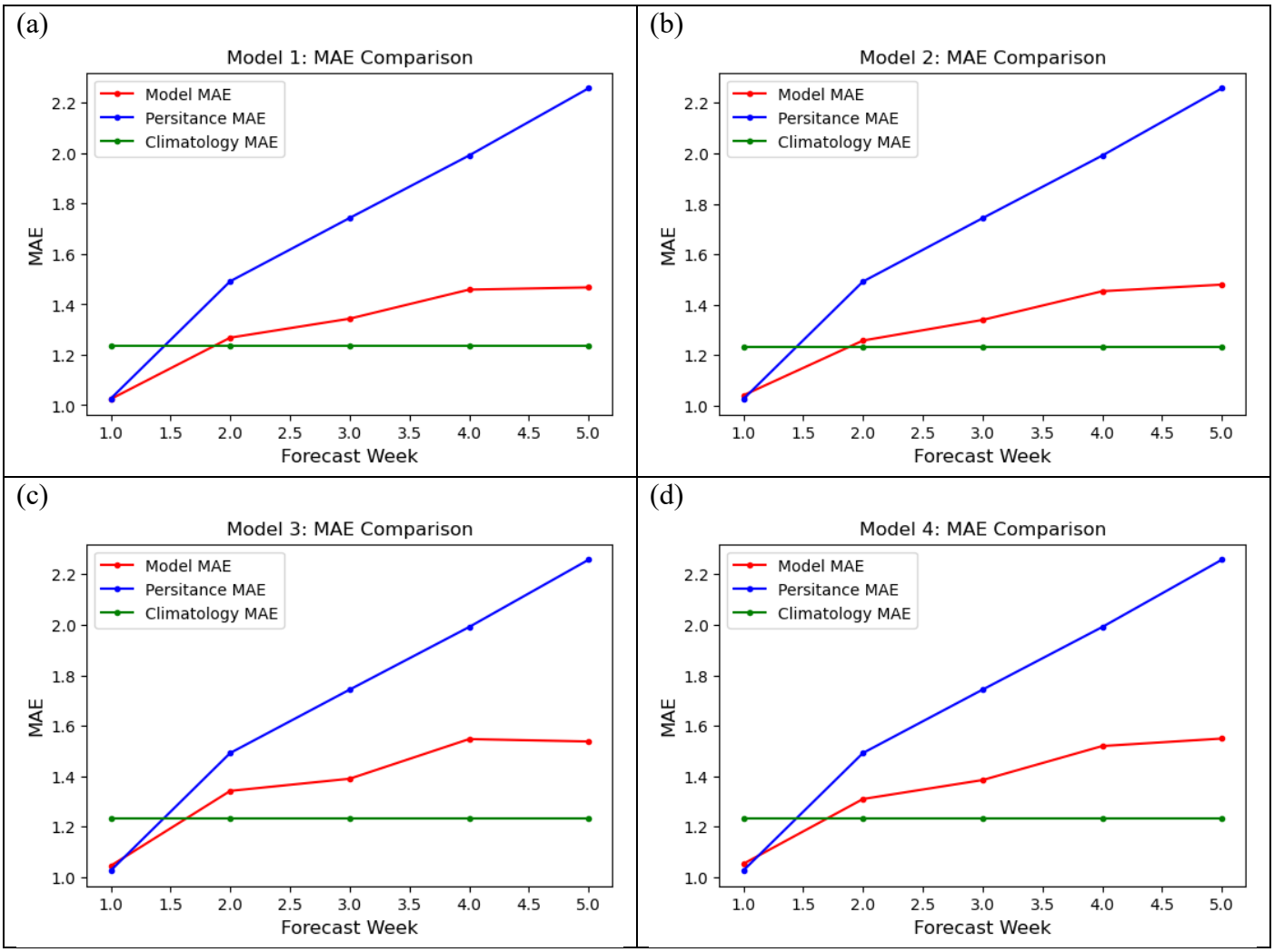


Figure A.9) Plotted MAE values for Hexel 10 showing Model MAE, Climatology MAE, and Persistence MAE for each of the four models (a to d) at one to five week lead times.

***Hexel 11: Model MAE Comparisons***

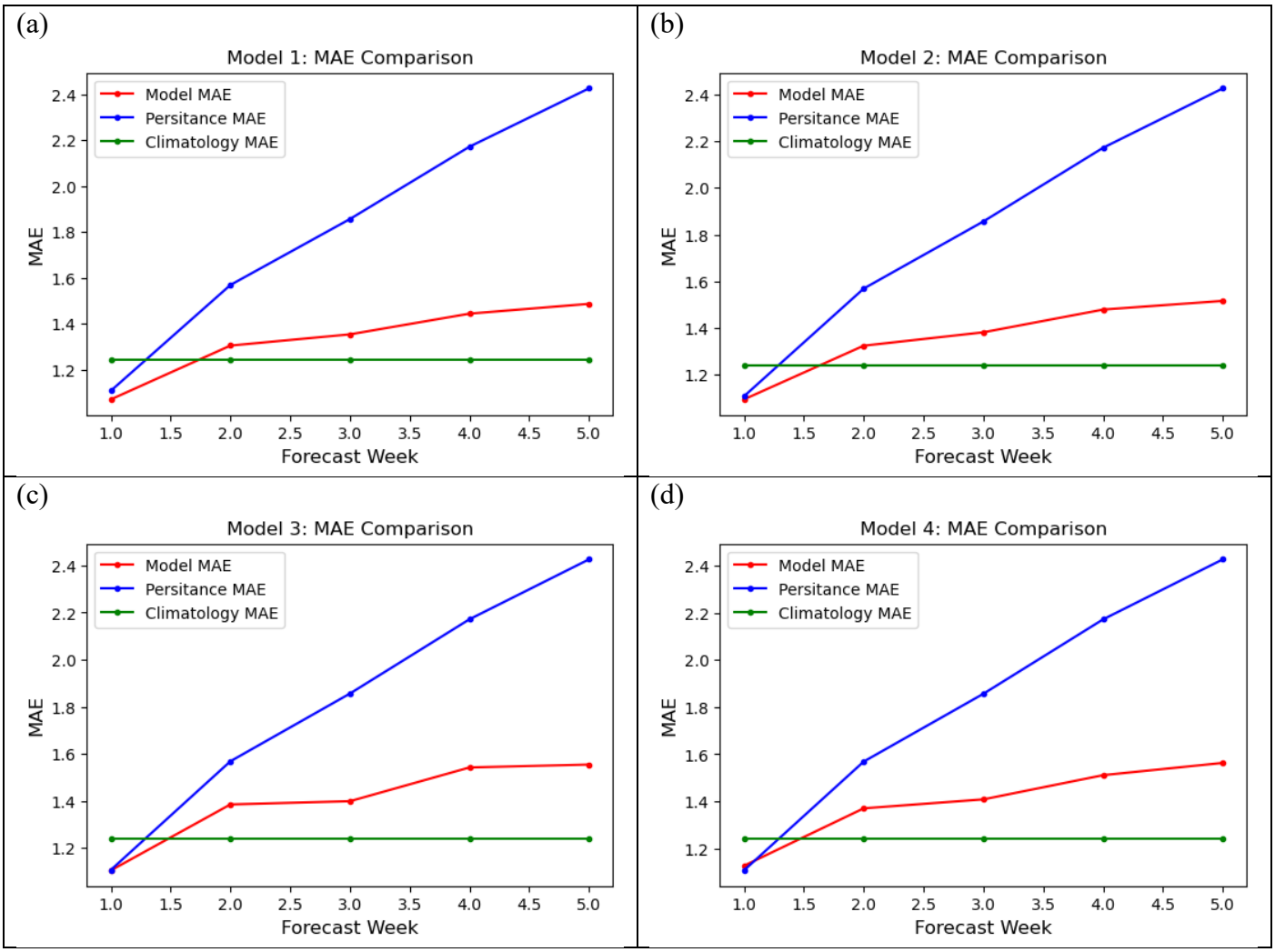


Figure A.10) Plotted MAE values for Hexel 11 showing Model MAE, Climatology MAE, and Persistence MAE for each of the four models (a to d) at one to five week lead times.

***Hexel 12: Model MAE Comparisons***

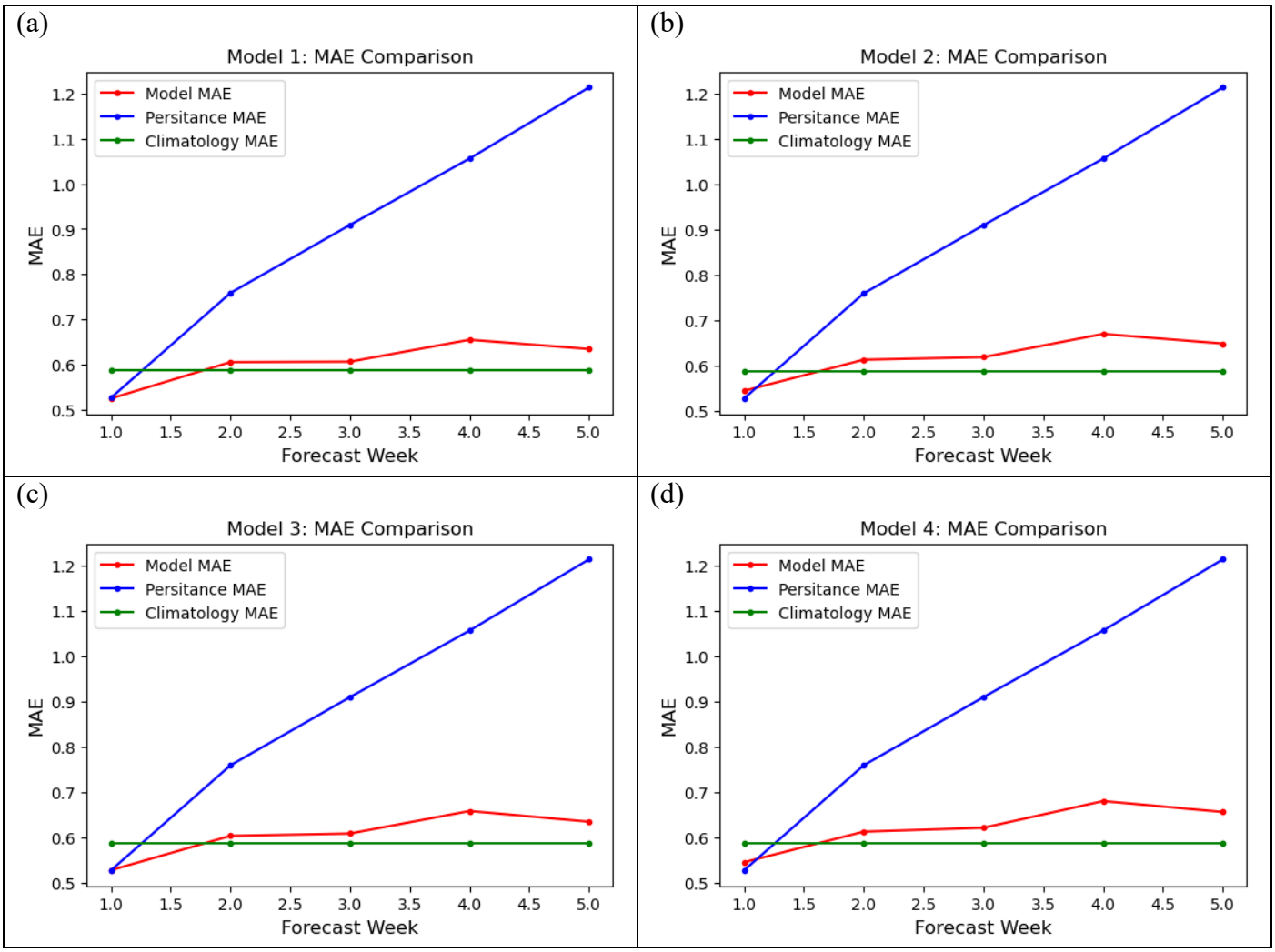


Figure A.11) Plotted MAE values for Hexel 12 showing Model MAE, Climatology MAE, and Persistence MAE for each of the four models (a to d) at one to five week lead times.

***Hexel 13: Model MAE Comparisons***

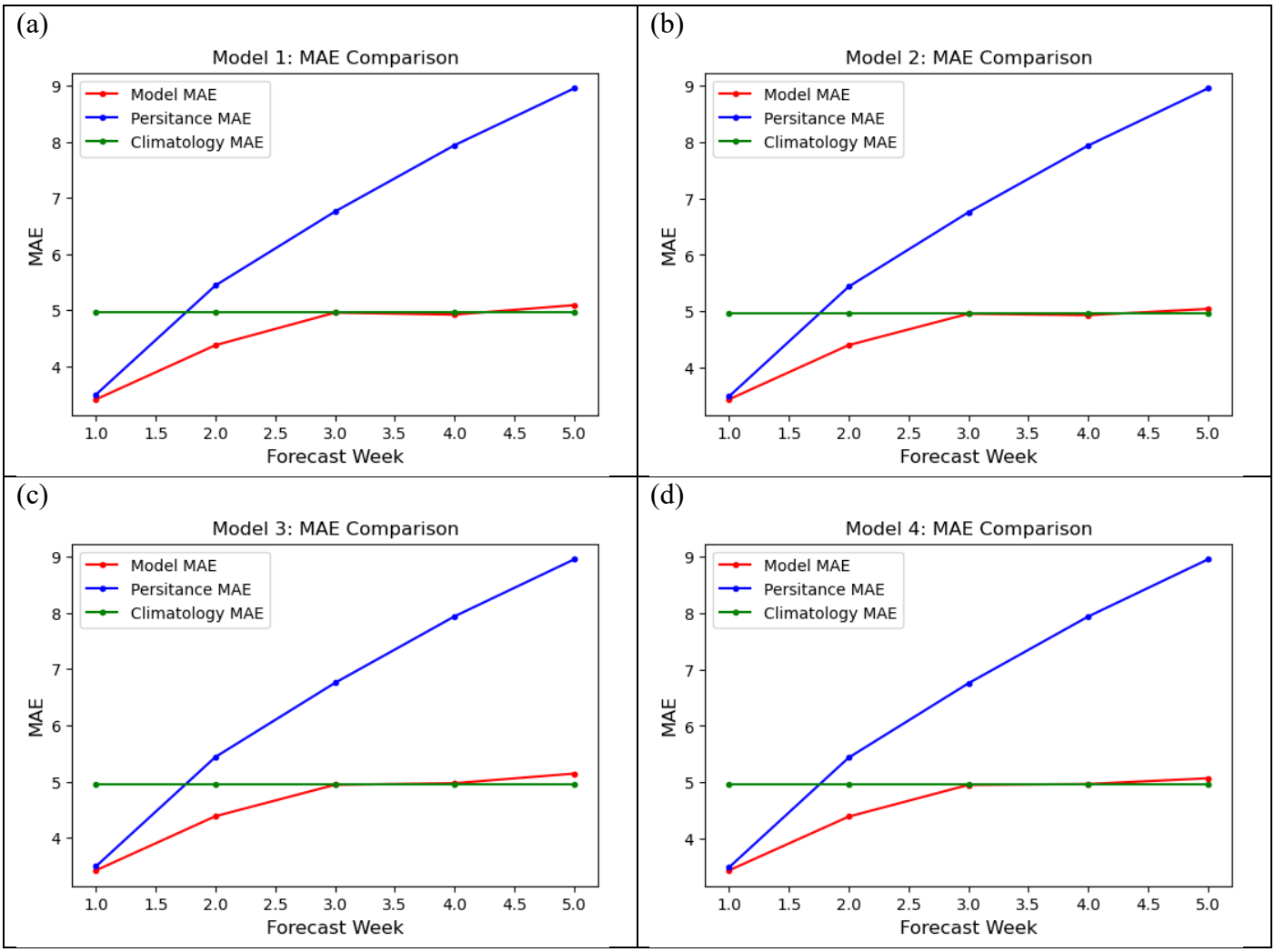


Figure A.12) Plotted MAE values for Hexel 13 showing Model MAE, Climatology MAE, and Persistence MAE for each of the four models (a to d) at one to five week lead times.

***Hexel 14: Model MAE Comparisons***

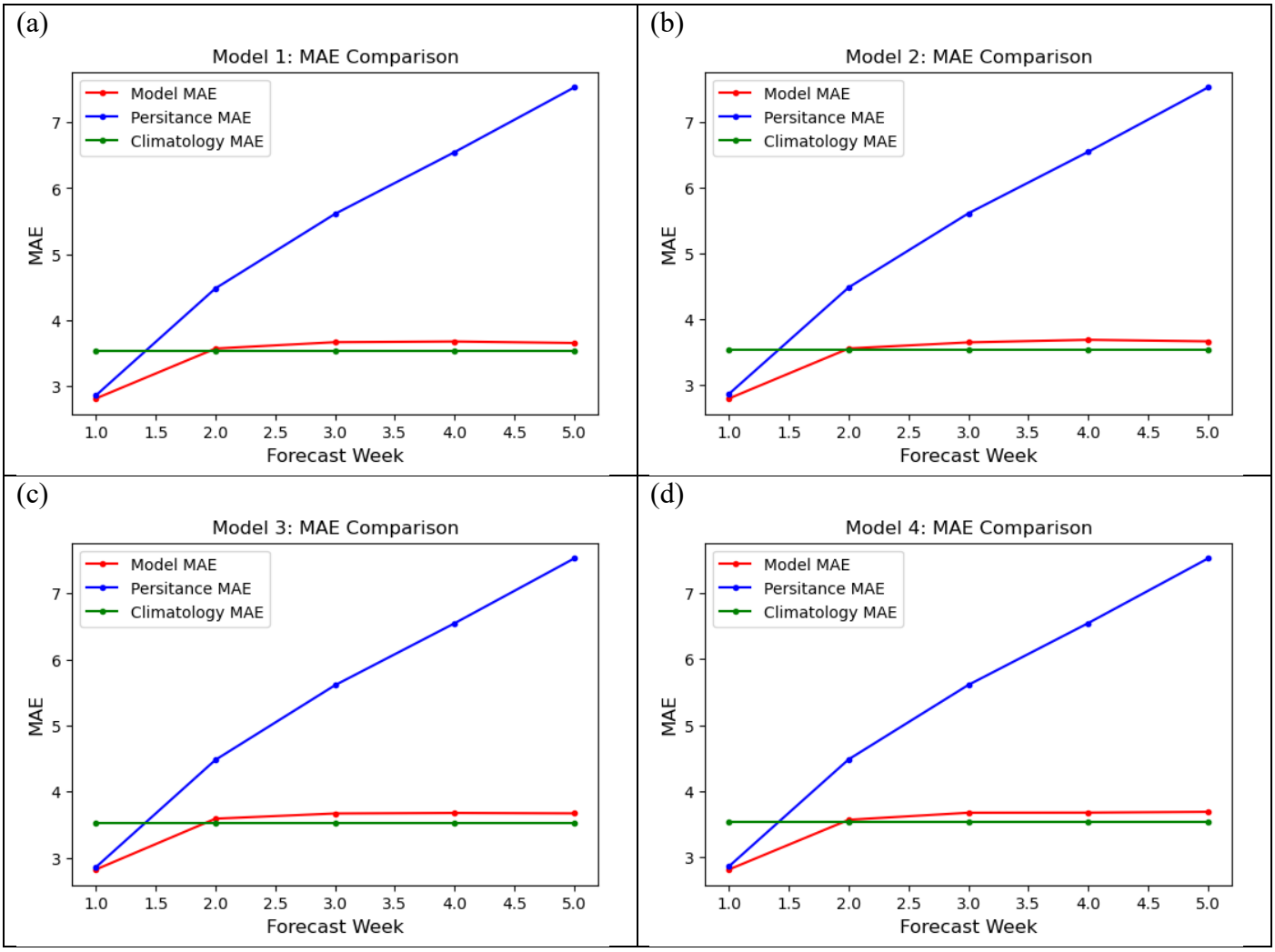


Figure A.13) Plotted MAE values for Hexel 14 showing Model MAE, Climatology MAE, and Persistence MAE for each of the four models (a to d) at one to five week lead times.

***Hexel 16: Model MAE Comparisons***

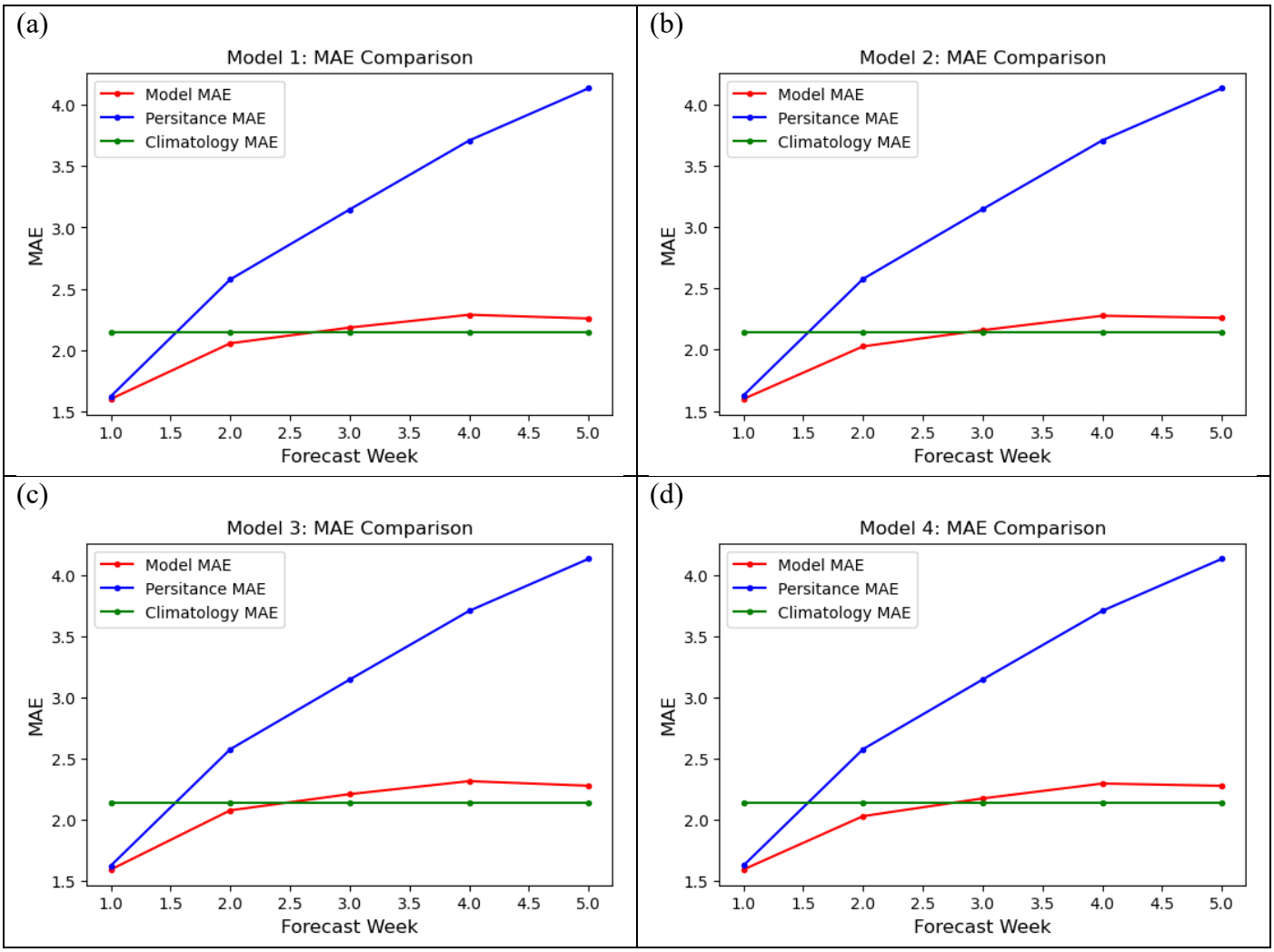


Figure A.14) Plotted MAE values for Hexel 16 showing Model MAE, Climatology MAE, and Persistence MAE for each of the four models (a to d) at one to five week lead times.

***Hexel 17: Model MAE Comparisons***

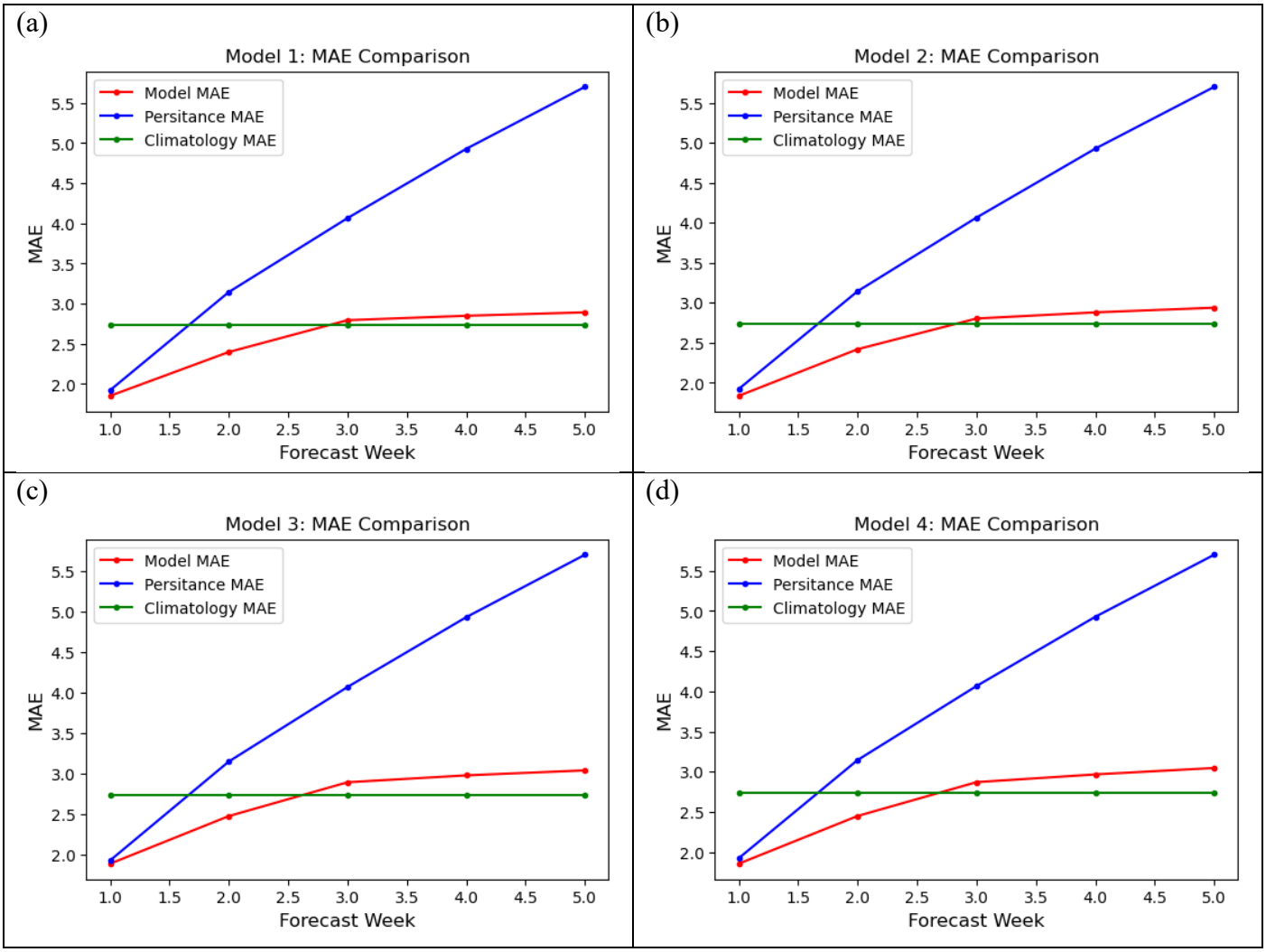


Figure A.15) Plotted MAE values for Hexel 17 showing Model MAE, Climatology MAE, and Persistence MAE for each of the four models (a to d) at one to five week lead times.

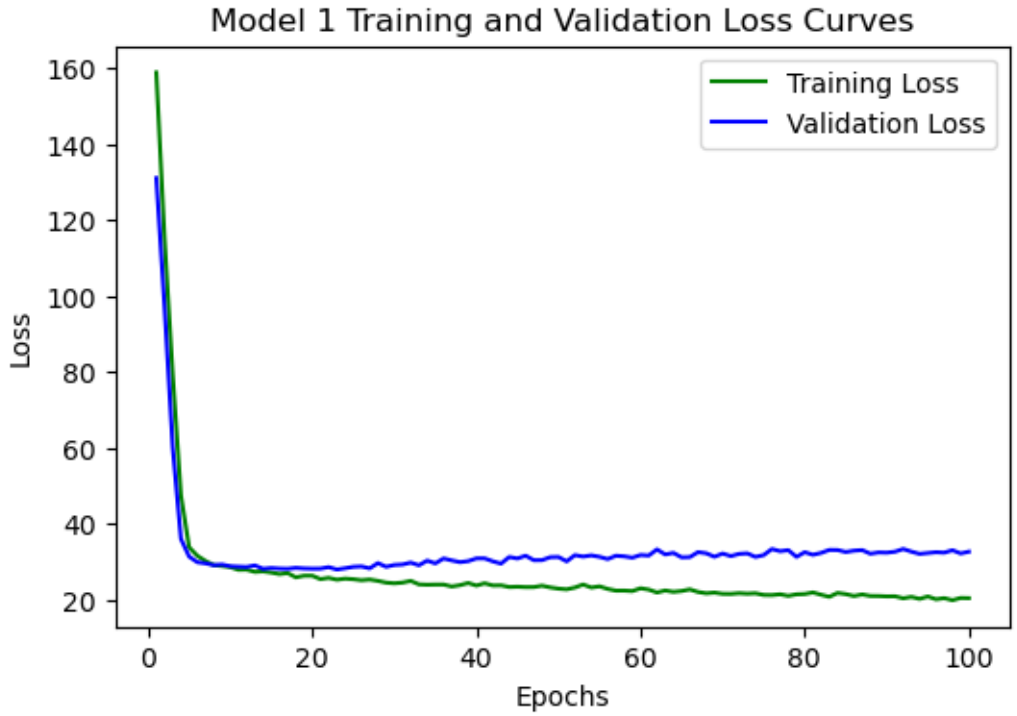


Figure A.16) Example of overfit training and validation loss curves using 100 epochs for Model 1, Hexel 8.

## Appendix B

```
# Split a multivariate sequence into samples
def split_sequences_multi(sequences, n_steps_in, n_steps_out):
	X, y = list(), list()
	for i in range(len(sequences)):

		# Find the end of this pattern
		end_ix = i + n_steps_in
		out_end_ix = end_ix + n_steps_out

		# Check if we are beyond the dataset
		if out_end_ix > len(sequences):
			break
		# Gather input and output parts of the pattern
		seq_x, seq_y = sequences[i:end_ix, :-1], sequences[end_ix:out_end_ix, -1]
		X.append(seq_x)
		y.append(seq_y)
	return np.array(X), np.array(y)
```

Figure B.1) Python code used for data pre-processing which creates two vectors of *n* timesteps.

```
# Pre-processed data division using Split_Sequences_Multi
# Split the training data
X, y = ss.split_sequences_multi(dataset_train, n_steps_in, n_steps_out)

# Split the testing data
Xtest, ytest = ss.split_sequences_multi(dataset_test, n_steps_in, n_steps_out)

# Build the LSTM Model
model = Sequential()
model.add(Dropout(0.20))
model.add(LSTM(150, activation='relu', input_shape=(n_steps_in, n_features)))
model.add(Dense(n_steps_out))
model.add(Dense(n_steps_out,activation='relu'))
optimizer = tf.keras.optimizers.Adam(0.00005)
model.compile(optimizer=optimizer, loss='mse')

# Run the LSTM model prediction
yhat_bui = model.predict(Xtest, verbose=0)
```

Figure B.2) Python code using Keras and TensorFlow libraries to create the LSTM model which includes various hidden layers. These layers are a dropout layer, two dense layers, and an LSTM layer. For the LSTM layer and the second dense layer, ReLU activation is used. As well, an Adam optimizer is included in the model architecture.